UNIVERSITY OF CALIFORNIA, SAN DIEGO

Neural Coding During Active Whisker Sensation.

A dissertation submitted in partial satisfaction of the
requirements for the degree Doctor of Philosophy
in
Computational Neurobiology

by

Shantanu Prafull Jadhav

Committee in charge:

Professor Terrence J. Sejnowski, Chair
Professor Daniel E. Feldman, Co-chair
Professor Eduardo J. Chichilnisky
Professor David Kleinfeld
Professor Larry R. Squire

2008

The dissertation of Shantanu Prafull Jadhav is approved, and it is acceptable in quality and form for publication on microfilm:

_____

_____

_____

_____
Co-Chair

_____
Chair

University of California, San Diego

2008

DEDICATION

To my mother, for her love, support and inspiration.

TABLE OF CONTENTS

LIST OF FIGURES

ACKNOWLEDGMENTS

I would like to thank my advisor Dan Feldman for his constant support and encouragement during my time in his lab. In good times as well as bad, he has been a patient guide and mentor, and has been an example of a model scientist and a good person. I also thank Massimo Scanziani for a collaboration on my first project in graduate school. He continues to be a mentor. Much of my thesis work was done in collaboration with Jason Wolfe. I have learnt a lot from Jason's ability to build experiments from scratch and focus on first principles. He continues to be a cherished friend. I also thank John Curtis and Samar Mehta for help with the chronic recording and spike sorting techniques respectively. In addition, I would like to thank other members of the Feldman lab for being great colleagues and friends, and my committee members for their feedback and guidance.

Outside of lab, I would like to thank my friends from IIT who are pursuing their PhDs in various universities across the country, and my Indian friends at UCSD for creating a home away from home. Finally, above all, I would like to thank my family for their love and constant support and encouragement in all my academic pursuits. My parents are my pillars of support, and my brother, Siddharth, takes pride in all my achievements.

The text of Chapter 2, in full, is a republication of the material as it appears in Gabernet,L., Jadhav S.P., Feldman D.E., Carandini, M., Scanziani, M. (2005): Somatosensory Integration Controlled by Dynamic Feed-Forward Inhibition. *Neuron*, **48**, 315–327. The dissertation author was the second author of this paper.

The text of Chapter 3, in full, is being prepared for publication, Jadhav S.P., Wolfe J.H., Feldman D.E., untitled. The dissertation author is the primary investigator and first author of this paper.

VITA

2002	B.Tech., Engineering Physics, Indian Institute of Technology (IIT) Bombay, India
2002-2003	Research Fellow, National Center for Biological Sciences (NCBS), Bangalore, India
2003-2008	Research Assistant, University of California, San Diego
2008	Ph.D., Computational Neurobiology, University of California, San Diego.

PUBLICATIONS

Gabernet, L., Jadhav, S.P., Feldman, D.E., Carandini, M., Scanziani, M. (2005): Somatosensory Integration Controlled by Dynamic Feed-Forward Inhibition. *Neuron*, **48**, 315–327.

Mitra, R., Jadhav, S., McEwen, B.S., Vyas, A., Chattarji, S. (2005): Stress duration modulates the spatiotemporal patterns of spine formation in the basolateral amygdala. *Proceedings of the National Academy of Sciences*, **102**, 9371–9376.

Vyas, A.*, Jadhav, S.*, Chattarji, S. (2006): Prolonged chronic stress induces amygdaloid neuronal hypertrophy and enhanced anxiety-like behavior. *Neuroscience*, **143**, 387–393.

ABSTRACT OF THE DISSERTATION

Neural Coding During Active Whisker Sensation.

by Shantanu Prafull Jadhav

Doctor of Philosophy in Computational Neurobiology

University of California, San Diego, 2008

Professor Terrence J. Sejnowski, Chair

Professor Daniel E. Feldman, Co-chair

A major goal in studies of sensory coding is to understand how neural activity represents stimuli in the external world. Rats actively palpate objects with their whiskers to discriminate tactile features of their environment. Although neural responses have been characterized in the whisker system in anesthetized animals for artificially applied whisker stimuli, circuit mechanisms underlying neural response properties and neural coding of sensory information in behaving animals are not well understood.

Precise timing of spikes is thought to be important for many aspects of neural coding in the whisker system. Chapter 2 of this thesis elucidates the cellular mechanisms underlying precise spike timing in primary somatosensory cortex (S1). Feed-forward thalamocortical inhibition is shown to dynamically regulate the integration time window of cortical neurons, thus enforcing temporal fidelity of spiking.

How surface properties are encoded by neural activity in awake and active animals is unknown. In Chapter 3, we describe an experiment to identify the fundamental features of whisker motion that are represented in S1 during natural

surface exploration. We simultaneously measured whisker motion and spiking responses of neurons in S1 in awake, behaving rats whisking across textured surfaces. We show that transient slip-stick events are encoded by a majority of S1 neurons with precisely timed spikes, leading to an increase in firing rate. The timing and amplitude of these events is encoded by S1 neurons. Slip-stick responses occurred with low probability, but led to a transient increase in synchronous activity of neurons, resulting in a sparse probabilistic population code. A simulation of the experimental data showed that slip-stick events can be efficiently decoded by synchronous spiking activity on a $\sim$20 ms time scale across small ($\sim$100 neuron) populations within a single S1 cortical column. These results demonstrate that slip-stick events are primary stimulus features encoded in S1 by a sparse ensemble representation during active surface whisking. Synchronous activity of a small subset of neurons efficiently represents slip-stick events, resulting in a population temporal code for surface properties.

I

Introduction

Active Sensation

Sensation is an active process. Animals explore the environment by actively sampling stimuli with their sensors. The movements of the sensory organs (eyes, finger-tips) results in dynamic streams of sensory input from which elementary features of the stimuli are extracted by the nervous system. The nature of this sampling strategy also strongly influences how the representations of complex, natural stimuli arise from integrating neural responses to fundamental sensory features. However, most studies of sensory coding in many modalities (vision, olfaction, tactile sensation) are performed in anesthetized animals with artificial, passive stimulation. Although these studies have revealed many neural response properties in primary sensory cortex, and led to hypothesis about the algorithms and mechanisms underlying perception and behavior, neural response properties in awake-behaving animals remain much less understood. In fact, recent studies have demonstrated that the behavioral state, attention and engagement of the entire sensory-motor loop in active animals completely alter processing of sensory information in cortex (Ferezou et al., 2007; Petersen, 2007; Fritz et al., 2007). Hence, in order to gain a better understanding of how the nervous system guides

behavior, it is necessary to characterize the principles of sensory encoding under active conditions in the behaving animal.

Active Tactile Sensation in the Rat Vibrissa/Whisker System

Active touch is a common behavior that animals use to discern the shape, size, location and texture of nearby objects. The rodent vibrissa/whisker system is an excellent model system for studying active tactile sensing. In primates, the glabrous (hairless) skin of hands provides the main cutaneous surface for sensory discrimination. For rats, arrays of whiskers on the face serve as the primary tactile organ. Rats palpate objects by sweeping their whiskers in a rhythmic forward-backward cycle at 5-15 Hz. Each"whisk" provides the animal with a snapshot of the tactile environment, and information is presumably integrated across many whisking cycles to generate a tactile percept. Just like the motion of fingertips and palms, whisker motion generates spatio-temporal patterns of input that are transmitted via the activation of mechanoreceptors to higher brain centers to discriminate features of the object (Kleinfeld et al., 2007; Brecht, 2007). During exploration and palpation of objects, whiskers are under motor control and haptic signals are continuously used to finely tune the position and motion of whiskers. Rats thus employ a combined sensorimotor strategy while executing tactile behaviors.

Behavior in the Whisker System

It is necessary to study animals performing well-defined tasks in order to gain insight into the perceptual basis of decisions, the starting point of which is sensory processing. Ethologically, whiskers are very important for rats. Whiskers mediate a wide range of behaviors and many natural tactile behaviors occur very rapidly (Petersen C.C., 2007; Brecht M., 2007). The behavioral tasks can be

roughly divided into two main categories: A) object location (the "where" question) and B) object properties (the "what" question). With regards to object location, the following tasks have been described in literature. (i) Rats can detect the presence of a platform across a gap with their whiskers (the gap-crossing task, Hutson and Masterton, 1986). (ii) They can discriminate the widths of apertures (Krupa et al., 2004). (iii) They can determine the location of an object in head-centered coordinates (Mehta et al., 2007; Knutsen et al., 2005). With regards to object properties, (i) rats can discern the size, shape (Brecht et al., 1997, Anjum et al., 2006) and (ii) texture of objects (Guic-Robles et al., 1989; Carvell and Simons, 1990; von Heimendahl, et al., 2008). The neural codes underlying these behaviors remain to be elucidated.

Neural Pathways of the Whisker System

The whisker system has a remarkable specialization in S1, where each whisker is represented by a discrete and well-defined, barrel shaped cluster of neurons in layer 4 (Woolsey and Van der Loos, 1970), hence the name "barrel" cortex. This specialization makes the whisker system an attractive model for sensory physiology. The major central projections from whiskers to S1 are depicted in Figure 1 (the lemniscal pathway; Petersen, 2007). Each whisker follicle is densely innervated by mechanoreceptors which respond to deflections of the whisker (Rice et al., 1986). Sensory information is transmitted via afferents, whose cell bodies lie in the trigeminal ganglia, to the brainstem where the first synapse is located. Within the lemniscal pathway, information then ascends to the ventral posterior medial (VPM) sector of the thalamus where the second synapse is located. From VPM the pathway ascends primarily into layer 4 of primary somatosensory cortex (S1) where the third synapse is located.

In all three structures along this ascending pathway, each whisker is rep-

resented by a distinct cluster of cells. Neurons of the sensory afferents in the trigeminal ganglion respond with action potentials only to the deflection of the one whisker which it innervates. These make excitatory connections in the principal trigeminal nucleus, where the trigemino-thalamic neurons are organized into somato-topically arranged "barrelettes" (Veinante and Deschenes, 1999). The next stage, the VPM nucleus is also somatotopically laid out into anatomical units termed "barreloids". VPM neurons respond rapidly and precisely to whisker deflection, with one "principal" whisker evoking stronger responses than all other (Simons and Carvell, 1989; Brecht and Sakmann, 2002). Further, the axons of VPM neurons project to S1 forming discrete clusters within the barrels in layer 4. The layer 4 barrel map is arranged identically to the layout of the whiskers in the periphery, and is repeatable from animal to animal. These topographically arranged anatomical projections strongly suggest a labeled-line single-whisker signaling pathway from the periphery to the barrel cortex, and indeed, principal whisker responses dominate throughout the pathway. Neurons in a single cortical column defined by a barrel have a receptive field centered around the principal whisker, which evokes strongest responses in the column. In addition to the lemniscal pathway, two additional, parallel pathways have been described (Yu et al 2006, Pierret et al 2000). The paralemniscal pathway (projecting via the PoM nucleus of the thalamus) has been shown to primarily represent proprioceptive information about whisker position. The extralemniscal pathway has been recently described. Here we concentrate on the lemniscal pathway, because it conveys precise information about whisker deflections ,and its response properties have been well characterized (Castro-Alamancos 2004; Temereanca and Simons 2003; Pinto et al., 2003).

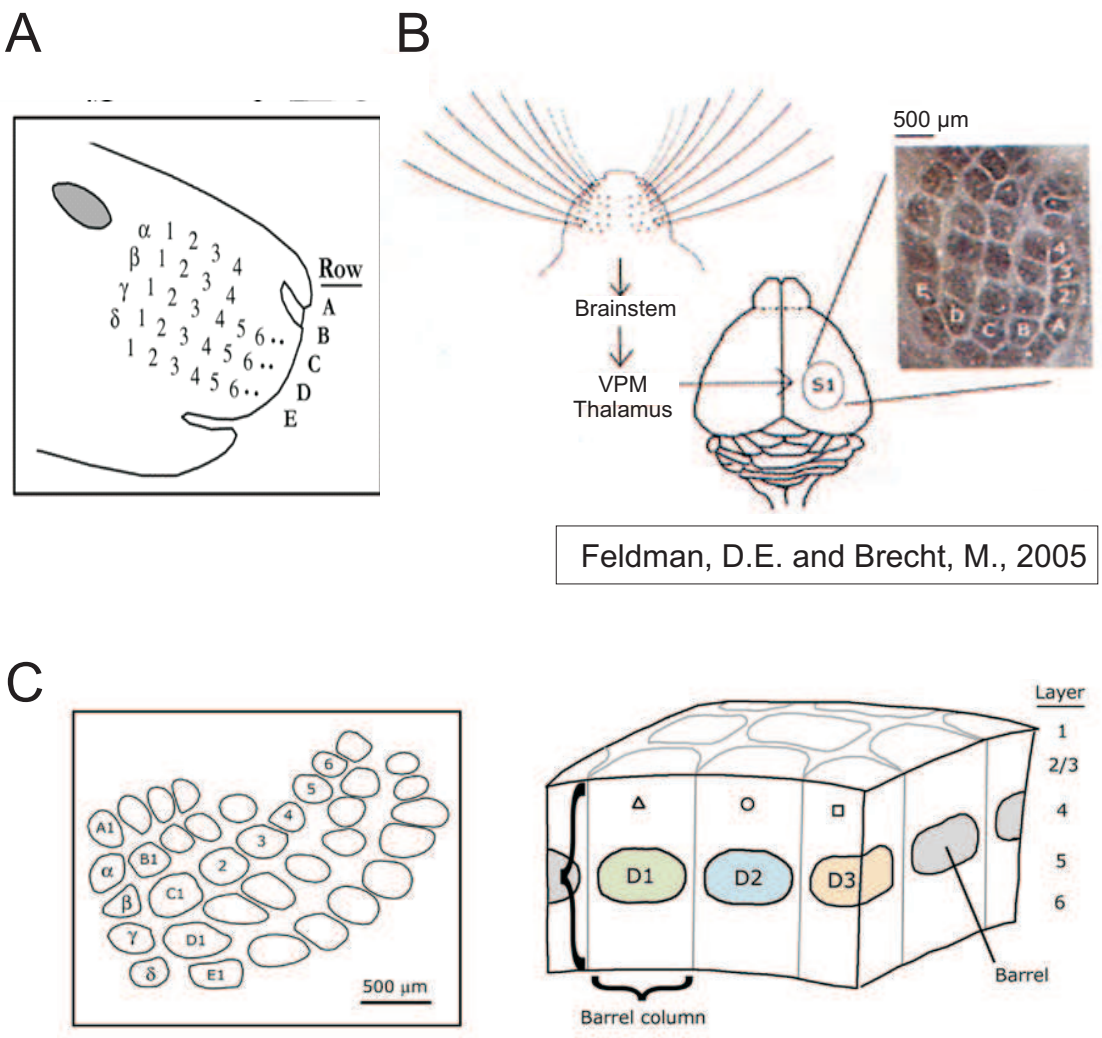

I.1 **Neural pathways of the whisker system.** (A) Whiskers are arranged in rows and arcs. (B) The lemniscal pathway of the whisker system. Primary neurons in the trigeminal ganglion corresponding to each whisker project via the brainstem and VPM thalamus to discrete cortical columns in S1. Inset shows a cytochrome oxidase stained tangential section through layer 4 (L4) of 'barrel' cortex. (C) The barrel map in S1. *Left* Discrete clusters of cells in L4 ('barrels') underlie a map of whiskers on the face. *Right* Cortical columns are centered on the barrels in L4

Neural Responses in the Whisker System

A majority of physiology studies in the whisker system have studied neural coding of passive, experimentally applied whisker stimulation in anesthetized

animals. Neurons in the trigeminal ganglion are sensitive to kinematic parameters (position, velocity and acceleration) of whisker motion (Jones, et al., 2004). Neurons in VPM thalamus and S1 respond rapidly and precisely to deflection of the principal whisker, with weaker and slower responses to surround whiskers. Responses in S1 increase in strength with increasing velocities of deflections, and are also known to be direction-selective (Bruno et al., 2003). Studies in VPM and S1 using this approach have characterized the size of receptive fields, precise timing of spikes to transient onsets and offsets of stimuli, and adaptation of responses to repetitive stimulation (Pinto, et al., 2003, Brumberg et al., 2003, Minnery et al., 2003). Precisely timed spiking responses in S1 are thought to be important for many aspects of neural coding in S1: 1) Precise timing may underlie a mechanism by which temporal features of tactile stimuli can be encoded by spiking activity in S1 (Panzeri et al., 2001). 2) Precise timing can regulate of size of whisker receptive fields (Bruno and Simons, 2002). 3) Spike timing controls plasticity of synapses in cortex and hence may be tightly regulated (Celikel, et al., 2004).

Chapter 2 of this thesis describes experiments which elucidate the cellular mechanisms of precise timing in the thalamo-cortical pathway. A feed-forward inhibitory circuit in L4 of S1 is shown to control the integration window of thalamocortical synaptic potentials in excitatory neurons in S1, resulting in a narrow time window of spiking, thus enforcing temporal fidelity during passive stimulation of whiskers in vivo. During rapid whisker stimulation, the strength of thalamocortical synaptic potentials decrease due to synaptic depression, resulting in weaker spiking responses. In addition, the accompanying decrease in feed-forward inhibition results in a broadening of the integration window, due to which jitter of responses also increases. These results show that inhibition sharpens the temporal resolution in S1, and can be dynamically modulated to change the temporal precision of responses.

Neural Responses and Sensory Coding in the Awake, Active Animal

Little is known about responses in S1 in the awake, active animal. Recent studies have shown that responses to even simple passive stimuli are strongly modulated by the engagement of sensory-motor loops during whisking and the attentional state of the animal (Petersen, 2007). One such study found that behavioral state can can modulate whether a sensory response even occurs to a simple deflection of a whisker (Ferezou, et al., 2005). Crucially, since whisking is an active process, the nature of the sensory input in a behaving animal is determined by the precise movement of whiskers, which may differ across behavioral states as sampling strategies. Understanding the neural basis of natural sensation thus requires the description of two processes in the awake-behaving animal: a) The physical transformation from object properties to kinematics of whisker motion, and b) The neural transformation from whisker kinetics to spiking responses along the sensory pathway.

Recent studies in this direction have led to a better understanding of coding of object location (the "where" question) in the whisker system. Using artificial whisking paradigms by stimulating the motor nerve (which generates rhythmic whisker motion similar to natural exploratory whisking), it has been shown that neurons in the periphery (trigeminal ganglion) are sensitive to phase of whisking and contact (Szwed, et al., 2003). Spiking responses in S1 neurons have also been shown to be phase-locked to the whisking cycle in awake-behaving animals (Fee et al., 1997). As a result of these studies, a picture has emerged for how rats detect the location of an object in head-centered co-ordinates using their whiskers: As rats whisk rhythmically back and forth in space and make contact with objects, distinct sets of receptors encode phase of whisking and the contact event. These two signals are propagated via parallel pathways (lemniscal and para-

lemniscal pathways; Szwed, et al., 2003; Yu, et al., 2006) to S1. These two signals are combined in phase and contact sensitive neurons in S1 which have strongest responses when contact occurs at the preferred phase of the neuron. (Curtis and Kleinfeld, submitted), resulting in a computation of object location.

Very little, though, is known about fundamental response properties or algorithms during object recognition tasks (the "what" question), like texture and shape of objects. The representation of surface roughness (texture) is currently a topic of intense interest. Rats can discriminate between fine differences in surface roughness, with an acuity that rivals that of the human fingertip (Carvell and Simons, 1990). There are two current hypotheses on how rats encode and discriminate surface roughness (Figure 2; Kleinfeld, et al., 2006; Mehta and Kleinfeld, 2004). The first hypothesis stems from the observation that whiskers show a gradation in their intrinsic resonance frequencies from the back of the whisker pad to the front due a gradation of whisker lengths (increase in resonance frequency due to decrease in length; Neimark, et al., 2003, Andermann, et al., 2004). According to this hypothesis, as the vibrissae sweep along a textured surface, the vibrissa with a resonance frequency which is most well-matched with the texture-induced input frequency will transmit the greatest vibration amplitude to the follicle. This leads to a spatial code for texture, with the increase in firing rate at a specific position within the map of vibrissa position in S1 cortex indicating the predominant frequency of whisker vibration and, consequently, the identity of the texture.

The second hypothesis is that whisker contact with a surface is dominated by damping. This leads to suppression of resonance vibrations, while vibrations that reflect the topology of the surface dominate the stimulus-induced motion of the vibrissa (Arabzadeh, et al., 2005). Thus, the spatial modulation of the surface is reflected in whisker kinetics, which is faithfully reproduced by the temporal pattern of spiking in the corresponding cortical column. This hypothesis relies on

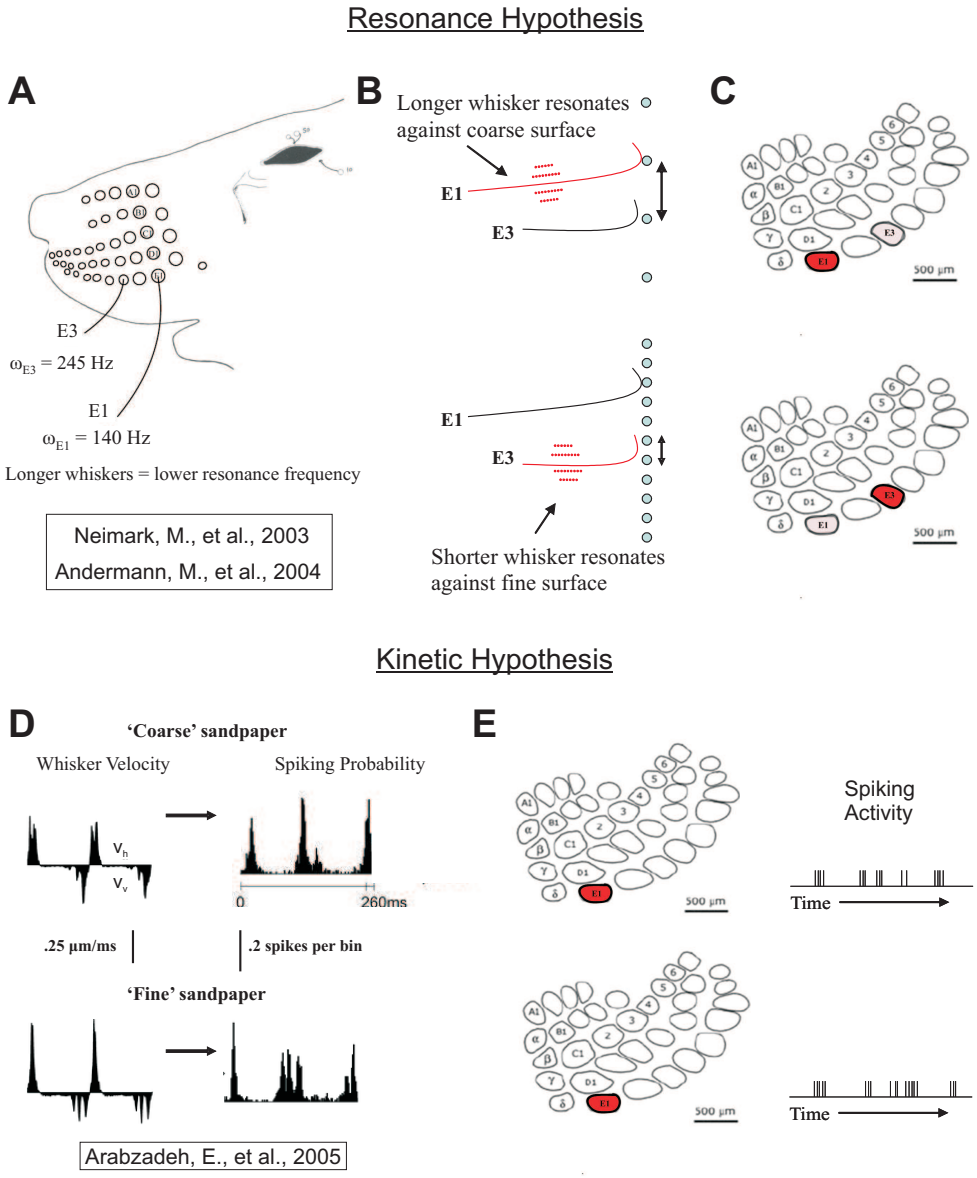

I.2 **The resonance and kinetic hypotheses for texture discrimination in the rat whisker system.** (A) Resonance frequencies of whiskers increase as whisker length decreases from the back of the whisker pad to the front. (B) Schematic illustrating selective activation of whisker resonance vibrations by textures of varying roughness. (C) Texture roughness is encoded by the *spatial* distribution of activity in S1 in the resonance hypothesis. (D) During artificial whisking on textures of varying roughness, whisker motion shows distinct kinetic patterns. Spiking activity in S1 faithfully represents passively applied whisker stimulation with varying kinetics. (E) Texture roughness is encoded by the *temporal* pattern of activity in S1 in the kinetic hypothesis.

the proposition that temporal precision of spiking in S1 reflects whisker movements on the surface. Also, this is a temporal, rather than a spatial code, and predicts that rats do not need more than one whisker to perform texture discrimination.

These hypotheses are yet to be tested in awake, behaving animals. In support of the resonance hypothesis, during passive deflections of whiskers at different frequencies in anesthetized animals, the resonance frequency evokes the highest amplitude whisker oscillations, and hence the highest firing rate in trigeminal and S1 neurons (Andermann, et al., 2004). In support of the kinetic hypothesis, during artificial whisking on textures in anesthetized animals, whiskers have a distinct kinetic profile (velocity transients) on different textures, which is faithfully represented in spiking in the trigeminal ganglion and in single S1 neurons across many repeated trials (Arabzadeh, et al., 2005). Additionally, rats can perform texture discrimination with single whiskers (Carvell and Simons, 1990), albeit with reduced performance accuracy. Conclusive proof for either of the hypothesis is currently lacking.

Determining the actual neural coding scheme for any surface property, including roughness, requires the measurement of the two transformations occurring in an active, behaving animal (Figure 3): a) Physical transformation - the prominent features of surface-driven whisker kinetics. b) Neural transformation - the features of whisker motion on surfaces that are encoded by neural responses. Thus, understanding surface coding requires the resolution of what elementary whisker motion elements are encoded in neural responses during active surface palpation. Two recent studies which measured the physical transformation during in awake, behaving animals showed that whisker motion is dominated by transient slip-stick-ring events driven by friction, and that amplitude of these events may underlie a code for surface roughness (Ritt et al., 2008; Wolfe, et al., submitted). These results suggest that slip-stick-ring events may be one of the primary features

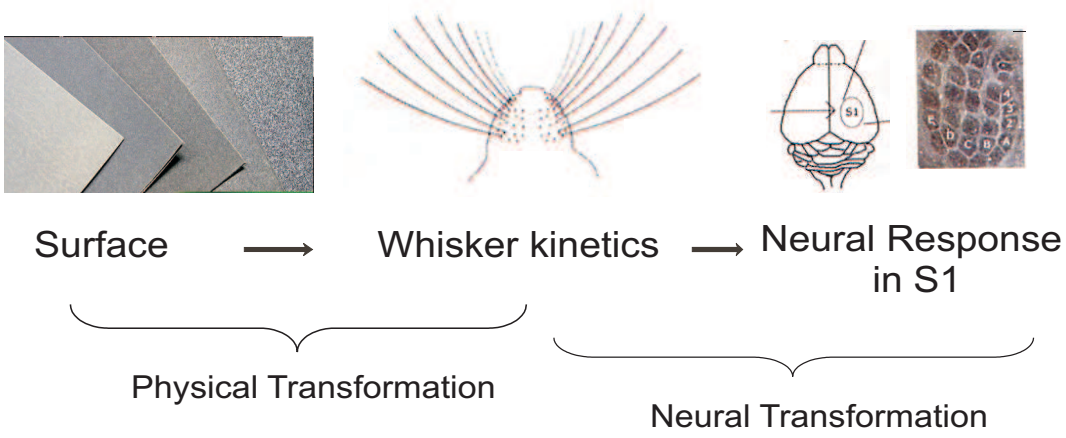

I.3 **Transformation from object properties to neural responses.** Schematic illustrating the two transformations that need to be measured in the awake, active animal. Surface properties are transduced into whisker kinetics during active palpation, which are represented in neural activity in S1.

of surface-driven whisker kinetics. Simultaneous measurement of both the transformations will allow us to identify the fundamental features of whisker motion on surfaces that are encoded by S1 neurons. Understanding this key element will also answer the outstanding questions in literature. Are slip-stick events represented in S1? Is resonance motion excited and encoded at all in the behaving animal? Are whisker kinetics faithfully represented by single S1 neurons? What underlies the increase in firing rate that has been observed in multiunit S1 activity during whisking on rough surfaces (von Heimandahl, et al., 2008). The ultimate goal of such an experiment will be to describe the nature of sensory representation in S1 in awake, behaving animals.

Neural Representation of Surface Properties in S1 in Awake-Behaving Rats

Chapter 3 of this thesis describes experiments and analysis to determine the fundamental response properties of S1 neurons and how natural inputs are represented in S1 during active surface whisking. A recent study described an op-

tical technique to measure high-resolution whisker motion in one-dimension (Wolfe, et al., submitted). We developed a technique to measure the spiking activity of multiple single neurons in a barrel column using tetrodes implanted in a chronic micro-drive. With these two techniques, we simultaneously measured whisker motion and spiking responses of neurons in S1 cortex in awake, behaving rats trained to whisk across textured surfaces.

Using this approach, we show that transient slip-stick-ring events are fundamental whisking features encoded by S1 neurons with precisely timed spikes, and slip-stick responses drive increase in firing rates in majority of the neurons during surface whisking. The amplitude and direction of these events is encoded in the spiking probability of S1 neurons. Thus, the temporal structure and amplitude of slip-stick events is encoded in S1. The damped resonance oscillations following slip-stick events ("ringing") have much weaker responses and serve primarily to amplify the responses to slip-sticks. Hence, whisker resonance is unlikely to code for surface features.

Instead, our results suggest that during continuous whisking on surfaces, frictional interaction drives sequences of slip-stick events in whisker motion marked by high-velocity and high-acceleration transients. These transient motion events of the principal whisker are encoded by spiking of neurons in the corresponding S1 column with high-precision. In addition, responses are sparse, resulting in a sparse probabilistic population code for slip-stick events. Slip-stick events cannot be identified by spiking in a single neuron; rather, they drive a transient increase in synchronous spiking in a fraction of neurons in S1, which is detectable in simultaneously recorded neurons. Using a simulation of the experimental data, we show that slips can be efficiently decoded by synchronous spiking activity on a $\sim$20 ms time scale across small ($\sim$100 neuron) populations within a single S1 cortical column. As a result, it is the synchronous population activity in S1 that encodes

whisker kinetics on surfaces.

These results show that surface properties are represented by a population temporal code in S1. They also add to a growing body of evidence that perception and behavior can be guided by small number of neurons in S1, and suggest that the key element of a sensory code in such sparse representations is precise timing of spikes and synchrony in the population.

I.A References

Andermann ML, Ritt J, Neimark MA, Moore CI (2004). Neural correlates of vibrissa resonance; band-pass and somatotopic representation of high-frequency stimuli. Neuron. 42: 451-63.

Anjum F, Turni H, Mulder PG, van der Burg J, Brecht M (2006). Tactile guidance of prey capture in Etruscan shrews. PNAS USA. 103: 16544-16549.

Arabzadeh E, Zorzin E, Diamond ME (2005). Neuronal encoding of texture in the whisker sensory pathway. PLoS Biol. 3: e17.

Brecht M, Preilowski B, Merzenich MM (1997). Functional architecture of the mystacial vibrissae. Science. 84: 81-97.

Brecht, M (2007). Barrel cortex and whisker-mediated behaviors. Curr Opin Neurobiol 17: 408-416.

Brecht M, Sakmann B (2002) Whisker maps of neuronal subclasses of the rat ventral posterior medial thalamus, identified by whole-cell voltage recording and morphological reconstruction. J Physiol 538: 495-515.

Brumberg JC, Khatri V, Pinto DJ, Simons DJ (2003). Cortical columnar processing in the rat whisker-to-barrel system. J Neurophysiol 82: 1808-1817.

Bruno RM, Simons DJ (2002). Feedforward mechanisms of excitatory and inhibitory cortical receptive fields. J Neurosci 22: 10966-10975.

Bruno RM, Khatri V, Land PW, Simons DJ (2003). Thalamocortical angular tuning domains within individual barrels of rat somatosensory cortex. J Neurosci 23: 9565-9574.

Carvell GE, Simons, DJ (1990). Biometric analyses of vibrissal tactile discrimination in the rat. J Neurosci 56: 2638-2648.

Castro-Alamancos, M A (2004). Absence of rapid sensory adaptation in neocortex during information processing states. Neuron 41: 455-464.

Celikel T, Szostak VA, Feldman DE (2004). Modulation of spike timing by sensory deprivation during induction of cortical map plasticity.

Curtis J, Kleinfeld D. submitted.

Fee M, Mitra PP, Kleinfeld D (1997). Central versus peripheral determinants of patterned spike activity in rat vibrissa cortex during whisking. J Neurophysiol 78: 1144-9.

Feldman DE, Brecht M (2005). Map plasticity in somatosensory cortex. Science. 310: 810-815.

Ferezou I, Bolea S, Petersen, CC (2006). Visualizing the cortical representation of whisker touch: voltage-sensitive dye imaging in freely moving mice. Neuron 50: 617-629.

Fritz JB, Elhilali M, David SV, Shamma SA (2007). Adaptive changes in cortical receptive fields induced by attention to complex sounds. J Neurophysiol 98: 2337-2346.

Guic-Robles E, Valdivieso C, Guajardo G (1989). Biometric analyses of vibrissal tactile discrimination in the rat. J Neurosci 56: 2638-2648.

Hutson KA, Masterton, RB (1986). The sensory contribution of a single vibrissa's cortical barrel. J Neurophysiol 56: 1196-1223.

Jones LM, Depireux DA, Simons DJ, Keller A (2004). Robust temporal coding in the trigeminal system. Science 304: 1986-9.

Kleinfeld D, Ahissar M, Diamond, ME (2006). Active sensation: insights from the rodent vibrissa sensorimotor system. Curr Opin Neurobiol 17: 408-416.

Knutsen PM, Pietr M, Ahissar E (2006). Haptic object localization in the vibrissal system: behavior and performance. J Neurosci 26: 8451-8464.

Krupa DJ, Wiest MC, Shuler MG, Laubach M, Nicolelis MA (2006). Visualizing the cortical representation of whisker touch: voltage-sensitive dye imaging in freely moving mice. Neuron 50: 617-629.

Mehta SB, Kleinfeld D (2004). Frisking the whiskers: patterned sensory input in the rat vibrissa system. Neuron 141: 181-184.

Mehta SB, Whitmer D, Figueroa, Williams BA, Kleinfeld D (2004). Active spatial perception in the vibrissa scanning sensorimotor system. PLoS Biol. 5: e15.

Minnery BS, Bruno RM, Simons DJ (2003). Response transformation and receptive-field synthesis in the lemniscal trigeminothalamic circuit. J Neurophysiol 90: 1556-1570.

Neimark MA, Andermann ML, Hopfield JJ, Moore CI (2004). Vibrissa resonance as a transduction mechanism for tactile encoding. J Neurosci 23: 6499-509.

Panzeri S, Petersen RS, Schultz SR, Lebedev M, Diamond ME (2001). The role of spike timing in the coding of stimulus location in rat somatosensory cortex. Neuron 29: 769-77.

Petersen, CC (2007). The functional organization of the barrel cortex. Neuron 56: 339-355.

Pierret T, Lavallee P, Deschenes M (2000). Parallel streams for the relay of vibrissal information through thalamic barreloids. J Neurosci 20: 7455-7462

Pinto DJ, Brumberg JC, Simons DJ (2003). Circuit dynamics and coding strategies in rodent somatosensory cortex. J Neurophysiol 83: 1158-1166.

Rice FL, Mance A, Munger BL(1986). A comparative light microscopic analysis of the sensory innervation of the mystacial pad. I. The common fur between the vibrissae. J Comp Neurol 252: 154-174.

Ritt JT, Andermann ML, Moore CI (2008). Embodied information processing: vibrissa mechanics and texture features shape micromotions in actively sensing rats. Neuron 57: 599-613.

Simons DJ, Carvell GE (1989). Thalamocortical response transformation in the rat vibrissa/barrel system. J Neurophysiol 1989 61: 311-30.

Szwed M, Bagdasarian K, Ahissar E (2003). Encoding of vibrissal active touch. Neuron. 40:621-30.

Temereanca S, Simons DJ (2003). Local field potentials and the encoding of whisker deflections by population firing synchrony in thalamic barreloids. J Neurophysiol 2003 89: 2137-45.

Veinante P, Deschenes M (1999). Single- and multi-whisker channels in the ascending projections from the principal trigeminal nucleus in the rat. J Neurosci 19: 5085-95.

von Heimendahl M, Itskov PM, Arabzadeh E, Diamond ME (2007). Neuronal activity in rat barrel cortex underlying texture discrimination. PLoS Biol 5: e305.

Wolfe JH, Hill D, Kleinfled D, Pahlavan S, Feldman DE (submitted). Encoding of texture by slip-stick events versus differential resonance in the rat whisker system.

Woolsey TA, Van der Loos H (1970). The structural organization of layer IV in the somatosensory region (SI) of mouse cerebral cortex. The description of a cortical field composed of discrete cytoarchitectonic units. Brain Res 17: 205-42.

Yu C, Derdikman D, Haidarlu S, Ahissar E (2006). Parallel thalamic pathways for whisking and touch signals in the rat. PLoS Biol 4: e124.

II

Somatosensory Integration Controlled by Dynamic Thalamocortical Feed-Forward Inhibition

II.A Summary

The temporal features of tactile stimuli are faithfully represented by the activity of neurons in the somatosensory cortex. However, the cellular mechanisms that enable cortical neurons to report accurate temporal information are not known. Here, we show that in the rodent barrel cortex, the temporal window for integration of thalamic inputs is under the control of thalamocortical feed-forward inhibition and can vary from 1 to 10 ms. A single thalamic fiber can trigger feed-forward inhibition and contacts both excitatory and inhibitory cortical neurons. The dynamics of feed-forward inhibition exceed those of each individual synapse in the circuit and are captured by a simple disynaptic model of the thalamocortical projection. The variations in the integration window produce changes in the temporal precision of cortical responses to whisker stimulation. Hence, feed-forward inhibitory circuits, classically known to sharpen spatial contrast of tactile inputs,

also increase the temporal resolution in the somatosensory cortex.

II.B Introduction

Timing is a basic attribute of sensory stimuli and needs to be faithfully represented by the nervous system to allow accurate stimulus identification and discrimination. Accordingly, temporal features of stimuli are accurately encoded and conveyed through the thalamus to the sensory cortex in several different sensory modalities (Arabzadeh et al., 2005; Buracas et al., 1998; DeWeese et al., 2003; Phillips et al., 1988; Reinagel and Reid, 2000; Wehr and Zador, 2003). For example, the timing of spikes in somatosensory cortex precisely reflects the temporal sequence of stimuli generated while touching an object (Phillips et al., 1988), and momentto- moment changes in spiking probability of barrel cortex neurons precisely reflect instantaneous variations in the velocity of a whisker sweeping over a surface (Arabzadeh et al., 2005).

Although this temporal precision is likely to be crucial for sensory representation, the cellular mechanisms that enable cortical neurons to follow the temporal structure of their thalamic inputs with such fidelity is currently unknown. In the cortex, individual thalamic afferent fibers impinging on principal neurons mediate excitatory postsynaptic potentials (EPSPs) that are small (Gil et al., 1999; Stratford et al., 1996) compared to the depolarization necessary to trigger a spike (Brecht and Sakmann, 2002). Hence, EPSPs resulting from several fibers have to summate to reach threshold for action potential generation. The time window within which EPSPs can effectively summate (Lloyd, 1946) is called the integration window (IW). The shorter the IW, the more coincident the activity of presynaptic fibers has to be to trigger a spike (Koch et al., 1996; Konig et al., 1996; Pouille and Scanziani, 2001). The IW, thus, dictates how precisely the activity of a neuron

can report the temporal structure of the activity of its inputs.

To establish the basis for spike timing precision in the initial steps of sensory processing in the somatosensory cortex, we determined the cellular mechanisms that control the IW of principal (excitatory) layer 4 neurons to thalamic inputs. Here, we demonstrate that the IW of layer 4 principal neurons has a broad dynamic range that can vary over an order of magnitude in an activitydependent manner. The duration of the IW is dynamically regulated by an efficient and temporally precise thalamocortical feed-forward inhibitory circuit. Feed-forward inhibitory circuits are well known to participate in the enhancement of spatial contrasts of somatosensory stimuli (Mountcastle, 1968; Mountcastle and Powell, 1959). Our data show that these circuits also enforce and modulate temporal resolution of tactile information.

II.C Results

Dynamic Control of Spike-Timing Precision in Barrel Cortex In Vivo

Spiking responses of regular spiking (RS) units, which represent presumed excitatory neurons in layer 4 of barrel cortex, were measured for low frequency (0.5 Hz) principal whisker (PW) deflections in anesthetized rats. Spikes were tightly time locked to the stimulus (jitter, 4.05 $\pm$ 0.28 ms; n = 105) (Figure 1A), despite occurring with relatively low probability (0.25 $\pm$ 0.02), consistent with previous observations of high temporal precision in barrel cortex (Arabzadeh et al., 2005; Petersen et al., 2001; Shimegi et al., 1999). Repetitive stimulation of the whisker at 10 Hz, similar to natural whisking frequency, however, led to a significant increase in jitter of layer 4 RS units (jitter; fourth stimulus, 5.79 $\pm$ 0.32 ms [$p < 0.01$]; sixth stimulus, 7.93 $\pm$ 0.43 ms [$p < 0.001$]; paired t test; n = 105) (Figures 1B and 1C), along with an adaptation (decrease in spike probability) and increased

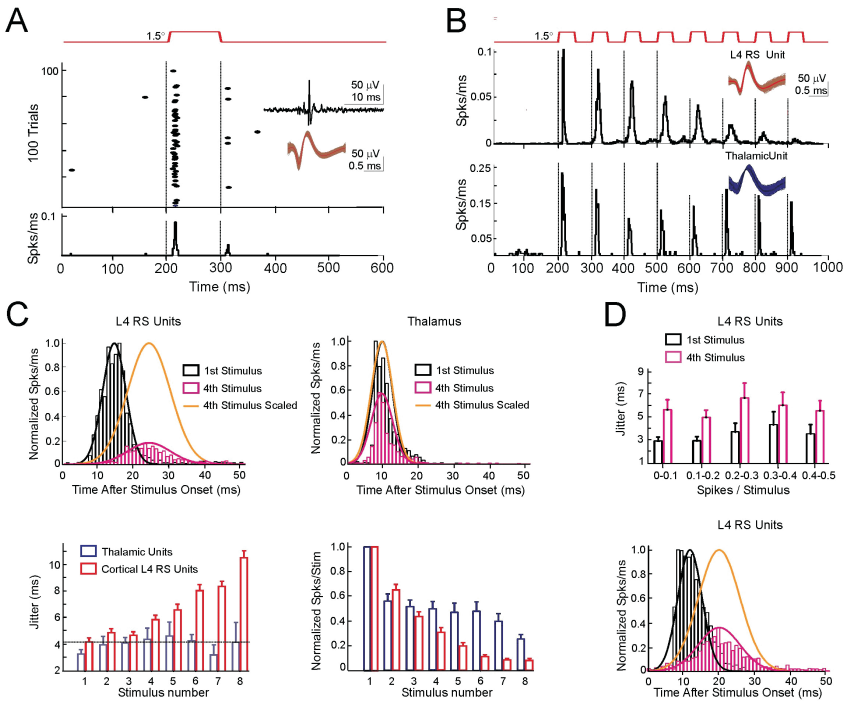

II.1 **Increased spike jitter of Layer 4 RS units in vivo by repetitive whisker stimulation.** ((A) Raster plot and peri-stimulus time histogram (PSTH) of the response of a single RS unit to PW deflection (1.5, 0.5 Hz, 100 trials). Insets: raw voltage recording and representative spike waveforms (red) and mean waveform (black) for the RS unit after spike sorting. (B) PSTHs of the responses of a layer 4 RS unit and a thalamic (VPM) unit to 10 Hz principal whisker (PW) deflection. Insets: single-unit spike waveforms. (C) Effects of 10 Hz stimulation across the population of layer 4 RS and thalamic units. Top: population PSTHs for onset responses to first and fourth stimuli in the 10 Hz train. Curves represent Gaussian fits. Bottom left: spike jitter increased with stimulus number in the train for RS units, but not for thalamic units. Bottom right: adaptation of whisker-evoked spike count for the population of RS (n = 105) and thalamic units (n = 22). RS units adapted significantly faster than thalamic units (RS, adaptation index (AI) = 0.19 ± 0.03; thalamus, AI = 0.47 ± 0.07; $p < 0.001$, t test). (D) Increase in jitter during trains is not due to decreased spike count. Top: jitter for RS units grouped by whisker-evoked spike count to the first stimulus. Bottom: population PSTHs for first and fourth stimuli for RS units tested with a longer recovery time between each train (10 s, n = 22) to produce less adaptation.

latency. To determine whether the increase in spike jitter reflects dynamic changes in the thalamocortical circuit, rather than in the periphery or the brainstem, we recorded from thalamic units in the VPM nucleus, which provide input to layer 4. VPM units showed virtually no increase in jitter during 10 Hz principal whisker stimulation, indicating that the temporal precision of cortical spiking responses is dynamically regulated downstream of the thalamus. Because 10 Hz whisker stimulation reduced whisker-evoked spikes for RS units (Chung et al., 2002; Khatri et al., 2004) (Figures 1B and 1C), the increased jitter could merely reflect weaker excitatory input to RS units or increased contamination of weak whisker-evoked responses by spontaneous spikes. To address this possibility, we tested whether spike jitter was correlated with spike probability across RS units. No correlation existed ($r = 0.04$) (Figure 1D). In addition, an identical increase in jitter occurred when long recovery times were used between 10 Hz trains, a protocol that leads to less adaptation and more spikes (Figure 1D). Thus, the increase in spike jitter during trains was not due to reduced excitation of RS neurons or the small number of whisker-evoked spikes.

These data show that the temporal precision of cortical responses to somatosensory stimuli is dynamically regulated by a circuit downstream of the thalamus. To establish what controls this dynamic range, we determined the integration window (IW) of cortical units to thalamic inputs in vitro.

Dynamic Integration Window in Cortical RS Neurons

To determine the IW of cortical neurons to thalamic inputs, we recorded from layer 4 RS neurons in thalamocortical slices and stimulated their thalamic afferents with an extracellular electrode placed in the ventrobasal complex (VB; see Experimental Procedures). Thalamic stimulation evoked an EPSP/IPSP sequence, consistent with previous reports (Agmon and Connors, 1991; Gil and Amitai, 1996;

Porter et al., 2001). Artificial excitatory postsynaptic potentials (aEPSPs) were evoked in RS neurons (with either current or dynamic clamp; see Experimental Procedures) at different intervals after thalamic stimulation.

RS neurons exhibited a very narrow IW to thalamic inputs. To effectively summate (i.e., to depolarize the membrane more than the peak-positive value of the thalamic response), we had to evoke aEPSPs withinw1ms (range, <1 to 3 ms; n = 6) after the onset of the thalamic EPSP (Figures 2A2C). An IW of 1 ms is extremely narrow, particularly when compared with the membrane time constant (17 ± 1 ms; n = 9). This result suggests that RS neurons operate as coincidence detectors.

The IW, however, was broadened by a factor of ten after repetitive stimulation. Repetitive thalamic stimulation at 10 Hz led to a pronounced and reversible increase in the IW by about one order of magnitude (to w10 ms after four to five stimuli; range 3 to >25 ms; n = 6) (Figure 2C). This broadening of the IW was caused by an increase in the half width of thalamically evoked postsynaptic potentials (PSPs; from 1 ± 0.3 ms after the first stimulus to 20 ± 5 and 18 ± 5ms after the fourth and fifth, respectively; n = 8) (Figure 2D) and by a reduction in the shunt (Coombs et al., 1955) of aEPSPs evoked shortly after the onset of thalamic EPSPs (first stimulus, 17% ± 3% reduction of aEPSP amplitude; fifth stimulus, 4% ± 3% reduction) (Figure 2). Both effects the increase in half width of the thalamic PSP and the decrease in the shuntcould be explained if repetitive stimulation reduced synaptic inhibition.

We asked whether repetitive stimulation of VB would affect the amplitude of thalamocortical feed-forward inhibition. RS neurons were voltage clamped at 260 mV, i.e., between the reversal potentials for excitatory and inhibitory postsynaptic currents. VB stimulation elicited an EPSC followed with a delay of 1.2 ± 0.1 ms (n = 11) by an IPSC (Figure 3A). The brief delay between EPSC and

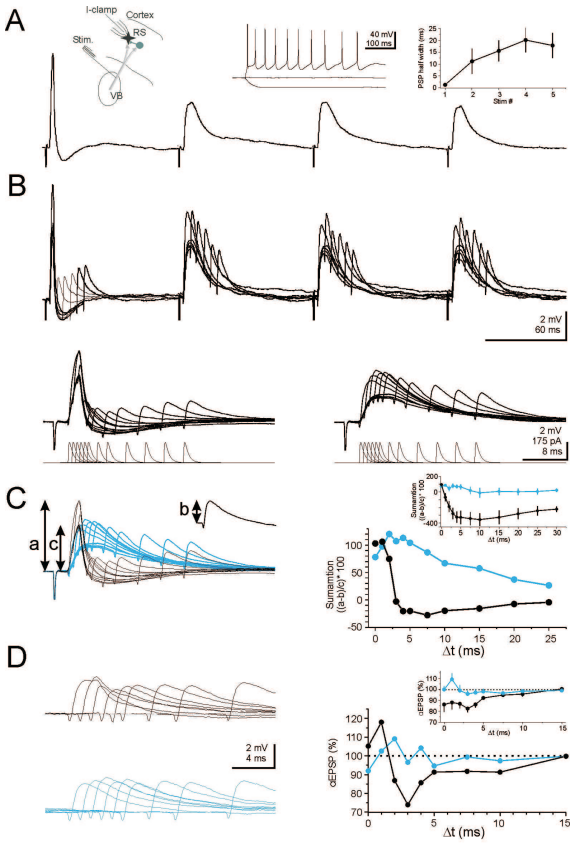

II.2 **Shift in the integration window of layer 4 regular spiking neurons.** ((A) Voltage response of a layer 4 RS neuron to four stimuli delivered at 10 Hz to the thalamus (Vm = 70 mV). Insets: Left: Schematic of the recording configuration Center: Voltage response of the neuron to square current pulses (-100; 0; +550 pA). Right: The half width of the postsynaptic potential is plotted against stimulus number (n = 7-8). (B) Upper panel: Six superimposed sweeps with artificial EPSPs (aEPSPs) triggered at different intervals after thalamic stimulation. Lower panel: Enhanced time scale for the first (left) and last (right) stimulus. (C) Left panel: The response of the neuron to the first (black) and last (blue) thalamic stimuli (same as in B) are superimposed to illustrate the different integration window. Right panel: The summation of the thalamic and aEPSPs for the first (black) and last (blue) stimuli plotted against the interval (t) between the onset of the thalamic and artificial EPSPs. (D) Left panel: aEPSPs evoked at different intervals after thalamic stimulation were"isolated" by subtracting the thalamic response. First stimulus: black traces; last stimulus: blue traces. Right panel: The amplitude of the aEPSP is plotted against the interval (t) between the onset of the thalamic and artificial EPSPs for the first (black) and last (blue) stimuli.

IPSC indicates that IPSCs were triggered in a feed-forward, disynaptic manner, i.e., by thalamic excitation of cortical GABAergic interneurons rather than by a feedback recruitment of interneurons via cortical RS neurons. The EPSC-IPSC sequence could be elicited even at very low stimulation intensities and the ratio between the peak EPSC and IPSC conductances was stable over a relatively wide range of stimulation intensities (Figure 3D). Repetitive 10 Hz thalamic stimulation, however, altered this balance through a striking decrease in the amplitude of feed-forward IPSCs. Although after five stimuli, EPSC amplitude decreased by 51% ± 4% (n = 7), feed-forward IPSCs decreased by 89% ± 3% (n = 8) (Figures 3A and 3B). Repetitive stimulation, therefore, increased the ratio between excitation and inhibition in RS neurons. Repetitive stimulation, moreover, progressively increased the delay between the EPSC and IPSC to 2.1 ± 0.4 ms (n = 5) after the fifth stimulus.

These data show that in the barrel cortex, thalamocortical feed-forward inhibition operates over a very broad dynamic range, allowing RS neurons to shift from coincidence detection to integration. We next determined the cellular basis of this dynamic range.

Mechanism Underlying the Dynamics of Thalamocortical Feed-Forward Inhibition

The activity-dependent reduction in the amplitude of thalamocortical feed-forward inhibition and the resulting increase in IW could be due to the depression of two distinct synapses: the glutamatergic synapse from thalamus to interneurons, or the GABAergic synapse from interneurons onto RS neurons. Depression of the second synapse would directly affect the amplitude of feed-forward inhibition; depression of the first synapse would reduce the fraction of interneurons that are excited above threshold for action potential generation and thus

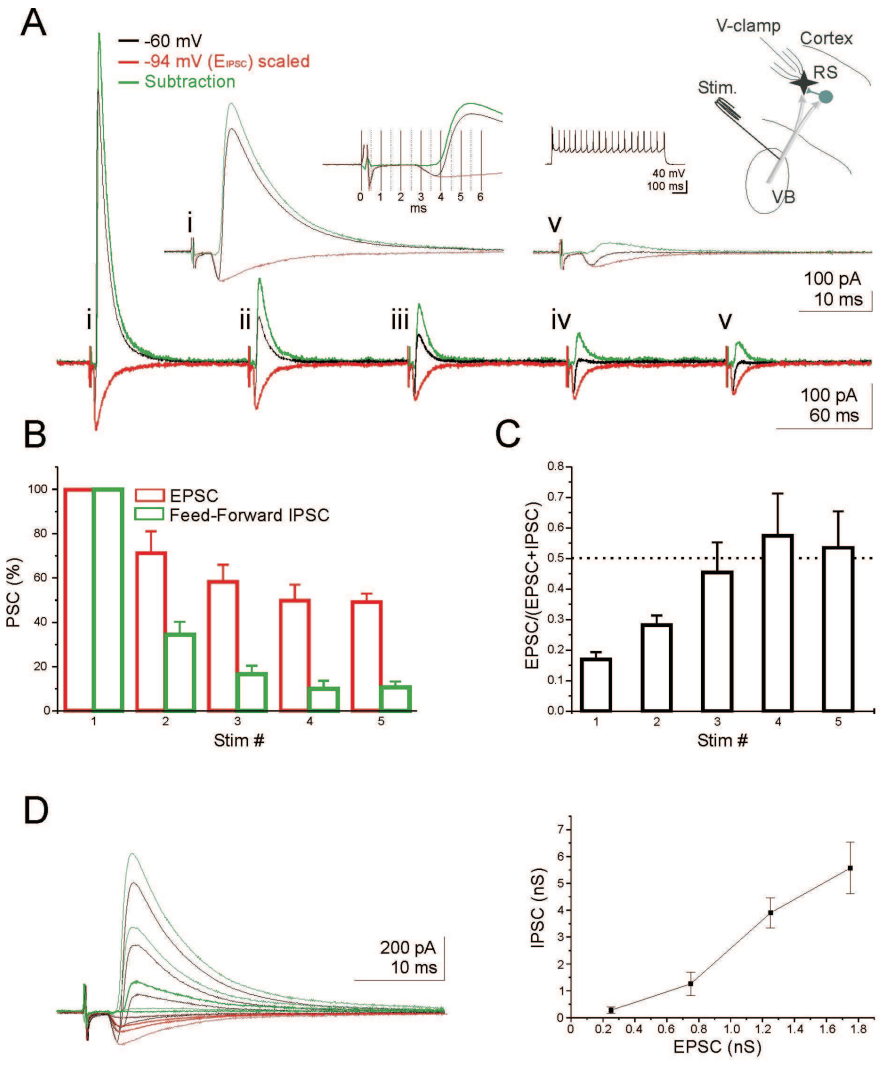

II.3 **Broad dynamic range of thalamocortical feed-forward inhibition.** (A) Response to 10 Hz thalamic stimulation of a layer 4 RS neuron voltage clamped at -60 mV (black trace) and at the IPSC reversal potential (red trace; the first EPSC on the red trace is scaled to the first EPSC on the black trace). The inset shows the responses to the first and last thalamic stimuli on an expanded time scale. (B) Summary graph of the EPSC and IPSC amplitude plotted against stimulus number (n = 8 for IPSC and 7 for EPSC). (C) Change in the excitation-inhibition ratio (peak conductances) plotted against stimulus number (n = 7). EPSC-IPSC sequences recorded at 5 different stimulation intensities (left, same cell as above) and summary graphs (right) where the peak conductance of the IPSC is plotted against the conductance of the EPSC (n = 5-6; bins: 0-0.249 nS; 0.24-0.749 nS; 0.75-1.249 nS; 1.25-1.75 nS).

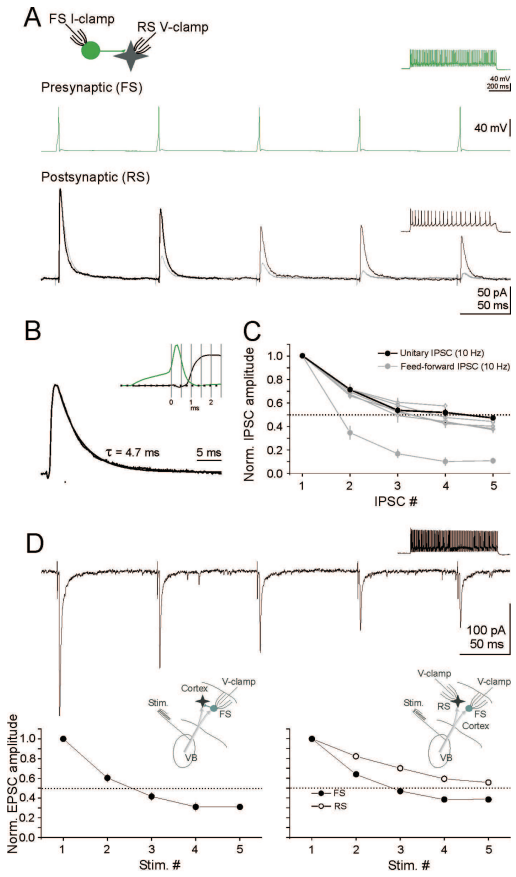

II.4 **Dynamics of the input and the output of cortical FS neurons.** (A) Paired recording between a presynaptic FS (green) and a postsynaptic RS (black) neuron. Brief current pulses were injected in the FS neurons to trigger series of five action potentials at 10 Hz. (B) Unitary IPSC from A on an expanded time scale. A mono-exponential fit is superimposed on the decay phase. The inset illustrates the delay between the presynaptic spike and the postsynaptic response. Summary graph: Black solid circles: unitary IPSCs evoked at 10 Hz (n = 6); Open symbols: Unitary IPSCs evoked at: 5 Hz (diamonds; n = 5), 20 Hz (down triangles; n = 5), 50 Hz (up triangles; n = 5), 100 Hz (squares; n = 5), 200 Hz (circles; n = 2). The reduction in amplitude of feed-forward IPSCs (gray solid circles; from figure 3B) evoked with thalamic stimulation at 10 Hz is included, for comparison. (C) Current trace: EPSCs recorded in an FS neuron in response to five thalamic stimuli delivered at 10 Hz. Summary graphs: Left: Normalized reduction in EPSC amplitude for 9 similar experiments plotted against stimulus number. Right Normalized reduction of EPSC amplitude for thalamic EPSC recorded simultaneously in FS (solid) and RS (open) neurons (n = 5).

participate in the generation of feed-forward inhibition.

We addressed both possible mechanisms by directly recording from GABAergic interneurons. Because layer 4 inhibitory fast spiking (FS) neurons are directly excited by thalamic inputs (Gibson et al., 1999; Keller and White, 1987; Staiger et al., 1996) and inhibit RS neurons (Beierlein et al., 2003; Tarczy-Hornoch et al., 1998), they are likely to represent the predominant source of thalamocortical feed-forward inhibition. We thus recorded from connected FS to RS neurons pairs.

FS neurons showed functional connections with approximately 50% of neighboring RS neurons. Unitary IPSCs triggered by individual FS neuron spikes occurred without failures, had an average peak conductance of 2.8 ± 0.85 nS (n = 6), and decayed with a time course of 6.2 ± 2.5 ms (Figure 4A). The decay of the unitary IPSCs was not significantly different than the decay of feed-forward inhibition (6.5 ± 0.62 ms; n = 10; p = 0.79) evoked by thalamic stimulation, consistent with the idea that layer 4 FS neurons are the predominant mediator of thalamocortical feed-forward IPSCs. The latency between the action potential (steepest point in its rising phase) triggered in the FS neurons and the onset of unitary IPSCs (5% of peak amplitude) recorded in the RS neuron averaged 0.6 ± 0.03 ms (n = 5). This indicates that the first half of the 1.2 ms delay between the EPSP and the feed-forward IPSC determined above is used for thalamic EPSPs to reach threshold for action potential generation in FS neurons, whereas the second half is taken by spike propagation and GABA release.

Depression at the synapse from FS to RS neurons was pronounced but not enough to account for the reduction in thalamocortical feed-forward inhibition with repetitive thalamic stimulation. Trains of spikes triggered at 10 Hz in FS cells resulted in unitary IPSCs that depressed to 47% ± 1% of their original amplitude after the fifth stimulus (Figures 4A and 4C). Even when triggered at higher frequencies, unitary IPSCs did not depress to less than ∼40% (Figure 4C). The

dynamics of the GABAergic synapses, therefore, cannot account for the observed ~90% reduction in thalamocortical feed-forward inhibition.

These results suggest that during repetitive thalamic stimulation, progressively fewer FS neurons participate in mediating feed-forward inhibition after each stimulus in the train. By comparing the depression of unitary IPSCs (uI_5/uI_1) with the decrease in thalamically evoked feed-forward inhibition (FFI_5/FFI_1), one can estimate the maximal fraction of GABAergic interneurons still participating in feed-forward inhibition by the fifth stimulus (N5/N1) to be only about 20% of those active at the beginning of the train ($FFI_5/FFI_1 = [uI_5/uI_1] \times [N_5/N_1]$).

We thus tested the possibility that excitation of FS neurons by thalamic afferents may depress during repetitive thalamic stimulation, thereby reducing the fraction of recruited interneurons. When elicited at 10 Hz, thalamic EPSCs recorded in FS neurons showed a marked depression (to 31% ± 3% of the original amplitude after five stimuli; n = 9) (Figure 4D) that was, in fact, significantly larger than the depression of thalamic EPSCs onto RS neurons (to 49% ± 4%; n = 7; see Figure 3; p = 0.0014). We confirmed this target cell specificity in thalamic EPSC depression by recording thalamic EPSCs simultaneously in FS and RS neurons. Again, thalamic EPSCs recorded in FS neurons depressed significantly more than those recorded in RS neurons (to 39% ± 2% versus 56% ± 3%; n = 5; p = 0.013) (Figure 4D).

These results indicate that the broad dynamic range of thalamocortical feed-forward inhibition is primarily achieved by varying the fraction of thalamically recruited FS neurons and, to a lesser extent, by the dynamics of the FS to RS synapse.

Thalamic Excitation of Cortical GABAergic Interneurons

For feed-forward inhibition to effectively control the IW of RS neurons,

it is expected that action potentials are readily triggered in FS neurons also in response to relatively weak thalamic stimuli.

Figure 3D shows that this is indeed the case as feedforward inhibition on RS neurons can be triggered even at low stimulation intensities, when the average peak conductance of thalamic EPSCs recorded in RS neurons is below 0.25 nS. This suggests that either activation of a limited number of thalamic fibers is sufficient to trigger a spike in FS neurons or FS neurons have a higher probability of being contacted by a thalamic fiber than RS neurons. We addressed both possibilities.

If the probabilities of a thalamic axon to form synaptic contacts with FS and RS neurons are similar, the ratio of the amplitude of unitary thalamic EPSCs (EPSCs evoked by stimulating a single thalamic fiber [Beierlein and Connors, 2002]) recorded in FS and RS neurons should be similar to the ratio of the amplitude of compound EPSCs (EPSCs evoked by stimulating several thalamic fibers). Minimal stimulation of the thalamus was used to isolate unitary thalamic EPSCs in FS and RS neurons. The amplitude of unitary thalamic EPSCs was defined as the amplitude of the successes measured over a stimulation range in which, starting from failures only, increasing stimulation intensity reduced failure rate without affecting the average amplitude of successes. Unitary thalamic EPSCs recorded in FS neurons had a peak amplitude that was 3.5 times larger than the one recorded in RS neurons (FS neurons, 200 $\pm$ 42 pA; n = 6; RS neurons, 57 $\pm$ 15 pA; p = 0.023; n = 4) (Figures 5A and 5B). EPSC recorded in FS neurons also had faster decay kinetics than EPSC in RS neurons (1.5 $\pm$ 0.3 ms versus 4.5 $\pm$ 0.4 ms; p = 3.35×10^{-5}) consistent with the different kinetics of AMPA receptors expressed in these neurons (Jonas et al., 1994). Strikingly, also the amplitude of compound EPSCs recorded simultaneously in FS and RS neurons was 3.5 $\pm$ 0.6 times larger in FS neurons (n = 6), indicating that thalamic fibers contact FS and RS neurons with similar probabilities (Figures 5C and 5D).

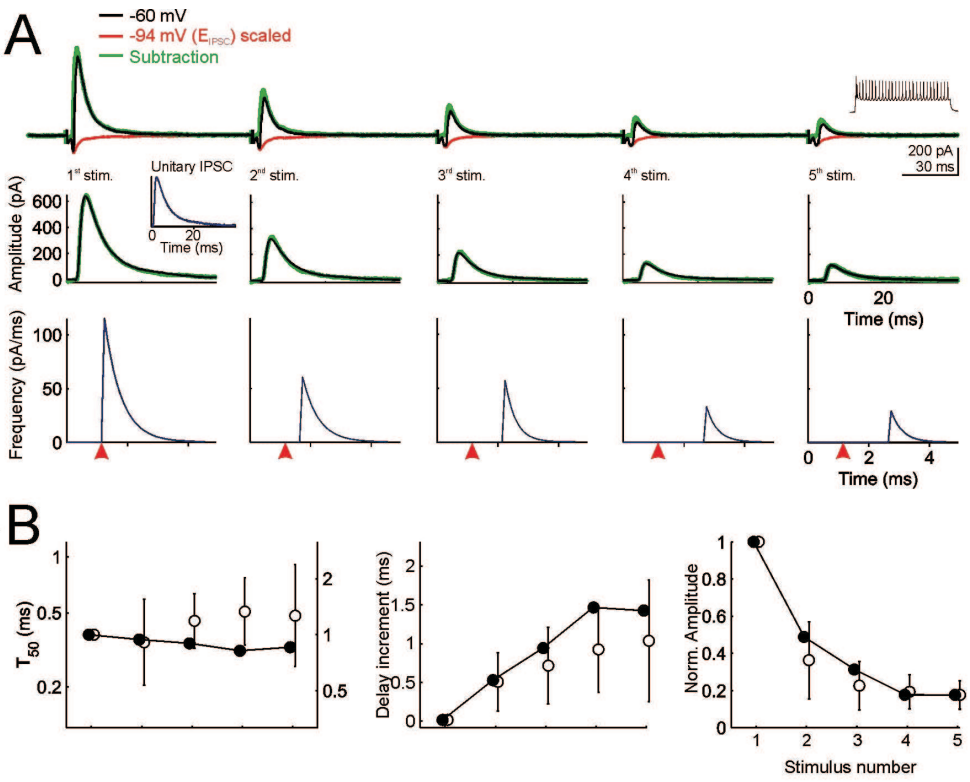

II.5 **Temporal precision is preserved in FS neurons during repetitive stimulation.** (A) Top row: Response to 10 Hz thalamic stimulation of a layer 4 RS neuron voltage clamped at -60 mV (black trace) and at the IPSC reversal potential (red trace; the first EPSC on the red trace is scaled to the first EPSC on the black trace). The feed-forward IPSC (green trace) was isolated by subtracting the red trace from the black trace. Middle and lower rows: Convolution of the "standard" unitary IPSC (inset, middle row) with the function $f(t) = (A/\tau * exp(-t/\tau)$ (blue traces, lower row) provided a good fit (black traces, middle row) to the isolated feed-forward IPSC (green trace, middle row). Note, in the lower panel, the progressively increasing delay of the onset of feed-forward inhibition after each stimulus. The delay in response to the first stimulus is marked by a red arrowhead. (B) Left panel: Time at which the integral over f(t) reaches 50% of its maximal value (T_{50}), plotted against stimulus number. The summary data (open symbols) are normalized by the T_{50} of the first stimulus (right ordinate). Note that T_{50} changes little after each stimulus, despite the increase in delay (middle panel) and the decrease in amplitude (right panel) of feed-forward inhibition.

The experiment shown in Figure 5A also demonstrates that an individual thalamic afferent can contact both FS and RS neurons. In this particular example,

not only were the minimal stimulation criteria satisfied for both neurons simultaneously, but failures and successes were absolutely correlated, indicating that they were contacted by the same fiber.

We then determined the minimal number of thalamic fibers necessary to trigger a spike in FS neurons. For this, we compared the amplitude distribution of unitary EPSCs with the average size of thalamic EPSCs on FS neurons when stimulating the thalamus at threshold to induce feed-forward inhibition in simultaneously recorded RS neurons. Clearly, the distribution of the amplitudes of unitary EPSCs (range, 51289 pA) (Figure 6) was similar to the distribution of the amplitudes of EPSC (average, 170 $\pm$ 64 pA; range 52400 pA; n = 5) (Figure 6) recorded in FS neurons when stimulating at threshold for eliciting feed-forward inhibition in RS neurons. A comparison between the lower and the higher values in the two distributions of EPSC amplitudes suggests that one to eight thalamic fibers are sufficient to trigger a spike in FS neurons. Thus, even a single thalamic fiber can evoke feed-forward inhibition.

These data show that despite the similar probabilities of thalamic neurons to contact FS and RS neurons, strong thalamic input on FS neuron ensures efficient feed-forward inhibition and an accordingly narrow IW even in response to very weak thalamic activity.

Temporal Precision of FS Neurons

Despite the reduced fraction and increased delay of FS neuron recruitment, FS neuron activity remained remarkably synchronous during repetitive thalamic stimulation (Figures 7A and 7B). To estimate the degree of synchrony of FS neurons recruited after each thalamic stimulus, we deconvolved the time course of feedforward inhibition recorded in RS neurons with the time course of a "standard" unitary IPSC (i.e., the averaged time course of unitary IPSCs recorded in

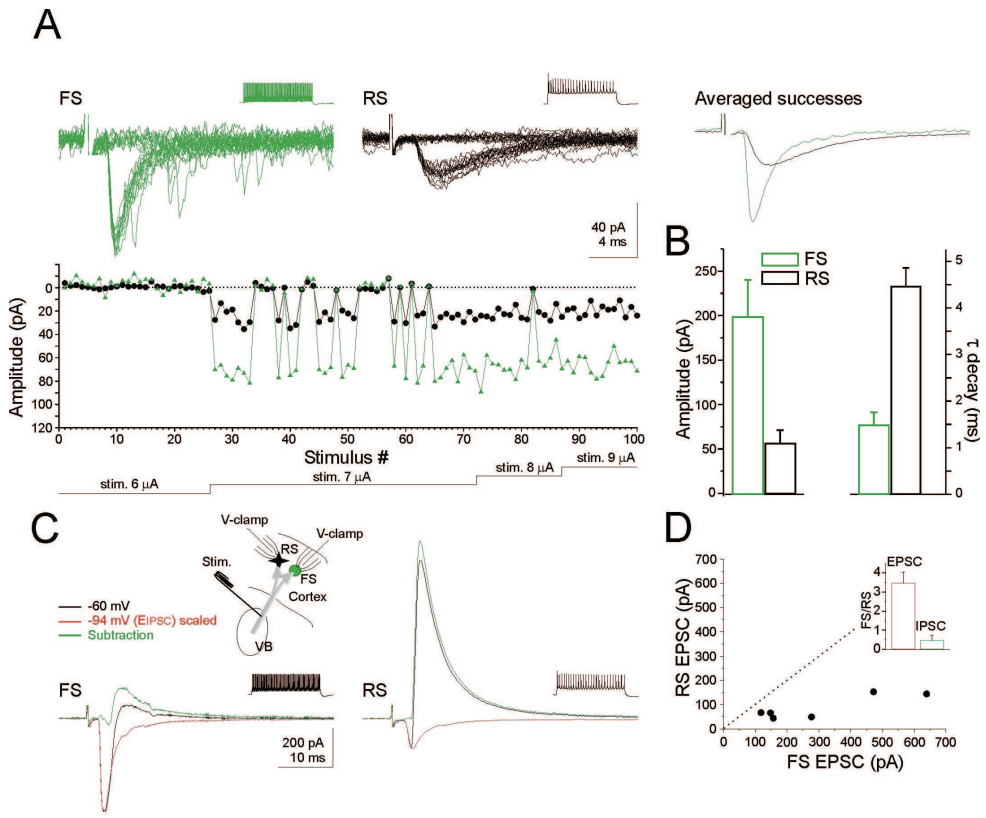

II.6 **Functional divergence of thalamic afferents onto FS and RS neurons.** (A) Simultaneous voltage clamp recording from an FS (green traces) and RS (black traces) neuron during minimal stimulation of the thalamus (23 superimposed individual sweeps each). Stimuli were delivered at 0.2 Hz. The amplitude of the EPSC is plotted against stimulus number. The intensity of stimulation is plotted below the graph. (B) The amplitude and decay kinetics of minimally evoked EPSCs recorded in FS (green; n = 6) and RS (black; n = 4) neurons. With the exception of the experiment illustrated in A, for the rest of the experiments minimal stimulation conditions were satisfied only for one neuron at the time (as in C). (C) Simultaneous recording from a FS and RS neuron in response to "non-minimal" thalamic stimulation. Both neurons were voltage clamped at -60 mV (black trace) and at the IPSP reversal potential (red trace; the EPSC on the red trace is scaled to the EPSC on the black trace). The feed-forward IPSC (green trace) was isolated by subtracting the red trace from the black trace. (D) The amplitude of the EPSC recorded in the RS neuron is plotted against the amplitude of the simultaneously recorded EPSC in FS neurons for six experiments. Inset: Ratio between responses in FS and RS neurons. Red column: EPSCs; green column IPSCs.

our six connected FS to RS pairs) (Figure 7A). This analysis indicates that 50%

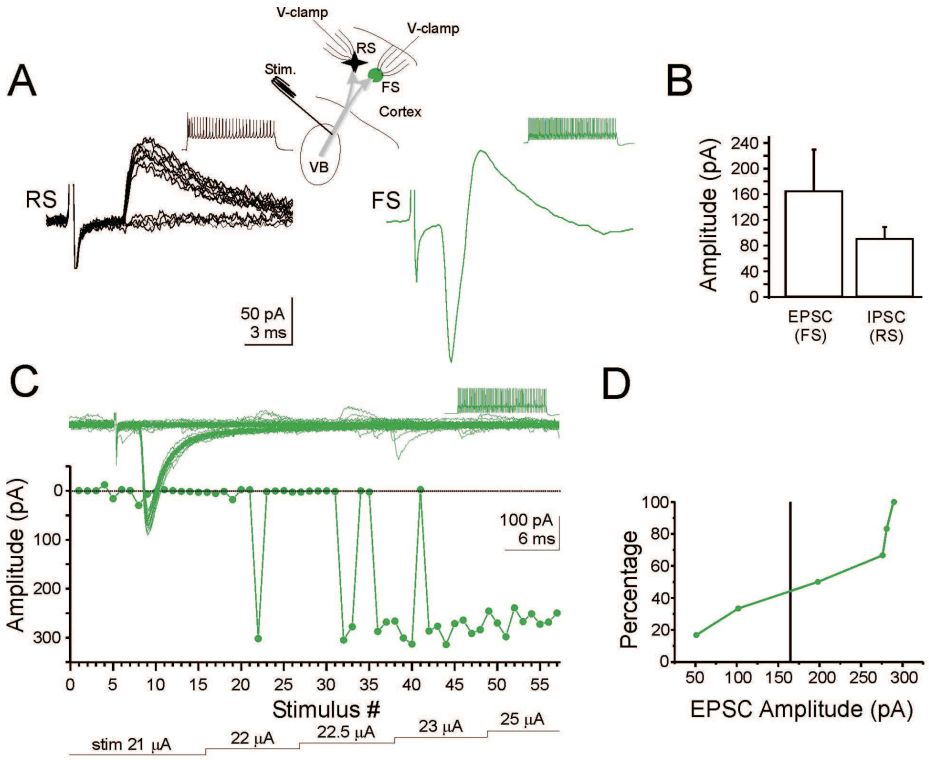

II.7 **Very few thalamic inputs are sufficient to trigger feed-forward inhibition .** (A) Simultaneous voltage clamp recording from a RS (black traces) and a FS (green traces) neuron while stimulating the thalamus at threshold for eliciting feed-forward inhibition in the RS neuron. Note that in this particular example feed-forward inhibition in the RS neuron occurred at stimulation intensities below what necessary to activate of a direct thalamic EPSC on the recorded neuron. (B) Summary graph illustrating the average amplitude of thalamic EPSCs recorded in FS neurons while stimulating the thalamus at threshold for triggering feed-forward inhibition in RS neurons (left column) and average amplitude of feed-forward IPSCs (successes only) simultaneously recorded in RS neuron (left column, n = 5). (C) Voltage clamp recording from a FS neuron during minimal stimulation of the thalamus (58 superimposed sweeps). Note the relatively large amplitude of the unitary EPSC. (D) Distribution of minimally evoked thalamic EPSCs recorded in FS neurons (green symbols, same data as in 4B) in relation to the average amplitude of thalamic EPSCs recorded in FS while stimulating the thalamus at threshold for triggering feed-forward inhibition in RS neurons (vertical line; from B).

of FS neurons spiked within a window of 0.22 ± 0.23 ms during the first response and within a window of 0.52 ± 0.41 ms during the fifth response of a train (n =

8). These results show that the degree of synchrony of FS neurons is only slightly affected by ongoing thalamic activity.

Spiking of FS Neurons In Vivo

The dynamic properties of the thalamocortical feedforward inhibitory circuit observed in vitro leads to two predictions in the intact animal. First, because of the strong depression of the thalamus to FS synapse, repetitive whisker stimulation will markedly reduce spike probabilities in FS units. Second, despite a reduction in spike probabilities, spike jitter should remain constant in FS units. We found this to be clearly the case. We recorded single RS and FS units in layer 4, identified by extracellular spike waveform (Bruno and Simons, 2002; Swadlow, 1989) (Figure 8A). FS units had broader receptive fields, consistent with previous reports (Bruno and Simons, 2002). By the fifth stimulus in a 10 Hz PW deflection train, spiking probabilities of FS units adapted to less than 15% of the initial probabilities. However, in striking contrast to RS units, the spike jitter did not significantly increase during the stimulus train (first stimulus, 4.07 $\pm$ 0.78; fifth stimulus, 4.55 $\pm$ 0.71; n = 34; $p > 0.05$) (Figure 8B). These results are in good agreement with the in vitro data reported above and strongly suggest that the temporal precision of cortical responses to whisker stimuli is dynamically regulated by a thalamocortical feed-forward inhibitory circuit.

A Simple Disynaptic Model for Thalamocortical Feed-Forward Inhibition

To test whether the cellular and synaptic properties determined above are sufficient to account for the dynamics of thalamocortical feed-forward inhibition, we devised a simple model of the circuit (Figure 9). The model includes an RS neuron and a pool of FS neurons and three types of synapse: from VB to FS, from

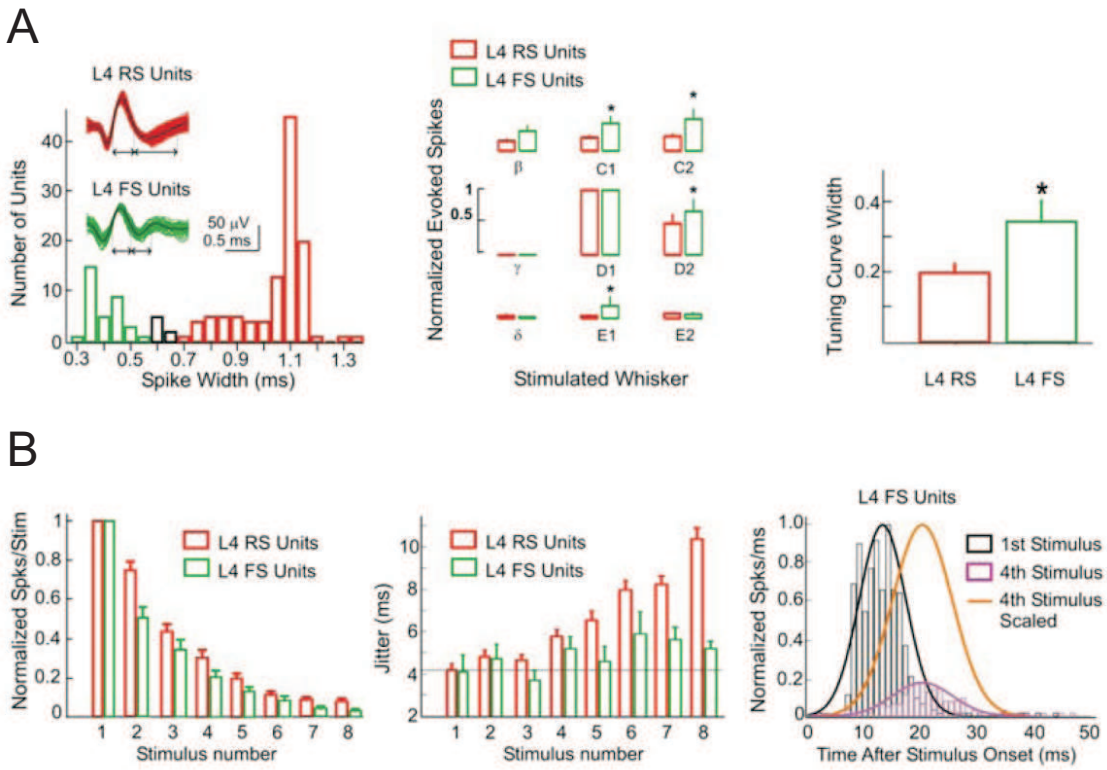

II.8 **Spiking of FS neurons in vivo.** (A) Identification of RS and FS units by total spike width (width of initial positive spike plus after hyperpolarization) in vivo. Left, histogram of total spike width across the population showing RS (red) and FS (green) units. Insets show examples of RS and FS unit waveforms. Center, mean whisker tuning curve for recording sites in D1 barrel. FS units had significantly broader tuning curves than RS units (asterisks, significant difference between FS and RS responses; $p < 0.05$; paired t-test). Right, tuning curve width (mean ratio of adjacent surround whisker response to PW response) for all RS ($n = 105$) and FS ($n = 34$) units. Summary graphs show mean ± SEM. (B) Response of RS and FS units to 10Hz whisker deflection. Left, spiking probability decreased for RS ($n = 105$) and FS ($n = 34$) units during the train. Both RS and FS units showed rapid adaptation (RS, AI = 0.19 *pm* 0.03; FS, AI = 0.13 ± 0.02, $p > 0.05$, t test). Middle, FS units did not show increased spike jitter during trains. Right, population PSTHS for first and fourth stimuli in train for all FS units. Note constant spike jitter despite adaptation and increased delay. Summary graphs show mean ± SEM.

FS to RS, and from VB to RS neurons. Model parameters were measured and fitted independently for each cell type and for each synapse type. All three synapse types exhibit depression to account for the experimental data (Figure 9A). We modeled

synaptic depression as a decrease decrease in resource (such as vesicles) available after each spike followed by recovery with an exponential time constant (Abbott et al., 1997; Tsodyks and Markram, 1997).

Because of the depression of the synapse from VB to FS neurons, after each stimulus, progressively fewer FS neurons reach threshold (Figure 9B). By the fifth stimulus, the fraction of FS neurons that reached threshold for action potential generation was down to about 20%. The reduced number of FS neurons spiking, combined with depression at synapses from FS to RS (Figure 8B), causes a pronounced decrease in feed-forward inhibition onto RSneurons (Figure 9C). Just as seen in the experimental observations (dots), the model (traces) predicts that by the end of the stimulus train feed-forward inhibition has decreased by about 90%. The effect of this decrease on the responses of the RS neuron is to substantially broaden the IW (Figure 9D). The components of this simple model are not only sufficient to explain the decrease in feed-forward inhibition (Figure 8C), but also necessary. Depression at the inhibitory synapse, on its own, is insufficient (Figure 9A, middle). The decrease in number of FS neurons that reach threshold, caused by the depression of the synapse onto FS neurons, is also insufficient on its own, especially to account for the pronounced reduction seen already at the second stimulus (Figure 8B). Only the combination of these effects achieves the observed decrease (Figure 9C).

This minimal model of the thalamocortical projection demonstrates how a disynaptic circuit accounts for a dynamic range of feed-forward inhibition that exceeds the dynamic range of each individual synapse in the circuit. Under the dynamic control of disynaptic IPSCs, RS neurons can act over a range of IWs, rapidly shifting from precise coincidence detectors to integrators.

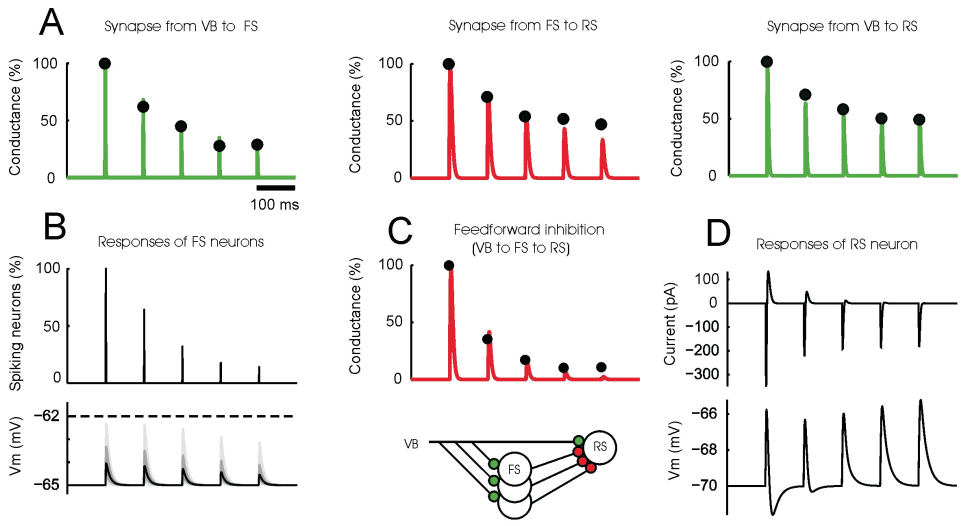

II.9 **A simple disynaptic model for thalamocortical feed-forward inhibition.** (A) Conductance time-course for the three synapses involved in the thalamocortical circuit (continuous traces) and experimental data (from figs. 3 and 4; filled symbols) plotted against time. (B) Upper panel: Spiking probability of FS neurons (normalized by the probability in response to the 1st stimulus) plotted against time. Lower panel: Distribution of membrane potentials in a simulated population of 100 FS neurons plotted against time. The dotted line indicates firing threshold. (C) Upper panel: Time-course of inhibitory conductances in RS neurons (feed-forward inhibition) resulting from the activity in the population of FS neurons. Lower panel: Schematic illustration of the modeled circuit. (D) Current (upper panel) and voltage (lower panel) time-course in model RS neurons in response to 10Hz thalamic activity. Note the progressive broadening of the half width of the postsynaptic potential.

II.D Discussion

Keeping Time

Somatosensory stimuli trigger precisely time-locked responses in cortical neurons (Arabzadeh et al., 2005; Phillips et al., 1988). Such temporal accuracy is essential for sensory representation. We have found that thalamocortical feed-forward inhibition generated by a simple disynaptic circuit governs this temporal precision. We show that this circuit can narrow the integration IW to ∼1 ms in

barrel cortex neurons and thus may account for the temporal precision of these neurons to whisker stimulation (Arabzadeh et al., 2005; Petersen et al., 2001; Shimegi et al., 1999). Moreover, we show that the temporal window within which cortical neurons integrate thalamic activity (IW) is not fixed but can increase over an order of magnitude depending on the strength of feed-forward inhibition. The detailed in vitro analysis of the circuit resulted in testable predictions about the dynamics of RS and FS units during repetitive whisker stimulation in vivo. These predictions were verified by in vivo measurements of whiskerevoked spikes, strongly suggesting that feed-forward inhibitory circuits control temporal integration of somatosensory stimuli in vivo. Future manipulation of GABAergic transmission in vivo will allow more direct quantification of the contribution of inhibitory synapses to the encoding and behavioral discrimination of temporal stimulus features.

Feed-forward inhibitory circuits are ubiquitous in the brain (Shepherd, 1998) and have been shown to control neuronal excitability in time (Berger and Luscher, 2003; Blitz and Regehr, 2005; Brunel et al., 2004; Mittmann et al., 2005; Pouille and Scanziani, 2001; Wehr and Zador, 2003) and space (Laaris et al., 2000; Lavallee and Deschenes, 2004; London et al., 1989; Mountcastle and Powell, 1959; Petersen et al., 2001). The presence of thalamocortical feed-forward inhibitory circuits in the somatosensory "barrel cortex" is well documented both anatomically (Keller and White, 1987; Staiger et al., 1996) and physiologically (Agmon and Connors, 1991; Agmon and ODowd, 1992; Gil and Amitai, 1996; Porter et al., 2001; Swadlow and Gusev, 2000; Wilent and Contreras, 2004; Zhu and Connors, 1999).

We show that the efficiency of feed-forward inhibition in reducing the IW of neurons in the barrel cortex results from the concurrent action of at least four factors: first, a powerful thalamic synapse onto GABAergic fast spiking (FS) interneurons, such that the activity of only one or a few inputs is sufficient to

trigger a spike; second, a fast "monosynaptic" delay (between the onset of the thalamic EPSC and the onset of the feed-forward IPSC) comprising 0.6 ms for thalamic EPSPs to reach spike threshold in FS neurons and additional 0.6 ms for the spike in FS neurons to propagate and release GABA on RS neurons; third, a high probability of connection between FS and RS neurons; and fourth, a large unitary IPSC conductance in RS neurons.

A caveat to the present findings is that our measure of the IW in RS neurons is based on the interaction between thalamically evoked EPSP-IPSP sequences and artificial EPSPs imposed with a somatic recording pipette. Thalamic afferents, however, impinge on the dendrites of RS neurons (Keller, 1995), whereas FS neurons preferentially (although not exclusively) project on the somatic/ perisomatic compartment (Kawaguchi and Kubota, 1997; Markram et al., 2004; Somogyi et al., 1998). The spatial separation between excitatory and inhibitory inputs is likely to result in less shunting of thalamic EPSPs by feed-forward inhibitory conductances as compared to what observed on artificial EPSPs, suggesting that the duration of the IW in RS neurons may have been underestimated. This potential underestimation must be small, however, because the reduction of the amplitude of the artificial EPSP attributed to the shunt was only 15%.

Our recordings indicate that thalamic EPSCs in FS neurons are three times larger than in RS neurons, and this holds true for both unitary (Beierlein and Connors, 2002) and compound EPSCs. Hence, the stronger thalamic excitation of inhibitory FS as compared to excitatory RS cortical neurons is not merely due to an increased connectivity of thalamic inputs onto FS neurons. We propose that the large thalamic EPSC recorded in FS neurons may account, at least in part, for the high responsiveness of FS neurons to whisker stimulation (Bruno and Simons, 2002; Swadlow, 1989) and to spontaneous, single-thalamic spikes (Swadlow and Gusev, 2000) observed in vivo. Several not mutually exclusive possibilities could account

for the difference in EPSC amplitude between FS and RS neurons, including a larger number of release sites per unitary input, a larger probability of release, a larger quantal amplitude, or a reduced membrane filtering of the postsynaptic EPSC. Elucidating the exact mechanism underlying this difference is the goal of future studies. The stronger depression of thalamic EPSCs onto FS neurons suggests that differences in release probability may account for at least part of the bias.

The faster decay kinetics of thalamic EPSCs on FS as compared to RS neurons is consistent with the kinetic differences observed for AMPA receptors obtained from these two types of neuron (Jonas et al., 1994) and, hence, is unlikely to be uniquely attributed to a difference in the membrane filtering of the signal. A large and fast EPSCis likely to significantly contribute to the temporally precise triggering of spikes in FS neurons (Fricker and Miles, 2000; Geiger et al., 1997; Jonas et al., 2004) and lead to the time-locked feed-forward IPSC.

Modulating the Integration Window

The dynamic range of the amplitude of thalamocortical feed-forward inhibition exceeds that of each individual synapse in the circuit and is responsible for the shift in the IW of RS neurons during repetitive thalamic stimulation. In principle, several properties of the circuit could contribute to the dynamic range, including the fraction of GABAergic interneurons recruited after each stimulus, the degree of synchrony of the recruited interneurons, the amount of GABA released on principal neurons, and their sensitivity to GABA. We show that spiking of FS neurons (in contrast to RS neurons) remains tightly time locked to each stimulus during the train, both in vivo and in vitro, suggesting that changes in synchrony do not contribute to the dynamics of feedforward inhibition. The amplitude of the unitary IPSC decreased during repetitive presynaptic activity, but the magnitude

of this depression is not sufficient to account for the full reduction in feed-forward inhibition. Rather, our data demonstrate that the broad dynamic range principally reflects the change in the fraction of GABAergic interneurons that are recruited by each thalamic stimulus. Our model shows that this change in fraction of recruited FS neurons can be well accounted for by the short-term dynamics of the thalamic input onto FS neurons. Although an activity-dependent reduction in the excitability of FS neurons could, in theory, also account for the observed reduction in the fraction of recruited FS neurons, two lines of evidence argue against this possibility. First, fast-spiking neurons show little spike adaptation to constant current injections and are, hence, expected to adapt even less to brief phasic excitation separated by 100 ms. Second, the probability of spiking of FS neurons in response to a given whisker stimulus in a train is identical regardless of the success of the previous stimulus in the train to trigger a spike (data not shown).

The depression of thalamic EPSCs onto FS neurons is significantly larger than on RS neurons. This difference could be due to a postsynaptic property, namely a difference in the amount of and recovery from desensitization of AMPA receptors on the two types of neurons or to a presynaptic property, like the dynamic of transmitter release. We favor the second possibility because desensitization of AMPA receptors expressed in FS neurons recovers faster than in RS neurons (Jonas et al., 1994). Our physiological demonstration that a single thalamic fiber can impinge on both FS and RS neurons is consistent with anatomical evidence (see Figure 6F in Staiger et al., [1996]) and indicates that release properties from the thalamus are target cell specific.

Acute slices and anesthetized animals have low spontaneous activity compared to behaving animals. Thus, we were able to measure feed-forward inhibition at synapses that have fully recovered from previous activity, thus promoting strong feed-forward inhibition and narrow IWs. Increasing stimulus frequency to natural

whisking frequency revealed the decrease in feed-forward inhibition and broadening of IWs. Thus, our experiments allowed us to explore the full dynamic range of thalamocortical feed-forward inhibition. In contrast, ongoing spontaneous thalamic activity in awake animals may depress thalamic inputs onto FS neurons even before the beginning of a whisking event (Castro-Alamancos, 2004), thereby reducing the dynamic range of feedforward inhibition. However, in awake, behaving animals, neuromodulators and network activity may depolarize GABAergic interneurons such that even "depressed" thalamic inputs may be able to bring them to threshold for spike generation (Swadlow and Gusev, 2000), which would reduce the dynamic range of feed-forward inhibition but maintain narrow IWs. Hence, the actual magnitude of thalamocortical feedforward inhibition, its dynamic range, and the resulting width of the IW in layer 4 neurons is likely to be strongly dependent on the behavioral state of the animal. The data presented here therefore illustrate the potential strength and dynamic range of thalamocortical feedforward inhibition and demonstrate that this circuit can powerfully control and modulate temporal integration during the initial steps of somatosensory processing.

II.E Experimental Procedures

All experiments were carried out in accordance with the guidelines set forth by the University of California.

Slices

Thalamocortical slices (400 μm) were prepared from 1425 day old ICR White or C57BL/6 mice (Agmon and Connors, 1991; Porter et al., 2001) incubated for 40 min in an interface chamber at 35C with an artificial cerebrospinal fluid equilibrated with 95% O_2 and 5% CO_2, containing (in mM): 119 NaCl, 2.5 KCl, 1.3 $NaHPO_4$, 1.3 $MgCl_2$, 2.5 $CaCl_2$, 26 $NaHCO_3$, 20 glucose, and subsequently kept in the same chamber at room temperature for 06 hr until being transferred in a submerged chamber at 30C33C for electrophysiological recordings.

In Vitro Thalamic Stimulation

Thalamic nuclei and barrels in the somatosensory cortex were first visualized with a low magnification objective with bright-field illumination and connectivity between the thalamus and the cortex assessed with a field-recording electrode (a patch pipette filled with 2 M NaCl) placed in the layer 4 of the barrel cortex while electrically stimulating thalamic afferents (stimulus duration, 100 μs; stimulus amplitude, 5100 μA) with a monopolar steel electrode placed in the ventrobasal nucleus (VB) close to the border with the nucleus reticularis thalami, near the fimbria. We considered field responses of above 100 μV amplitude as acceptable evidence for a reliable connection. To ensure that the observed responses resulted from orthodromic stimulation of thalamocortical axons rather than antidromic stimulation of cortico-thalamic axons, we routinely determined three electrophysiological parameters of the response, namely latency, paired pulse ratio, and supernormality

(Beierlein and Connors, 2002). We only considered experiments in which EPSPs recorded in layer 4 occurred at short latencies (<3.5 ms), showed paired pulse depression, and displayed no supernormality (i.e., decrease in latency of the second EPSP elicited 100 ms or less after the first).

In Vitro Recordings

Whole-cell recordings of visually identified neurons (infrared DIC videomicroscopy and water immersion objective [40X]) in layer 4 were obtained with patch pipettes (24 MΩ) containing (in mM): 150 K gluconate, 5 HEPES, 1.1 EGTA, 0.51 $MgCl_2$, 10 phosphocreatine, biocytin (0.1%0.5%), and the pH adjusted to 7.2 with gluconic acid.

The firing pattern of the recorded neurons was determined immediately after rupturing the membrane by injecting 800 ms current pulses of incremental amplitude (50600 pA) in the current-clamp mode. Regular spiking (RS) neurons were identified by their rapid adaptation of the instantaneous firing frequency in response to a square pulse of current (from a peak frequency of 161 ± 14 Hz [first two spikes] to a frequency of 29 ± 2 Hz [averaged over 100 ms, 400 ms after the beginning of the pulse]; 300600 pA current injection; steady state to peak frequency ratio, 0.2 ± 0.02), a relatively long membrane time constant (16.6 ± 1 ms), a high input resistance in response to a 50 pA negative current pulse (232 ± 16 MΩ), and a relatively depolarized spike threshold (249 ± 1 mV). Fast-spiking neurons were identified by a much less pronounced adaptation of the firing frequency (from a peak frequency of 106 ± 15 Hz [first two spikes] to a frequency of 92 6 11 Hz [averaged over 100 ms, 400 ms after the beginning of the pulse]; 400600 pA; steady state to peak frequency ratio, 1.1 ± 0.27), a faster membrane time constant (9.7 ± 1 ms), and a lower input resistance (81 ± 8 MΩ; spike threshold, 251 ± 1 mV; all values above were measured from a set of nine simultaneously recorded, FS/RS

pairs) (Feldmeyer et al., 1999; Gibson et al., 1999; Kawaguchi and Kubota, 1997; Mc- Cormick et al., 1985). Low threshold spiking interneurons (Beierlein et al., 2003) were not included in the study.

In Vitro Data Acquisition and Analysis

Data were recorded with Multiclamp 700A or Axopatch 200B amplifiers, digitized at 510 kHz, and analyzed offline. Voltage measurements were corrected for the experimentally determined junction potential of 12 mV. Average values are expressed as mean ± SEM. The Students t test was used for statistical comparisons. Electrophysiological traces illustrated in the figures represent the average averages about 10 to 40 individual sweeps, unless stated otherwise. To deconvolve the unitary IPSC from the feed-forward IPSC, we modeled the firing of FS neurons as occurring in a sharp onset followed by an exponential decay. This function is f(t) = (A/τ) X exp(-t/τ), with parameters A and τ. We obtained these parameters by minimizing the square difference between the measured feedforward IPSC and the convolution of f(t) with the unitary IPSC.

Dynamic Clamp

Dynamic clamp was used to simulate excitatory synaptic conductances, $g_{syn}(t)$, as follows: $I_{inj(t)} = g_{syn}(t)X(Vm(t) - V_{rev})$, in which $I_{inj}(t)$ is the current injected in the recorded neuron, Vm(t) is themembrane potential of the neuron, and V_{rev} is the reversal potential of the synaptic conductance to be simulated and was set at 0 mV. The time course of $g_{syn}(t)$ was given by the sum of two exponentials, t_{rise} and t_{decay}, of 0.15 and 1 ms, respectively. The amplitude ranged between 2 and 3 nS. The operation was performed with an analog circuit (5 MHz bandwidth) connected to the amplifier. Input and output signals were filtered at 5

kHz as described previously (Pouille and Scanziani, 2001). In three experiments, a standard current clamp configuration was used instead ($I_{inj}[t]$ independent of Vm) in which the time course of the I_{inj} was the same as g_{syn}, and the peak value of $I_{inj}(t)$ was either 100 or 200 pA.

In vivo Recording and Analysis

Long-Evans rats (P3045) were anesthetized with urethane (Sigma, 1.5g/kg, i.p.) and prepared for acute recording as described previously (Celikel et al., 2004). Recordings were obtained with glassinsulated carbon fiber electrodes (0.51 MΩ at 1 kHz), or tungsten microelectrodes (24 MΩ at 1 kHz). Signals were preamplified (1,000X), band-pass filtered (0.5-10 kHz), further amplified (5X), and digitized at 32 kHz with custom Igor routines (Wavemetrics). Spike sorting was performed offline with a published algorithm (Fee et al., 1996) implemented in Matlab (Mathworks) by S. Mehta and D. Kleinfeld. Whiskers were deflected with calibrated, computer- controlled piezoelectric actuators 9 mm from the face. Initial mapping was performed to locate the barrel column of interest and layer 4 identified by depth and response latency (Celikel et al., 2004). Whisker deflections (250 μm ramp-and-hold deflection, 50 or 100 ms duration, rise/fall time 4 ms) were delivered at 0.5 Hz or in 10 Hz trains. 100 trials were collected at each recording site. Anesthesia was maintained by additional urethane (10dose, i.p.) at a level that suppressed corneal and limb withdrawal reflexes and maintained breathing rate at $<$2 Hz. Columnar position and laminar location of all cortical recording sites were confirmed by lesion recovery (5 μA, 10 s) in cytochrome-oxidase-stained sections (Fox, 1992). Data analysis: spike counts and spike jitter were calculated for onset responses (spikes within 50 ms of deflection onset); spike jitter was defined as the standard deviation of the Gaussian fits of the onset PSTHs.

Model

This simple model of thalamocortical excitation and feed-forward inhibition includes three synapses (VB-FS, FS-RS, and VB-RS) each subject to synaptic depression (Figure 8). Each synapse type is described by only two parameters: a use factor u and the time constant of recovery τ_d. We obtained these parameters from responses to presynaptic trains at the following frequencies (in Hz): 2.5, 5, 10, 20, 50, and 100. Depression was pronounced at the synapse from VB to FS (u = 0.33, τ_d = 2.2 s) and less pronounced at the synapse from FS to RS (u = 0.26, τ_d = 4.1 s) and at the synapse from VB to RS (u = 0.60, τ_d = 0.2 s). FS neurons (n = 100) were described by an integrate-and-fire model with refractory period (Rinput = 100 MΩ; τ_{mem} = 9.7 ms; Vthresh = 251 mV) and received a variable number of thalamic inputs such that the mean conductance of the thalamic EPSPs was 7.5 nS (with reversal potential E_{exc} = 0 mV) and varied by a factor of ten. We modeled the RS neuron as a single passive compartment (Rinput = 200 MΩ; τ_{mem} = 16ms) that receives an EPSC from VB (with reversal potential E_{exc} = 0 mV) and, 1 ms later, an IPSC from FS neurons (with reversal potential E_{inh} = 285 mV).

Acknowledgement

This chapter, in full, is a republication of the material as it appears in Gabernet,L, Jadhav S.P., Feldman D.E., Carandini, M, Scanziani, M. (2005): Somatosensory Integration Controlled by Dynamic Feed-Forward Inhibition. *Neuron*, **48**, 315–327. The dissertation author was the second author of this paper.

II.F References

Abbott, L. F., Varela, J. A., Sen, K., and Nelson, S. B. (1997). Synaptic depression and cortical gain control. Science 275: 220–224.

Agmon, A., and Connors, B. W. (1991). Thalamocortical responses of mouse somatosensory (barrel) cortex in vitro. Neuroscience 41: 365–379.

Agmon, A., and O'Dowd, D. K. (1992). NMDA receptor-mediated currents are prominent in the thalamocortical synaptic response before maturation of inhibition. J Neurophysiol 68: 345–349.

Arabzadeh, E., Zorzin, E., and Diamond, M. E. (2005). Neuronal encoding of texture in the whisker sensory pathway. PLOS Biol 3 e17: .

Beierlein, M., and Connors, B. W. (2002). Short-term dynamics of thalamocortical and intracortical synapses onto layer 6 neurons in neocortex. J Neurophysiol 88: 1924–1932.

Beierlein, M., Gibson, J. R., and Connors, B. W. (2003). Two dynamically distinct inhibitory networks in layer 4 of the neocortex. J Neurophysiol 90: 2987-3000.

Berger, T., and Luscher, H. R. (2003). Timing and precision of spike initiation in layer V pyramidal cells of the rat somatosensory cortex. Cereb Cortex 13: 274-281.

Blitz, D. M., and Regehr, W. G. (2005). Timing and specificity of feed-forward inhibition within the LGN. Neuron 45: 917-928.

Brecht, M., and Sakmann, B. (2002). Dynamic representation of whisker deflection by synaptic potentials in spiny stellate and pyramidal cells in the barrels and septa of layer 4 rat somatosensory cortex. J Physiol 543: 49-70.

Brunel, N., Hakim, V., Isope, P., Nadal, J. P., and Barbour, B. (2004). Optimal information storage and the distribution of synaptic weights: perceptron versus Purkinje cell. Neuron 43: 745-757.

Bruno, R. M., and Simons, D. J. (2002). Feedforward mechanisms of excitatory and inhibitory cortical receptive fields. J Neurosci 22: 10966-10975.

Buracas, G. T., Zador, A. M., DeWeese, M. R., and Albright, T. D. (1998). Efficient discrimination of temporal patterns by motion-sensitive neurons in primate visual cortex. Neuron 20: 959-969.

Castro-Alamancos, M. A. (2004). Absence of rapid sensory adaptation in neocortex during information processing states. Neuron 41: 455-464.

Coombs, J. S., Eccles, J. C., and Fatt, P. (1955). The inhibitory suppression of reflex discharges from motoneurones. J Physiol 130, 396-413.

DeWeese, M. R., Wehr, M., and Zador, A. M. (2003). Binary spiking in auditory cortex. J Neurosci 23: 7940-7949.

Feldmeyer, D., Egger, V., Lubke, J., and Sakmann, B. (1999). Reliable synaptic connections between pairs of excitatory layer 4 neurones within a single 'barrel' of developing rat somatosensory cortex. J Physiol 521 Pt 1: 169-190.

Fricker, D., and Miles, R. (2000). EPSP amplification and the precision of spike timing in hippocampal neurons. Neuron 28: 559-569.

Geiger, J. R., Lubke, J., Roth, A., Frotscher, M., and Jonas, P. (1997). Submillisecond AMPA receptor-mediated signaling at a principal neuron-interneuron synapse. Neuron 18: 1009-1023.

Gibson, J. R., Beierlein, M., and Connors, B. W. (1999). Two networks of electrically coupled inhibitory neurons in neocortex. Nature 402: 75-79.

Gil, Z., and Amitai, Y. (1996). Properties of convergent thalamocortical and intracortical synaptic potentials in single neurons of neocortex. J Neurosci 16: 6567-6578.

Gil, Z., Connors, B. W., and Amitai, Y. (1999). Efficacy of thalamocortical and intracortical synaptic connections: quanta, innervation, and reliability. Neuron 23: 385-397.

Jonas, P., Bischofberger, J., Fricker, D., and Miles, R. (2004). Interneuron Diversity series: Fast in, fast out–temporal and spatial signal processing in hippocampal interneurons. Trends Neurosci 27: 30-40.

Jonas, P., Racca, C., Sakmann, B., Seeburg, P. H., and Monyer, H. (1994). Differences in Ca2+ permeability of AMPA-type glutamate receptor channels in neocortical neurons caused by differential GluR-B subunit expression. Neuron 12: 1281-1289.

Kawaguchi, Y., and Kubota, Y. (1997). GABAergic cell subtypes and their synaptic connections in rat frontal cortex. Cereb Cortex 7: 476-486.

Keller, A., and White, E. L. (1987). Synaptic organization of GABAergic neurons in the mouse SmI cortex. J Comp Neurol 262: 1-12.

Koch, C., Rapp, M., and Segev, I. (1996). A brief history of time (constants). Cereb Cortex 6: 93-101.

Konig, P., Engel, A. K., and Singer, W. (1996). Integrator or coincidence detector? The role of the cortical neuron revisited. Trends Neurosci 19: 130-137.

Laaris, N., Carlson, G. C., and Keller, A. (2000). Thalamic-evoked synaptic interactions in barrel cortex revealed by optical imaging. J Neurosci 20: 1529-1537.

Lavallee, P., and Deschenes, M. (2004). Dendroarchitecture and lateral inhibition in thalamic barreloids. J Neurosci 24: 6098-6105.

Lloyd, D. P. C. (1946). Facilitation and inhibition of spinal motoneurons. J Neurophysiol 9, 421-438.

London, J. A., Cohen, L. B., and Wu, J. Y. (1989). Optical recordings of the cortical response to whisker stimulation before and after the addition of an epileptogenic agent. J Neurosci 9: 2182-2190.

McCormick, D. A., Connors, B. W., Lighthall, J. W., and Prince, D. A. (1985). Comparative electrophysiology of pyramidal and sparsely spiny stellate neurons of the neocortex. J Neurophysiol 54: 782-806.

Mittmann, W., Koch, U., and Hausser, M. (2005). Feed-forward inhibition shapes the spike output of cerebellar Purkinje cells. J Physiol 563: 369-378.

Mountcastle, V. B., and Powell, T. P. (1959). Neural mechanisms subserving cutaneous sensibility, with special reference to the role of afferent inhibition in sensory perception and discrimination. Bull Johns Hopkins Hosp 105: 201-232.

Petersen, C. C., and Sakmann, B. (2001). Functionally independent columns of rat somatosensory barrel cortex revealed with voltage-sensitive dye imaging. J Neurosci 21: 8435-8446.

Phillips, J. R., Johnson, K. O., and Hsiao, S. S. (1988). Spatial pattern representation and transformation in monkey somatosensory cortex. Proc Natl Acad Sci U S A 85: 1317-1321.

Porter, J. T., Johnson, C. K., and Agmon, A. (2001). Diverse types of interneurons generate thalamus-evoked feedforward inhibition in the mouse barrel cortex. J Neurosci 21: 2699-2710.

Pouille, F., and Scanziani, M. (2001). Enforcement of temporal fidelity in pyramidal cells by somatic feed-forward inhibition. Science 293: 1159-1163.

Reinagel, P., and Reid, R. C. (2000). Temporal coding of visual information in the thalamus. J Neurosci 20: 5392-5400.

Shepherd, G. M. (1998). The Synaptic Organization of the Brain, fourth edn (New York, Oxford University Press).

Staiger, J. F., Zilles, K., and Freund, T. F. (1996). Distribution of GABAergic elements postsynaptic to ventroposteromedial thalamic projections in layer IV of rat barrel cortex. Eur J Neurosci 8: 2273-2285.

Stratford, K. J., Tarczy-Hornoch, K., Martin, K. A., Bannister, N. J., and Jack, J. J. (1996). Excitatory synaptic inputs to spiny stellate cells in cat visual cortex. Nature 382: 258-261.

Swadlow, H. A. (1989). Efferent neurons and suspected interneurons in S-1 vibrissa cortex of the awake rabbit: receptive fields and axonal properties. J Neurophysiol 62: 288-308.

Swadlow, H. A., and Gusev, A. G. (2000). The influence of single VB thalamocortical impulses on barrel columns of rabbit somatosensory cortex. J Neurophysiol 83: 2802-2813.

Tarczy-Hornoch, K., Martin, K. A., Jack, J. J., and Stratford, K. J. (1998). Synaptic interactions between smooth and spiny neurones in layer 4 of cat visual cortex in vitro. J Physiol 508 (Pt 2): 351-363.

Tsodyks, M. V., and Markram, H. (1997). The neural code between neocortical pyramidal neurons depends on neurotransmitter release probability. Proc Natl Acad Sci U S A 94: 719-723.

Varela, J. A., Sen, K., Gibson, J., Fost, J., Abbott, L. F., and Nelson, S. B. (1997). A quantitative description of short-term plasticity at excitatory synapses in layer 2/3 of rat primary visual cortex. J Neurosci 17: 7926-7940.

Wehr, M., and Zador, A. M. (2003). Balanced inhibition underlies tuning and sharpens spike timing in auditory cortex. Nature 426: 442-446.

Wilent, W. B., and Contreras, D. (2004). Synaptic responses to whisker deflections in rat barrel cortex as a function of cortical layer and stimulus intensity. J Neurosci 24: 3985-3998.

Zhu, J. J., and Connors, B. W. (1999). Intrinsic firing patterns and whisker-evoked synaptic responses of neurons in the rat barrel cortex. J Neurophysiol 81: 1171-1183.

III

Sparse Ensemble Coding during Active Tactile Sensation in Primary Somatosensory Cortex.

III.A Summary

Rats palpate objects with their whiskers to discriminate tactile features of their environment. However, the fundamental features of whisker motion that are encoded during natural surface exploration are unknown, and are critical to understanding how surface properties like texture and shape are encoded. To identify these features, we simultaneously measured whisker motion and spiking responses of neurons in somatosensory (S1) cortex in "awake, behaving" rats trained to whisk across textured surfaces. Results showed that during natural surface whisking, transient slip-stick events occur prominently and are encoded by a majority of S1 neurons with precisely timed spikes, leading to an increase in firing rate in S1. Slip-stick responses occurred with low probability, but led to a transient increase in synchronous activity of neurons, resulting in a sparse probabilistic population code for slips. A simulation of ensemble activity using the experimental data revealed

that slips can be efficiently decoded by synchronous spiking activity on a ∼20 ms time scale across small (∼100 neuron) populations within a single S1 cortical column. These results demonstrate that sparse ensemble representations exist in S1 during natural sensation. The synchronous activity of a small subset of neurons can efficiently represent slip-stick events, which are fundamental stimulus features during surface whisking, within this sparse activity.

III.B Introduction

In active sensation, animals explore the environment by actively sampling stimuli with their sensors. In active tactile sensation, the movement of fingertips or whiskers across objects creates dynamic input streams from which stimulus information must be extracted by the nervous system. Variations in sampling strategy may affect perceptual ability, and how the representations of complex, natural stimuli arise from neural responses to fundamental features. Though sensory coding has been studied in detail in anesthetized animals, the principles of sensory encoding under active conditions in the behaving animal are not yet understood.

The rodent whisker system is an excellent model system for studying active sensing. Rats palpate objects with their whiskers, which serve as arrays of highly sensitive detectors for acquiring tactile information. Whiskers, like primate fingers and palms, are scanned across objects to encode their tactile features. (Bensmaia, et al., 2006; Vega-Bermudez et al., 1991; Mehta and Kleinfeld, 2004; Kleinfeld, et al., 2007). Rats perform a range of tactile behaviors using their whiskers including identification of shape and size of objects (Brecht, et al., 1997; Anjum, et al., 2006; Mehta and Kleinfeld, 2004), object location (Szwed, et al., 2003; Mehta, et al., 2007; Knutsen et al., 2006), width of gaps (Krupa, et al., 2004) and surface texture (Guic Robles, et al., 1989; Carvell and Simons, 1990;

von Heimandahl, et al; 2007). The neural codes underlying these behaviors remain to be elucidated.

The whisker system is also an attractive system to study physiologically due to the specialized representation of whiskers in primary somatosensory cortex (S1). Each whisker is represented in S1 by a discrete, well-defined cell cluster, called a barrel, in cortical layer 4 (Woolsey and Van der Loos, 1970). Barrels are arranged isomorphically to the layout of whiskers on the snout. Information from each whisker is relayed via the trigeminal ganglion and VPM thalamus (lemniscal pathway; Simons and Carvell, 1989; Brecht and Sakmann, 2002) to L4 of a single cortical column. L4 neurons then project to L2/3 and L5 of the cortical column associated with that barrel. This results in a discrete map of whiskers, in which receptive fields of neurons in each cortical column are centered on the "principal whisker" for that column (Pinto, et al, 2003; Petersen, 2007). Studies of whisker system physiology in anesthetized animals have shown that S1 neurons respond with brief, phasic spiking responses to onset and offset of experimentally applied passive whisker deflections. Responses are rapid and precise for deflections of the principal whisker, with weaker and slower responses to surround whiskers. Higher velocity deflections drive stronger responses, and S1 neurons are also weakly sensitive to direction of whisker deflections (Bruno et al., 2003; Pinto et al., 2003; Brumberg et al., 2003). However, little is known about S1 coding of natural whisker stimuli in the awake, active animal. During whisking, rats move their whiskers back and forth in a 5-12 Hz rhythm (Fee et al., 1997). Whisker contact from air onto objects drives brief responses in S1 neurons, both in awake animals (Curtis and Kleinfeld, submitted) and in anesthetized animals induced to whisk artificially by stimulating the motor nerve (Szwed, et al., 2003). S1 neurons also also encode phase of whisking (Fee, et al., 1997), and a combination of phase and contact (Curtis and Kleinfeld, submitted). In contrast, almost nothing is known

about neural encoding of whisker movements on surfaces. Encoding of surface features must occur since rats can accurately discriminate texture and shape of objects, but what these features are and how they are encoded is unclear.

Two hypotheses have been proposed to explain how surface features are encoded (Kleinfeld, Ahissar and Diamond, 2006; Mehta and Kleinfeld, 2004). One hypothesis states that surface properties are read out by sustained vibration of whiskers at their resonance frequencies (Neimark, et al., 2003, Andermann, et al., 2004). In the other hypothesis, surface properties are encoded by discrete, high-velocity whisker motion events (Arabzadeh et al., 2005). Consistent with the latter hypothesis, direct measurement of whisker movement on surfaces in awake rats demonstrated the occurrence of discrete, high-velocity, slip-stick and slip-stick ring events, whose properties vary with texture (Wolfe, et al., submitted; Ritt, et al., 2008). However, whether these events are key, salient elements of whisker input that are encoded in S1 is unknown.

To address this question, we simultaneously measured whisker motion and spiking responses of neurons in the corresponding S1 barrel column in awake-behaving rats whisking across textured surfaces. We show that transient slip-stick events, marked by discrete high-velocity and high-acceleration epochs, are encoded by S1 neurons with sparse, precisely timed spikes. These responses encode the timing and amplitude of slip-stick events and contribute significantly to the increase in firing rates of neurons during surface whisking. Despite evoking sparse responses, slip-stick events are efficiently represented by a sparse, probabilistic population code across small ($\sim$100 neuron) populations within a single S1 cortical column. Our results demonstrate that slip-stick events are fundamental features of whisker motion on surfaces that are represented in neural activity and are encoded by sparse, synchronous firing of S1 neurons.

III.C Results

Behavior Task and Whisker Measurements

We trained freely behaving rats to whisk voluntarily in air and across textured sandpaper surfaces (Supplementary Video 1, Figure 1A, B, Wolfe et al., submitted). We trimmed all but one whisker, and simultaneously measured micro-motion of the intact whisker on the right side of the face and spiking in the corresponding cortical column in contralateral S1. The behavioral sequence during a trial is depicted in Figure 1B. Rats initiate a trial by entering the central nosepoke port in the task chamber. They were required to hold position in the nosepoke for $\sim$300 ms, and whisk across the surface a criterion number of times (Methods). A noise cue then indicated that a water reward was available at the lick port in the reward chamber, and rats withdrew from the nosepoke to drink. Well-trained rats performed > 100 trials per session.

Whisker motion was measured in the protraction-retraction plane (roughly rostro-caudal, parallel to the face) by automated tracking of shadows of the whisker cast by a collimated plane of laser light, onto a linear CCD imaging array below the training cage (Figure 1C, Methods, Wolfe, et al., submitted). Surfaces were positioned parallel to the face, less than 5 mm in from the whisker tips, and the whisker motion was measured 1-2 mm in from the surface. Whiskers could be tracked with high spatial ($\sim$5 μm) and temporal resolution (0.25 ms). The surfaces used were sandpapers of varying roughness (P150, P400, P800, P1200) mounted on an aluminum backing and positioned statically using a computer-controlled stepper motor (Methods). In some recording sessions (n = 3), interleaved trials with whisking in air were also included.

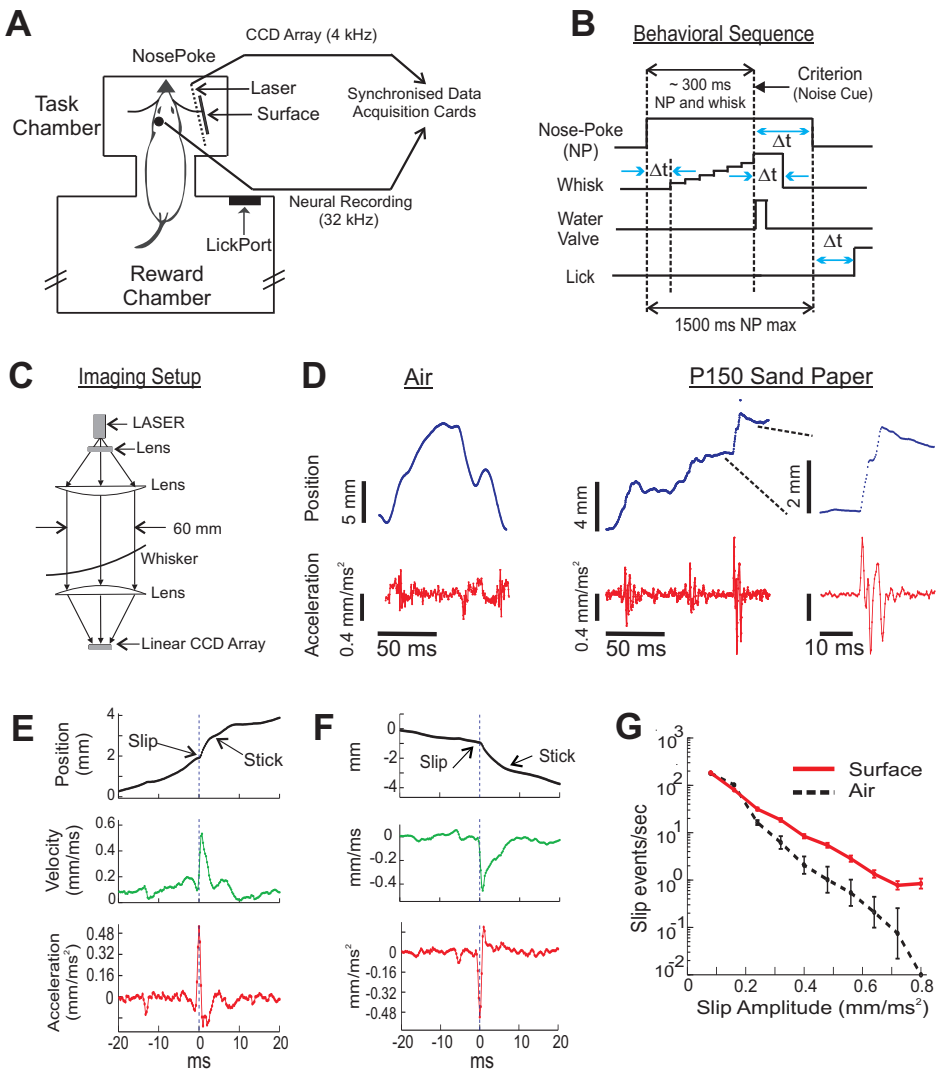

III.1 **Slip-stick events are prominent during whisking on surfaces.** (A) Behavior and recording setup to simultaneously measure whisker motion and spiking responses of S1 neurons during active surface palpation. (B) Sequence of events in a single behavior epoch. (C) Schematic of optical setup for measuring whisker motion. (D) Examples of whisker motion in air (*Left*), and on P150 sandpaper (*Right*). Inset illustrates slip-stick motion on a smaller time scale. (E),(F) Mean kinetics of all slips (threshold = 0.2 mm/ms^2) in one behavior session during (E) forward whisking motion (protraction) on surfaces (n = 566 slips) and (F) backward whisking motion (retraction) on surfaces (n = 746 slips). (G) Distribution of peak amplitude of acceleration (171 trials in air; 228 trials on surface) of slip-stick events on air and surface.

Slip-Stick events are prominent during whisking on surfaces

Whisking motion typically consisted of 5-12 Hz periodic motion with protraction (forward motion) and retraction (backward motion) epochs (Berg and Kleinfeld, 2003; Fee et al., 1997; Szwed et al., 2003). During surface whisking, transient slip-stick events were a prominent feature of whisker micro-motion. Representative motion traces (position and acceleration) for the D1 whisker in air and on P150 sandpaper are shown in Figures 1D, 2A (Wolfe et al., Ritt, et al., Arabzadeh, et al., 2005). Slip-stick motion consisted of sudden, discrete, high-velocity and high-acceleration movements, occasionally followed by damped oscillatory motion of the whisker ("ringing"). Slip-stick events occurred both during protraction and retraction, and were marked by prominent peaks in both, velocity and acceleration (Figure 1E, F; the average kinematics of slip-stick events on a P150 surface for D1 whisker in a single behavior session during protraction, n = 566 events, and retraction, n = 746 events). Slips and sticks generally occurred in quick succession, resulting in a sharp rise and fall of velocity, and biphasic peaks in acceleration. Occasional ringing motion following a slip-stick event led to a clustering of velocity and acceleration peaks. Thus, sequences of correlated high-velocity, high-acceleration events represent slip-stick-ring motion of whiskers along surfaces. In fact, the magnitude of instantaneous velocity and acceleration were highly correlated during the entire duration of natural whisking on surfaces (Figure 2B). Instantaneous velocity and acceleration magnitudes (40ms sliding windows, 20ms overlap) had highly significant correlation coefficients across trials (Fig 2B, single behavior session, R = 0.92, $p < 0.001$) and across behavior sessions ($R = 0.83 \pm 0.01$, n = 22 behavior sessions). Since velocity and acceleration peaks were correlated, we identified slip-stick events (referred to as 'slip-sticks', or 'slips') by using a threshold to detect acceleration transients (Methods). Ringing motion was identified by the occurrence of acceleration peaks in quick succession

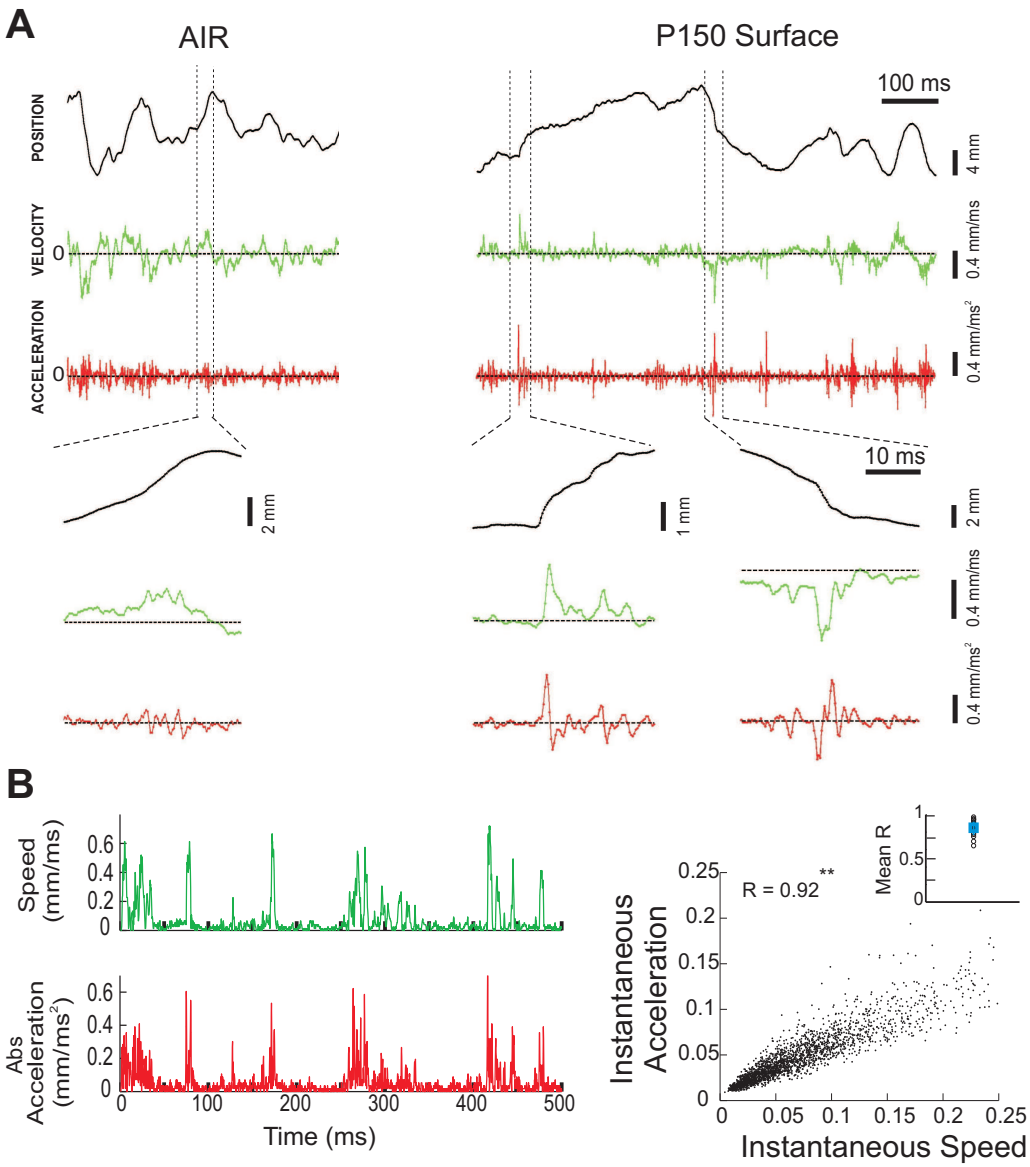

III.2 **Features of whisker motion during active whisking on surfaces.** (A) Example traces showing position, velocity and acceleration of whisker motion during whisking in air (*Left*) and on surfaces (*Right*). Insets below show slip-stick events on a smaller time scale. (B) Correlation between velocity and acceleration of whisker motion during surface whisking. *Left* Speed and absolute acceleration during a single trial of whisking. *Right* Correlation between magnitude of instantaneous speed and acceleration calculated in 40 ms moving windows for all trials during a behavior session. Inset shows mean correlation values for all behavior sessions.

(within 20ms, See Methods), and slips for which there was no preceeding acceleration peak for >=20 ms were referred to as 'first slips'. Peak acceleration was used to characterize amplitude of slips.

Whisking in air exhibited smoother motion that included low acceleration peaks, but generally not large slips (Figure 1D; whiskers vibrations in air are presumably due to the intrinsic resonance properties of the whisker and high-frequency drive by whisker muscles, Wolfe et al., submitted). Quantification of slip amplitudes (3 behavior sessions, 94 seconds in 171 trials in air, 115 seconds in 228 trials on surfaces) revealed that low-acceleration movements were common in air and on surfaces, but high-acceleration movements ($>0.2\ mm/ms^2$) were significantly more prevalent on surfaces than in air (Figure 1G). This is consistent with a simple model of frictional interaction between the whisker and the surface (Wolfe et al, submitted). In this model, as the whisker is forced across the surface, it bends and overcomes the force of friction, resulting in a ballistic, high-velocity, high-acceleration movement which releases the stored energy, before it sticks again. On surfaces, slips achieved displacements, velocities and accelerations higher than standard thresholds of passive deflections for driving spikes *in vivo* in anesthetized animals (3^o, $800^o/sec$, Pinto et al., 2003; Gabernet et al., 2005). In an example behavior session, slips (n = 1742) had an average displacement of 9 mm, an average peak velocity of 0.42 mm/ms, and an average peak acceleration of 0.32 mm/ms^2 (This corresponds to approximately 16^o, $800^o/sec$ and $600^o/sec^2$ respectively, assuming a whisker length of 30 mm). Awake, non-whisking rats can detect experimentally applied stimuli of much lower velocity and amplitude (Stuttgen et al., 2004; $3-12^o$, $750^o/sec$). Thus, it is likely that slip-stick events during surface whisking will drive spikes in awake behaving animals.

Neural recordings

To test whether slips are encoded in neural activity, we measured single-unit spiking in S1 recorded simultaneously with the whisker measurements. Following training, rats were implanted with a chronic electrode microdrive that held 4 independently moveable tetrodes (Figure 3A, Methods). The tetrodes were targeted to the whisker region of S1, aligned for radial electrode penetrations (Methods). After implantation, tetrodes were advanced into S1, and the principal whisker for each tetrode that successfully penetrated into S1 was physiologically determined by measuring spiking responses to manual or air puff deflection of whiskers under anesthesia. We then chose 1 principal whisker corresponding to one of the tetrodes, and trimmed all the other whiskers. Recordings were restricted to tetrodes in the cortical column corresponding to the spared whisker. We only recorded from tetrodes which had an unambiguous principal whisker in the arcs 1-3 of whisker rows C-E. Over the next 10-24 days, tetrodes were moved in small steps until spiking activity with good signal to-noise was observed. If the activity was stable for 15 minutes, recordings were made while the rats performed the behavior. In total, neural data was collected from 22 recording sites in 4 cortical columns in 3 animals, along with simultaneous whisker movement data (3-10 sites per penetration; 2 penetrations were in the D1 column, and one each in D2 and E1). At the end of the experiment, lesions were left at 3-4 locations along the recording track. Columnar penetrations and recording locations were verified by histology (Figure 3A *Right*, Methods). All the recordings were in L4 and L5 as determined by depth of recordings (700-1300 μm) and verified by histology (L4 recordings were in the granular "barrel" region of the column (700-1000 μm), and L5 recordings were sub-granular (1000-1300 μm), Celikel, et al., 2004; de Kock, et al., 2006).

Single neurons were isolated offline from tetrode recordings using a semi-automated spike-sorting algorithm implemented in Matlab (Methods, Fee et. al,

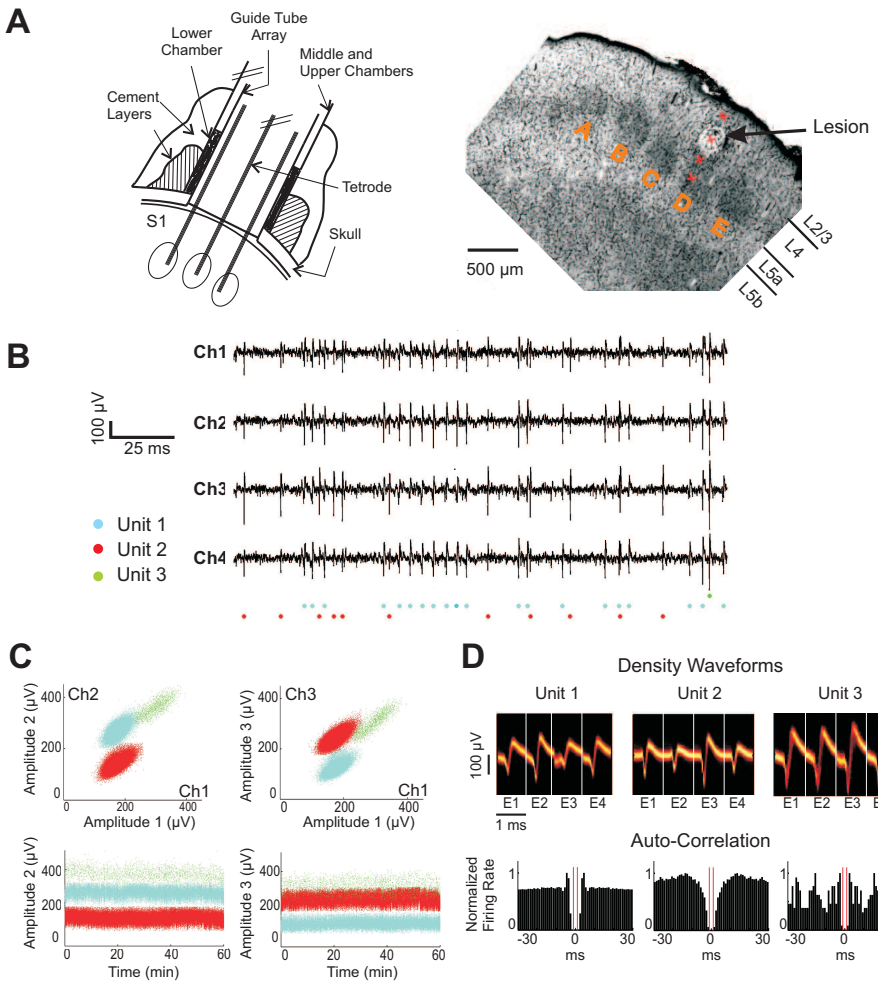

III.3 **Recording configuration and single unit sorting using tetrodes.** (A) Spiking activity was recorded using chronically implanted, moveable tetrodes in an ultra-minature microdrive in contralateral S1, and sorted offline to isolate stable S1 single units. Histology image on right illustrates a cytochrome-oxidase stained coronal section ($\sim 45^o$ to bregma-lambda line) across the 5 macrovibrissa rows (A, B, C, D, E), showing a lesion and the reconstructed recording track (red crosses). (B) Example of a tetrode recording with raw signal on all 4 channels of a tetrode. 3 isolated units (single neurons) are denoted with rasters below the raw traces. (C) *Above* Amplitude plots for the recording site illustrated in B, showing 3 clearly isolated units. *Below* The amplitudes of the 3 units were also stable throughout the entire recording session. (D) *Above* Density plots of the 3 units showing shape of waveforms on all 4 channels of the tetrode. *Below* Auto-correlation plots illustrating refractory periods for the 3 units. The red lines denote a 1 ms refractory period.

1999). A total of 90 single units were isolated (range: 2-6, mean = 4.1 units per site). Only units with good isolation and recording stability across the session were analyzed. Single units were required to have spikes with $< 0.5\%$ violations of a 1 ms refractory period. Cluster separation was evaluated with isolation distance (isolation distance > 20 for single units, Methods, Harris, et al., 2001). An example recording site with 3 well-isolated single units is shown in Figure 3. Cluster separation was apparent from amplitude on different channels of the tetrode and clusters were stable throughout the session (Figure 3C; raw tetrode signal in Figure 3B). Mean spike shapes are shown by density waveforms on each tetrode channel (Figure 3D *Above*). Auto-correlation plots showed no refractory period violations (Figure 3D *Below*).

Firing rate modulation during surface whisking

Neurons showed low average firing rate (0.3 Hz to 48 Hz, mean = 7.5 ± 0.8 Hz, median = 5.7 Hz; n = 90) when calculated over entire recording sessions including both whisking and non-whisking epochs, and a range of behavior states (30 minutes to 2 hours, Figure 4A). More than 75% of the neurons had firing rates below 10 Hz. This low firing rate meant that few spikes occurred per whisking epoch (Figure 4B). PSTH analysis of firing rate aligned to nosepoke onset or whisking onset (first appearance of whisker shadows in CCD image taken 1-2 mm from surface) showed that average firing rate increased during surface whisking. Some neurons showed sustained firing rate increase during the entire whisking period (Figure 4C, Neurons A and B; mean duration of whisker contact during the whole trial was 340.0 ± 41.9 ms); others showed a transient response followed by inhibition (Figure 4C, Neuron C).

Firing rate was analyzed across all whisking trials (range: 65 to 365, median = 160, inter-quartile range = 135-193) for each neuron. Three response

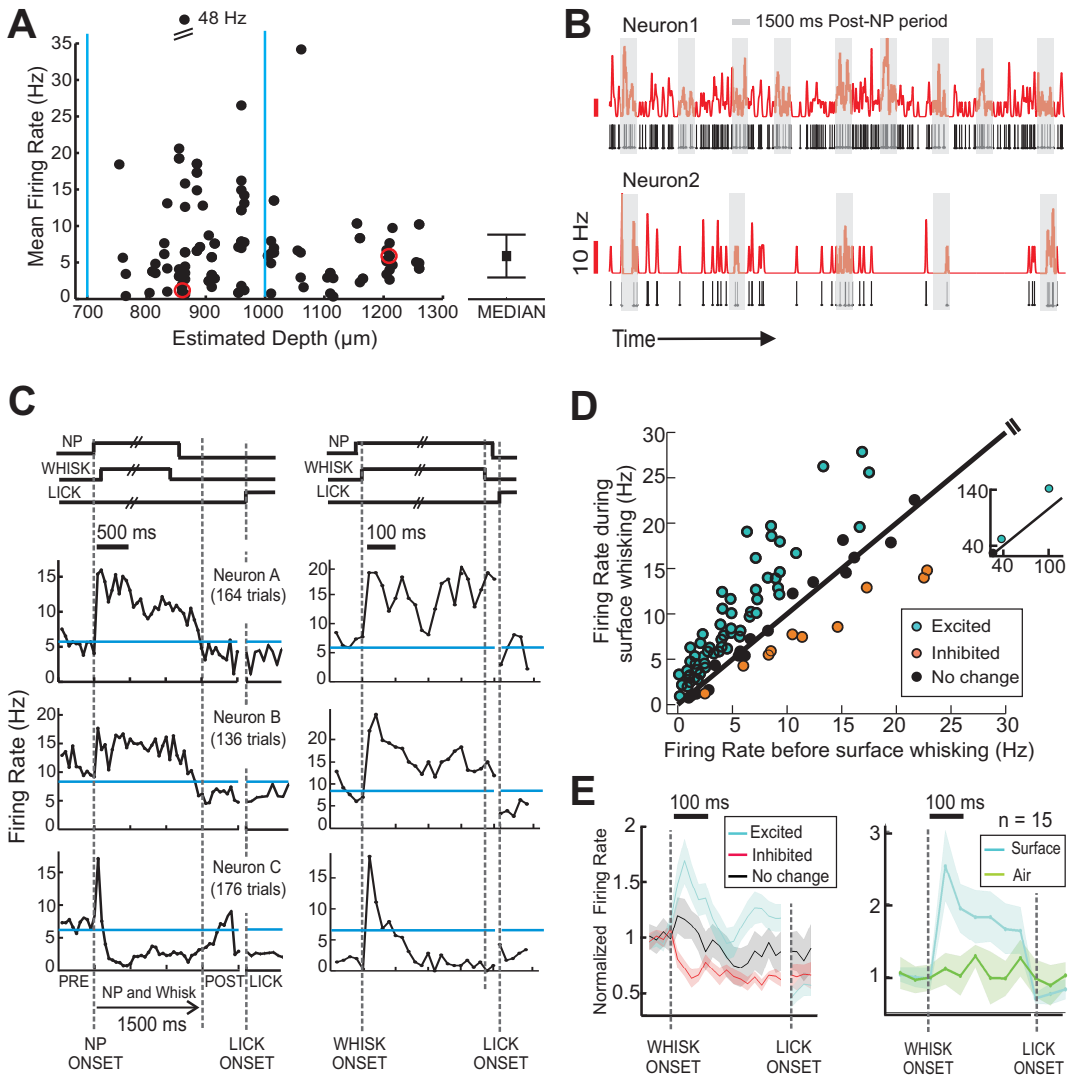

III.4 **Firing rate modulation of S1 neurons during active palpation on surfaces.** (A) Mean firing rates of 90 neurons in L4 and L5 during entire behavior sessions. The blue lines denote L4 barrel boundaries, as determined by histology. Inset denotes median firing rate of population with inter-quartile ranges. (B) Rasters and gaussian filtered PSTHs for 2 neurons (marked in (A) by red circles) during behavior sessions. Gray bars indicate the 1500 ms period beginning at onset of nosepoke during which whisker data was collected. (C) PSTHs aligned to onset of nosepoke (left), and onset of surface whisking (right), illustrated for 3 example neurons. (D) A comparison of firing rates during surface whisking with firing rates before onset of surface whisking. (E) Mean PSTHs with confidence intervals. *Left* For 3 response types during surface whisking. *Right* For the subset of neurons tested with interleaved trials of surface whisking and whisking in air.

classes were evident (Figure 4D, Methods). Surface-excited neurons ($\sim$ 70%, n = 62/90) significantly increased firing rate during whisking on surfaces relative to a pre-whisk baseline (t-test, $p < 0.05$). Surface-inhibited neurons (n = 10/90) showed a significant decrease in firing rate, and surface-nonresponsive neurons (n = 18/90) showed no significant change. These response types are shown by mean PSTHs aligned at whisking onset (Figure 4E *Left*). The mean fractional increase in population firing rate during surface whisking was 1.77 ± 0.11 for all 90 neurons, and 2.21 ± 0.13 for the 62 excited neurons. In 15 neurons tested with interleaved trials on surface and air (3 sessions, 228 trials on surface, 171 trials in air), firing rate increased during whisking on surfaces, but not during whisking in air (Figure 4E, *Right*). This indicates that surface interactions, not motor commands or sensory reafference from whisking itself, were responsible for the increased firing rate in S1 neurons.

Slips drive sparse, precisely timed spikes in S1 neurons

To determine whether whisker slips drive spikes on surfaces, we constructed slip-locked rasters and PSTHS by aligning spike trains to slips identified using acceleration thresholds (Figure 5A; threshold (Θ) = 0.32 mm/ms^2 used for quantification, See Methods). Sparse slip responses were apparent in raster plots in $\sim$ 20 ms following slips, illustrated in 2 example neurons (Figure 5B). Slip-locked PSTHs showed a strong transient peak response above the neurons' baseline firing rate (Figure 5C, D). Slips often occurred in tight clusters (first slips and rings), which affected PSTHs. PSTHs selectively compiled from first slips (no preceeding slip for >= 20 ms) showed a short-latency, narrow peak following the average slip event (Figure 5C). PSTHs compiled from all slips (slips and rings) also showed, in addition, a slow firing rate increase, reflecting spikes evoked by preceeding slips within the cluster.

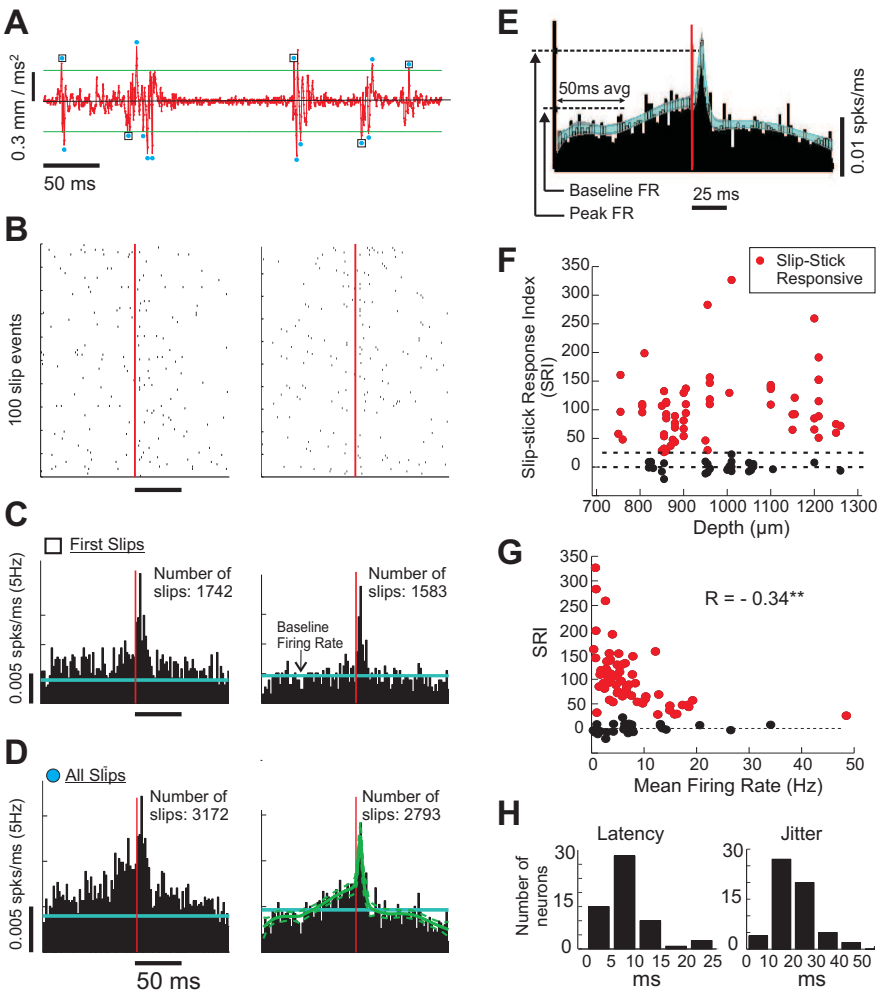

III.5 **Slips drive sparse, precisely timed spikes in S1 neurons.** (A) Example acceleration trace illustrating detection of slips using an acceleration threshold. Slips marked by blue circles are all acceleration threshold crossings. Black squares are first slips. (B) Spike rasters for 2 neurons aligned to 100 first slips, illustrating sparse responses to slips. (C)(D) PSTHs (2 ms bins) aligned to (C) first slips, and (D) all slips, for the neurons in (B), illustrating precisely timed, short-latency peaks. Baseline firing rates are marked by cyan lines. Right panel in (D) illustrating fits to the PSTHs. (E) Procedure for deriving the Slip Response Index (SRI). (F) Slip Response Index (% change in peak firing rate over baseline) vs recording depth for all 90 neurons recorded in L4 and L5. n=62/90 neurons were slip-responsive. (G) SRI showed a significant negative correlation with mean firing rate in the population. (H) Distribution of latency-to-peak and jitter of response in the population of slip-responsive neurons.

For each neuron, we fit the PSTH and defined a slip response index (SRI) as the percent change in the peak firing rate above baseline from the fit (Figure 5E, $\Theta = 0.32\ mm/ms^2$, Methods). Seventy percent (n = 62/90) of neurons showing significant slip peaks (quantified with confidence intervals by the fit, Figure 5F, Methods). Responsive neurons had SRI >= 25 (mean = 103.1±7.5, n = 62). Slip-responsive neurons were found both in L4 and L5. SRI correlated inversely with mean firing rates of neurons (Figure 5G), implying that neurons with low spontaneous rates responded more strongly to slips than neurons with high spontaneous rates. Latency to peak response (7.5 ±0.5 ms) and jitter (19.0±2.6 ms) were low (Figure 5H), indicating that the timing of slips is encoded in the population. These results show that as a whisker moves across a surface, slips are represented with high temporal precision in spiking activity of neurons in the corresponding barrel column.

Slips are fundamental features of whisking motion on surfaces encoded in S1 neurons

We performed several analyses to test whether slip-evoked spikes contribute substantially to firing rate increase on surfaces. First, n = 56/62 of surface-excited neurons were also slip-responsive, while only n = 6/28 surface-inhibited or surface-responsive neurons were slip-responsive. Moreover, Slip Response Index (SRI) correlated significantly with the increase in firing rate on surfaces (Figure 6A; r = 0.49, $p < 0.01$). Second, we performed an analysis analogous to boot-strap to estimate the fraction of surface-driven spikes attributable to slips. In this analysis, we compared for each slip-responsive neuron, a) the number of spikes that occurred within a 20 ms response response window after each first slip, with b) the number of spikes in an equivalent number of non-slip epochs, randomly chosen from the same trials, with c) the total number of spikes that occurred in those

trials. The first 250 ms of each trial was analyzed to avoid trivial correlations due

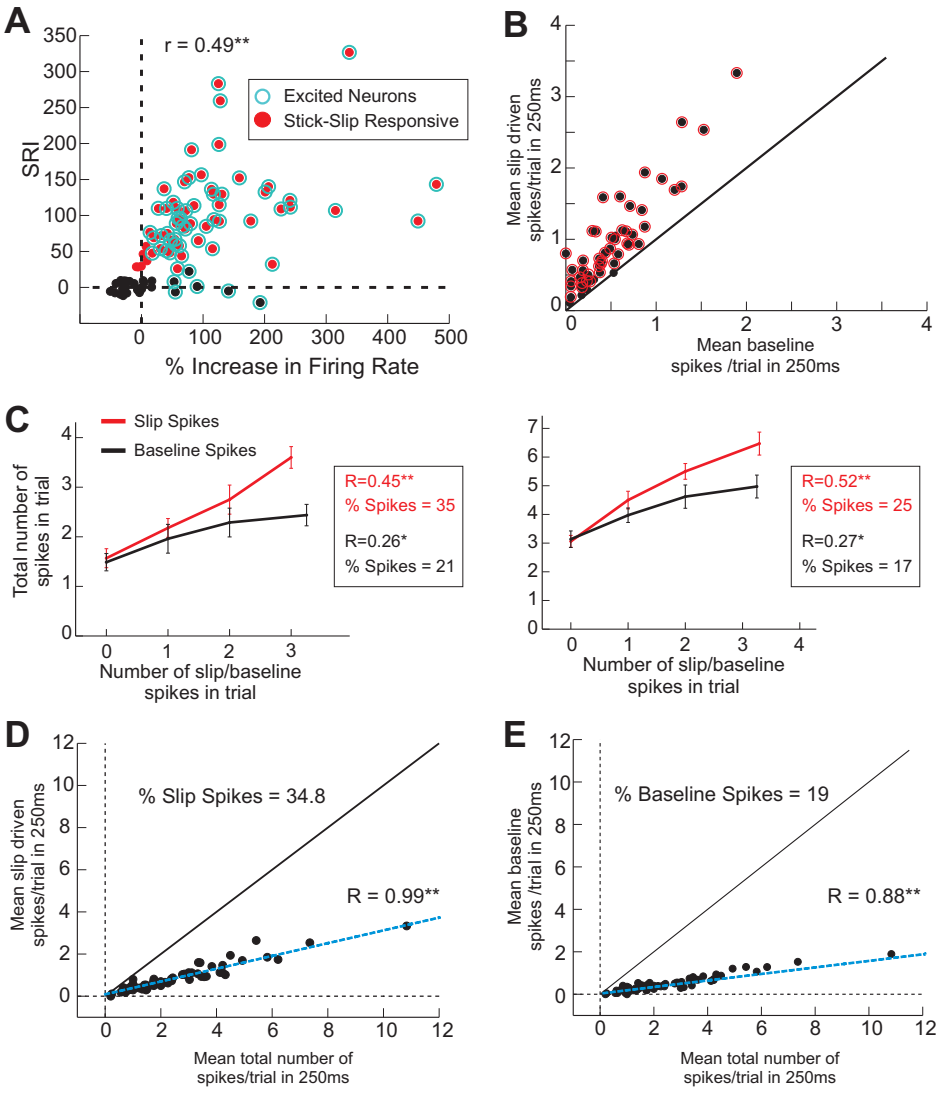

III.6 **Slips drive a significant fraction of spikes on surfaces.** (A) Correlation between the Slip Response Index and the % increase in firing rate observed during surface whisking. (B) Comparison of slip-driven spikes in a 20 ms response window per trial to baseline spikes in an equivalent number of random windows, for all 62 slip-responsive neurons. (C) Slip driven and baseline spikes in a 20 ms response window vs Total number of spikes per trial for 2 example neurons. Insets show correlation values and the % of total number of spikes for slip driven and baseline spikes. (D) Mean Slip driven spikes in a 20 ms response window per trial vs Mean total number of spikes per trial, in all 62 slip-responsive neurons. (E) Mean baseline spikes per trial in equivalent length windows vs Mean total number of spikes per trial.

to trial length, and a low slip detection threshold (Θ) of 0.16 mm/ms^2 ($\sim$2 s.d.s > mean) was used to incorporate all detectable slips. With this threshold, 3.4 ± 0.05 slips occurred per trial. Spikes in slip-response windows accounted for 34.8$\pm$1.4% (n = 62) of all spikes in the trials (mean 1.02 ± 0.18 spikes out of 3.07 ± 0.6 spikes in the entire 250 ms trial). These slip-driven spikes were significantly higher than those that occurred for non-slip epochs for n = 55/62 neurons (Figure 6 B,C; t-test across trials for each neuron individually, $p < 0.05$). In the population, spikes in non-slip epochs (baseline spikes) accounted for 19% of total spikes per trial, which was significantly lower than the percentage of spikes driven by slips (Figure 6D, E; 34.8$\pm$1.4% slip driven spikes vs 19.0$\pm$1.3% baseline spikes , n = 62, $p < 0.05$). The number of baseline spikes was trivially correlated with total number of spikes in a trial (Figure 6E), since both will co-vary with mean spontaneous rate. Thus, $\sim$16% (34.8%-19%) of total spikes on surfaces are driven by first slips. Because surface whisking increases firing rate of surface-excited neurons by $\sim$2.2. first slips account for $\sim$30% of this surface-induced increase in firing rate over pre-whisk firing. This number is a lower-bound because only first slips are considered. Since only 1.02 ± 0.18 spikes were elicited for across 3.4 ± 0.05 first slips per trial, this analysis confirms that the probability of slip-evoked spikes is low. However, despite being sparse, slip responses contribute significantly to the firing rate increase on surfaces.

Slip properties encoded by S1 neurons

In previous studies in anesthetized animals, the amplitude and direction of transient, passive deflections have been shown to be encoded by spiking responses in S1 (Simons and Carvell, 1989; Bruno et al., 2003; Pinto, et al., 2003). To test whether the amplitude of slips is encoded in awake rats, we separately calculated slip-evoked PSTHs using increasing slip amplitude thresholds. Slip ampli-

tude strongly modulated spiking responses (example in Figure 7A). Slip-responsive neurons varied in amplitude gain (Figure 7B, defined as the change in peak firing rate per unit acceleration amplitude of 0.1 mm/ms^2, mean = 4.2±0.3, n = 62). Amplitude response threshold (defined as the lowest slip amplitude at which a significant peak response was observed) was 0.16±0.01 mm/ms^2 (n = 62; Figure 7B), which is lower than amplitude of slips observed on surface (Figure 1F); indicating that neurons are sensitive enough, in principle, to encode all surface-relevant slips.

To test whether slip responses were modulated by direction of whisker motion during slips, we calculated slip-locked PSTHs separately for slips during protraction and retraction. A few neurons were strongly direction selective (Figure 7C, Left; direction-selectivity assessed by net spiking probability in a 20 ms window following a slip). However, in the population, neurons had weak direction selectivity. Only $\sim$ 43% (n = 27/62) of neurons show a significant modulation with direction (n = 19/62 neurons are retraction selective, n = 8/62 neurons are protraction selective), with low modulation depth (mean = 0.79±0.07, n = 27; fractional change in spiking probability with direction, see Methods).

Whiskers are resonant beams that show damped high-frequency vibrations after impulses (Hartmann, et al., 2003; Ritt et al., 2008; Wolfe, et al., submitted). Ringing at resonance frequency has been proposed to amplify neural coding of whisker input (Moore, 2005). Ringing of whiskers was frequently observed following slips (Figure 8D, $\Theta = 0.32\ mm/ms^2$, rings are detected by clustering of acceleration peaks within 20 ms as described previously, See Methods). Both, single slip sequences and slips associated with rings (slip-ring sequences) were prevalent on surfaces. To determine whether rings amplified responses to first slips, we separately calculated slip-response PSTHs for single slip and slip-ring sequences. We found that slip-ring sequences had significantly higher net spike responses than single slips (Figure 8E). However, responses to ringing motion were clearly weaker

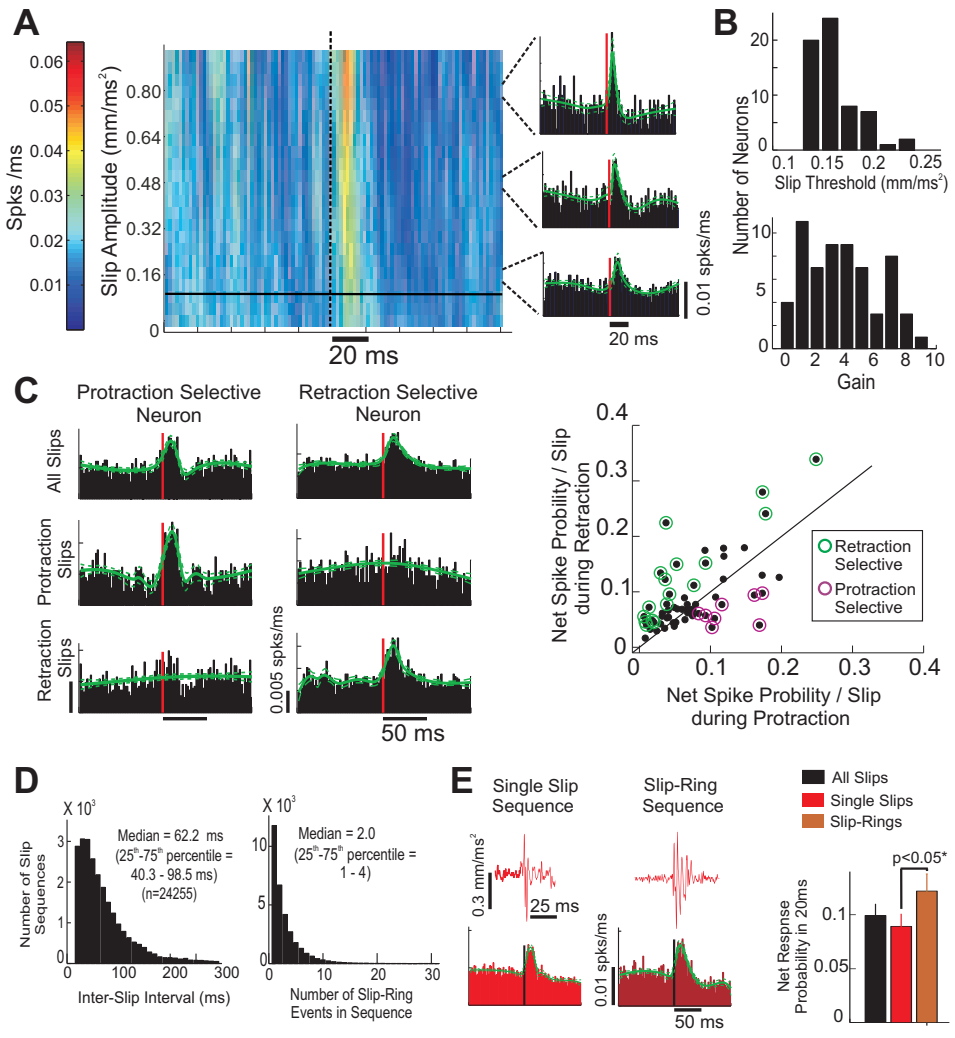

III.7 **Slip properties are encoded by S1 neurons.** (A) Amplitude of slips. Cumulative slip-amplitude response plot of an example neuron. Each row of the matrix is the normalized PSTH of spiking responses of 1 neuron for all slips above the corresponding slip amplitude (acceleration threshold). Horizontal line denotes threshold amplitude. Insets with PSTHs show increasing peak response with increasing slip amplitude. (B) Population plots show distribution of slip thresholds and amplitude gain for all slip-responsive neurons. (C) Direction of motion. 2 example neurons with direction selective responses to slips. *Left* Protraction (forward whisker motion) selective, *Right* Retraction (backward whisker motion) selective. Distribution of direction-selective neurons is shown in the population plot on the right. (D) Statistics of slip-ring sequences. (E) Ringing motion of whisker. Example neuron with response psths for single slip and slip-ring sequences. The plot on the right shows the net response probability in the population.

than slips and rings had a modest effect in the population. We estimated that in slip-ring sequences, they served to amplify the slip response by 39±11% (n = 62, $p < 0.05$). This increase in response was not due to variation in first-slip amplitude between these groups (mean amplitude of first slip for both groups was statistically similar for all thresholds tested, $p > 0.05$). Thus, ringing of whiskers following transient slip events modestly increases the probability of spiking due to slips.

Neural responses are insensitive to position

S1 neurons have been proposed to encode whisker position and phase within the whisker cycle, and phase sensitivity has been proposed to be important for coding of object location (Mehta, et al., 2004; Szwed, et al., 2003; Yu et al., 2006). Phase sensitivity during epochs of exploratory whisking in air has been shown to result in mainly a rearrangement of spikes in time, and has a modest increase in firing rate (∼10%; Fee, et al., 1997; Curtis and Kleinfeld, submitted). To test for position encoding, we compared number of spikes observed during retraction and protraction epochs (normalized for epoch length, Methods), We looked for modulation of spiking rate in all 90 neurons during retraction and protraction epochs of whisking, and found a very weak effect in the population. Only ∼ 20% (n = 18/90) neurons have significantly different responses depending on epoch (Figure 8, n = 15/62 neurons preferably spike during retraction, and n = 3/62 neurons during protraction, $p < 0.05$), and position modulation in these neurons is weak (mean = 0.47±0.05, n = 18; modulation depth is defined as the fractional change in spiking probability with epoch of whisking, see Methods). Part of the modulation of spiking by gross position while whisking of surfaces might also be due to direction-selective responses to slips. This is consistent with previous reports of weak modulation of total spike rate by position. (Fee, et al., 1997; Curtis

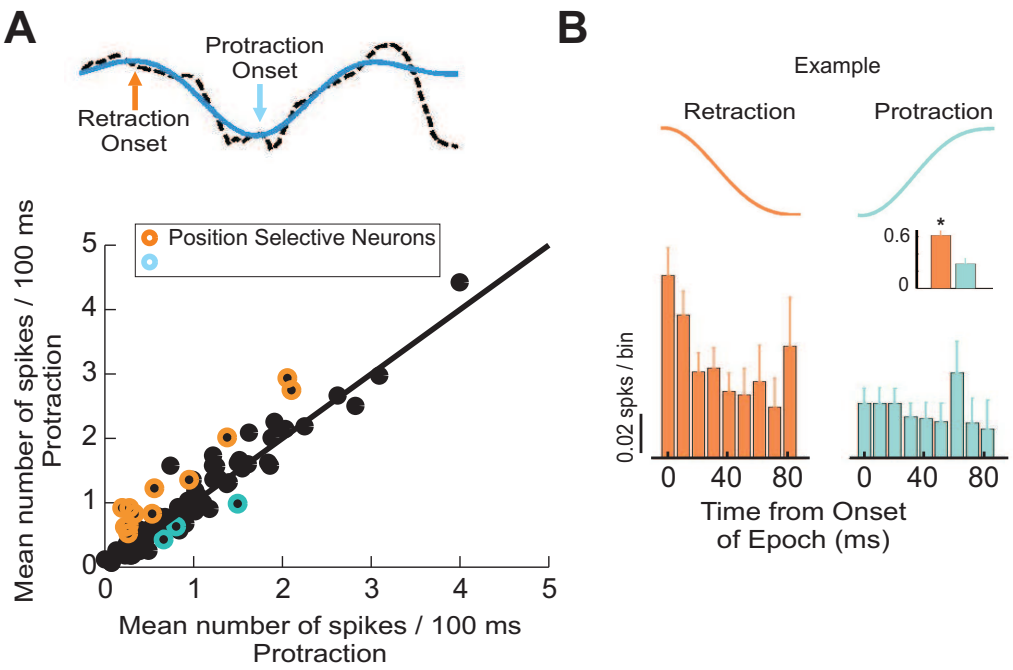

III.8 **Neural responses are insensitive to position.** (A) Net spiking probability in population during protraction and retraction, normalized for 100 ms epoch length. Schematic on top illustrates identification of retraction and protraction epochs from low-pass filtered whisker motion data. (B) Example neuron with significantly more spikes during retraction. Bin-size for spike probability is 10 ms.

and Kleinfeld, submitted).

Multiple Regression Analysis

To further verify that high-velocity, high-acceleration slips are the primary encoded features of whisker motion surfaces, we performed a multiple regression analysis. Firing rate of a neuron is fit with a linear combination of different kinetic parameters, and a significant prediction of variance indicates that those parameters are encoded by the neuron, with dependencies given by coefficients of regression (Itoh, et al., 2002; Watanabe, et al., 2003; Romo, et al., 2004; Lau and Glimcher, 2008). We performed 2 regression analysis, one predicting firing over full trials (Figure 9) and one on instantaneous firing rate (Figure 10). Mean speed of motion has been proposed to predict spiking during passive stimulation or arti-

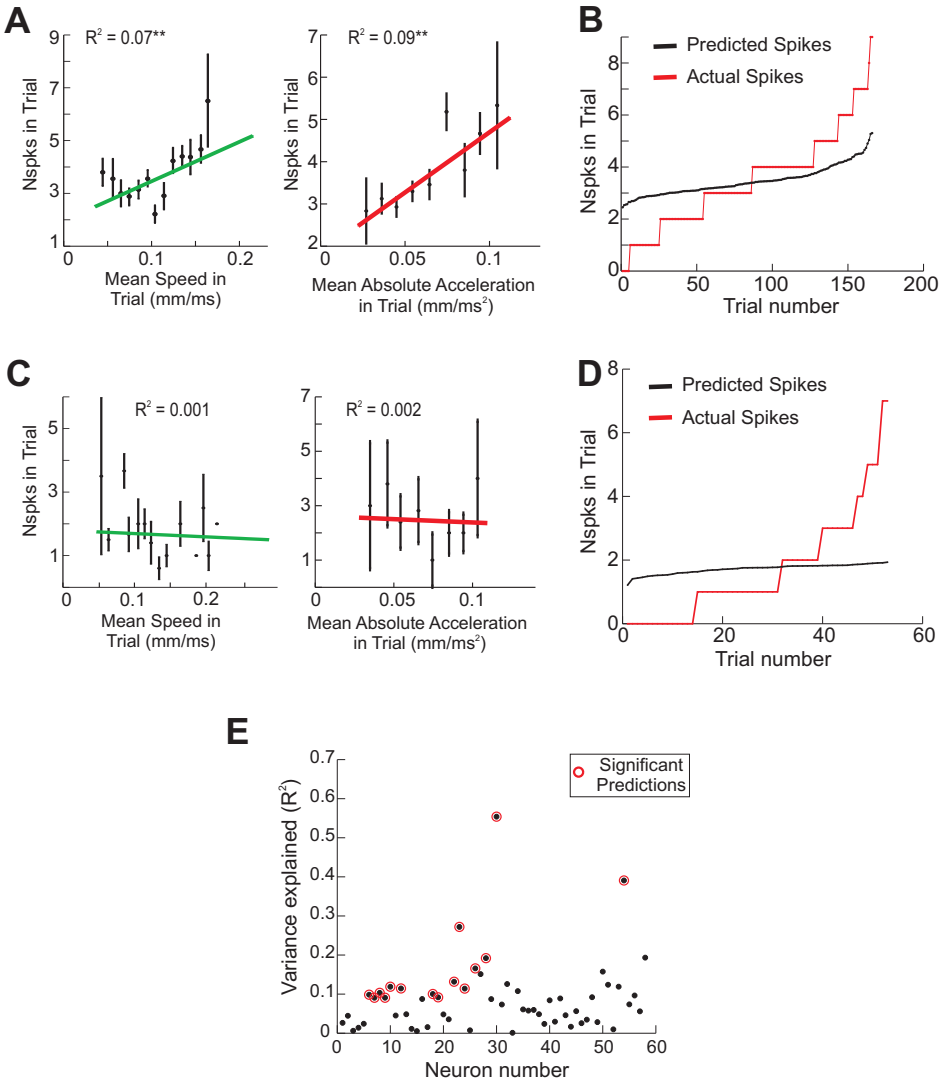

III.9 **Variance in firing rate over full trials is poorly predicted by kinematic parameters in the population.** (A) Firing rate/trial plotted against the mean speed (*Left*) and mean absolute acceleration (*Right*) for a neuron with significant predictions with a multiple regression analysis. Regression lines are overlaid. (B) Observed firing rate/trial and predicted firing rate with a speed+acceleration model for the neuron in (A). (C) Firing rate/trial plotted against the mean speed (*Left*) and mean absolute acceleration (*Right*) for a neuron which does not show significant regression. Most neurons in the population (n = 43/58) do not have significant predictions. (D) Observed and predicted firing rate/trial for the neuron in (C). (E) Variance explained by the speed+acceleration model across the population. Predictions are significant for only n = 15/58 neurons.

ficial whisking on surfaces (Arabzadeh et al., 2003, 2005). We used the regression: Nspks(trial) $= A_o + A_1 * MeanSpeed(Trial) + A_2 * MeanAbsAcceleration(trial) + A_3 * MeanPosition(Trial)$, to see if this was true for our data for awake, actively whisking animals (regression with all variables or with each variable individually, all trials of length 250 ms; See Methods). Position was not a significant predictor for any neuron, and only n = 15/58 ($\sim$25%) neurons had significant regression coefficients ($p < 0.05$) with the full model (4 neurons were discarded due to lack of sufficient trials of length 250 ms). Speed and absolute acceleration were also individually significant predictors for these neurons (only magnitudes of absolute values were used in this analysis, direction was ignored). Individual regression with speed and absolute acceleration for an example neuron with significant predictions is shown in Figure 7A. For this neuron, a significant fraction of the variance (9%) in firing rate/trial is explained with a speed+acceleration model (Figure 7B, observed spikes per trial and spikes predicted by the model). However, $\sim$75% (n = 43/58) neurons do not have significant predictions for any model (speed, absolute acceleration, or speed+absolute acceleration) for full-trial regression (Example: Figure 7C, D; Population: Figure 7E), and on average only 8.7$\pm$1.3% (n = 58) variance was explained in the population.

Since slip-driven spikes contribute a significant fraction of spikes for these neurons, and slips are marked by discrete high-velocity and high-acceleration epochs, we asked if variance in instantaneous spiking is better predicted by instantaneous parameters. Instantaneous spiking probability was calculated in sliding windows within a trial (20 ms windows, 10 ms overlap, trials of length 250 ms). Multiple regression was used to assess statistical significance of spiking dependence on instantaneous position, speed and absolute acceleration, across all trials using the model (Methods): Nspks(t) $= A_o + A_1 * MeanSpeed(t) + A_2 * MeanAbsAcceleration(t) + A_3 * MeanPosition(t)$. Indeed, $\sim$78% (n = 45/58) neurons had significant coef-

ficients of prediction ($p < 0.05$) for the full model (and, individually with both, speed and acceleration, but not position; Example neuron, Figure 8A; Predictions, Figure 8C). To estimate the time window over which spiking probability is predicted by kinetic parameters, we repeated the regression with increasing window size. The number of significant neurons decreases as the window size is increased from 20 ms to 160 ms (Figure 8B). This indicates that instantaneous peaks in velocity and acceleration on a 20 ms or shorter time scale modulate the moment-to-moment spiking probability of a majority of neurons. However, the variance explained for this analysis is only 2.5±0.4% (n = 58), due to the large number of time windows across all trials.

We therefore calculated if the temporal dynamics of spiking over the course of a trial can be predicted by the instantaneous parameters. Using 20 ms windows, we calculated regression coefficients for speed and absolute acceleration for *each* trial (with a speed+acceleration model). The mean predicted spike rate over the course of a trial was then computed with the mean coefficients of regression across all trials, and the mean values of instantaneous speed and acceleration in the time windows. Although each trial was different, the predicted spiking probability correlated significantly with the actual spike probability (Two examples in Figure 8D). We could thus predict the mean variation in spike probability over the course of a trial with the two coefficients for the instantaneous speed and absolute acceleration. Mean variance of instantaneous spiking rate for 20 ms windows explained in the population by a speed+absolute acceleration model was high (R^2 = 29.9±2.1%, n = 58). The mean variance explained individually by instantaneous speed or absolute acceleration is highly correlated across neurons (Figure 7E), as expected from the high degree of correlation between the two parameters. The coefficients for the two variables for all 58 neurons are shown in Figure 7F. These results confirm that acceleration and velocity transient (slips) drive a large fraction

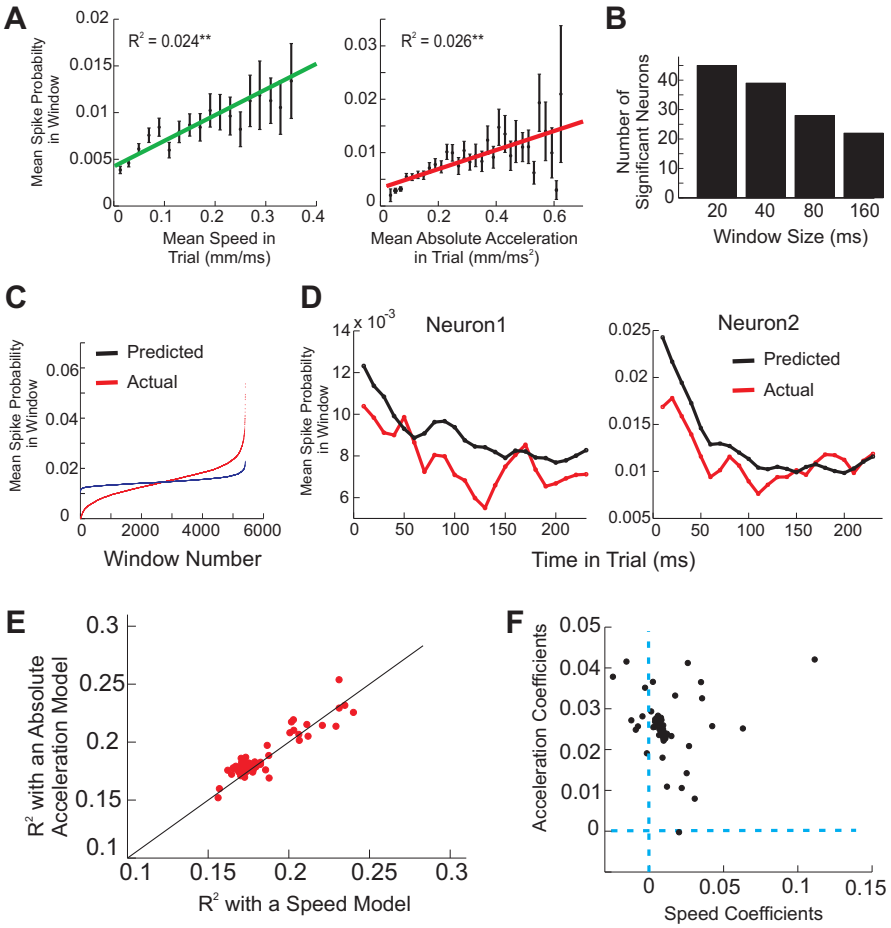

III.10 **Variance in instantaneous firing rate is well-predicted by kinematic parameters in the population.** (A) Mean Spike Probability/Window (window size = 20 ms) plotted against the mean speed (*Left*) and mean absolute acceleration (*Right*) in the window for a neuron with significant predictions with a multiple regression analysis. n = 45/58 neurons had significant predictions with a window size of 20 ms. (B) Number of neurons with significant regression for instantaneous spiking with a instantaneous speed+absolute acceleration model, plotted against the window size used. Predictions get poorer with increasing window size. (C) Observed and predicted spike probability/window(20 ms) with a speed+acceleration model for a neuron with significant regression. (D) Mean observed and predicted spike probability/window(20 ms) over the time course of a trial for 2 neurons. All variables and coefficients of prediction are means across trials. (E) Mean variance in instantaneous spike rate per trial explained by speed vs absolute acceleration. (F) Coefficients of regression for speed and absolute acceleration for the instantaneous model (computed as means across all trials).

of surface-driven spikes in S1, and can predict the temporal dynamics of spiking on a time scale $\sim$ 20 ms.

Slips are encoded by sparse, synchronous firing in small neuron ensembles

Slip-evoked spikes occurred only in a small proportion of slips, even for highly slip-responsive neurons (Figure 5B, SRI = 191.4; Figure 11A, SRI = 114.9). Across all 62 slip-responsive neurons, only 13.5$\pm$1.5% of slips drove any spikes ($\Theta = 0.32 mm/ms^2$), with single spikes being the pre-dominant response (12.2% slips have 1 spike response, 1.3% slips have >1 spike response). This was only a modest (but significant, $p < 0.05$) increase from spiking probability in pre-slip epochs (Figure 11B, mean number of background windows with spikes = 6.9 ± 0.9%, with 6% with 1 spike response and 0.9% with >1 spike response). For each neuron, we defined net spiking probability to a slip from slip-response PSTHs as the integrated response in the 20 ms after the slip minus the background response 20 ms before the slip. The strength of the population response across all neurons, including responsive and non-responsive neurons is illustrated by the distribution of net slip response probabilities (Figure 11C). For $\Theta = 0.32\ mm/ms^2$, the mean net spiking probability in the population was 0.09, indicating that a slip will evoke a net spike in 1/11 neurons. Net spike probability increase with amplitude (Figure 11C, Inset), but only modestly. Thus, at the single-neuron level, a slip response is a probabilistically sparse, single-spike signal on a sparse background, indicating that slips cannot be identified from the spiking activity of a single neuron.

To determine how detectable slips are in the neuronal activity in the population, we simulated the population response to a slip using neural response profiles drawn from all 90 recorded neurons. We first determined the population representation of a large slip ($0.8\ mm/ms^2$) of the principal whisker in the cor-

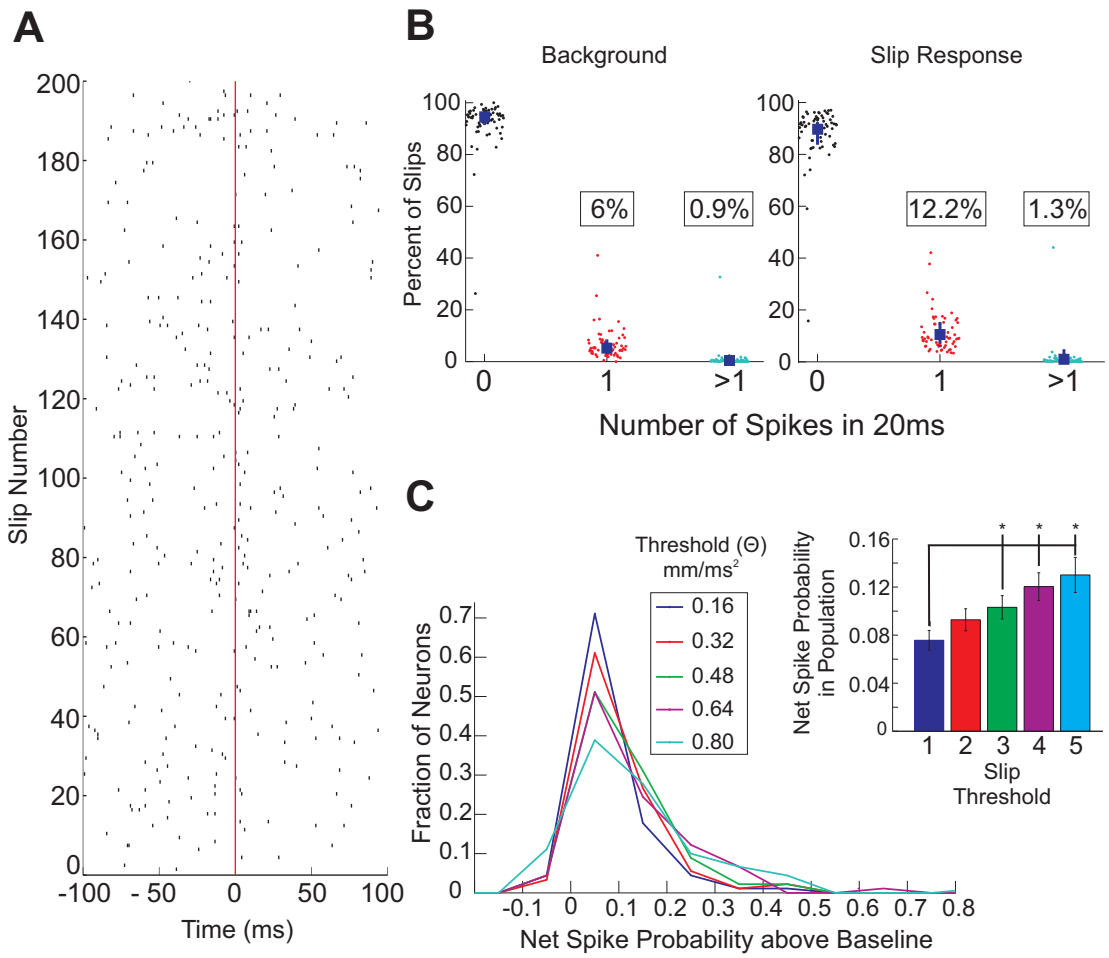

III.11 **Slip responses are sparse.** (A) Raster aligned to first slip for a neuron, illustrating sparse response. (B) Number of spikes in the 62 slip-responsive neurons before (Background, 20 ms) and after (Response, 20 ms) a slip, shown as percentage of total number of slips (Slip threshold 2 (Θ) - 0.32 mm/ms^2). (C) Net Spike Probability above background in the population of 90 neurons in response to a slip of of varying amplitudes. Slip Amplitude Thresholds vary from 0.16 mm/ms^2 to 0.8 mm/ms^2 (corresponding to Slip Threshold 1-5). *Inset* Mean net spike probability in the population of 90 neurons as a function of slip amplitude.

responding S1 column in small time windows (since slip responses are transient in time, the population response will be transient, implying synchrony). Given a simulation of n neurons, the ensemble response to each single slip in a time window of length t was constructed as follows (Figure 12A): Pick n random neurons from the experimental population of 90 with replacement. For each neuron,

use the integrated spiking probability from the slip-response PSTH (for slips of corresponding amplitude) in time t before and after the slip, to probabilistically generate a background and slip response (see Methods). Calculate the total number of spikes in the background and response window across all the neurons in the population. Repeat for 100 iterations. The major assumption of this model is the independence of responses between neurons, which is justified from the joint spiking probabilities observed in simultaneously recorded pairs of neurons in vivo (Figure 15C, D, see below).

Using this method, background and response distributions were generated for 100 iterations of the simulation (Figure 12B) for varying population sizes. An ROC analysis was used to quantify detectability of slips for each population size to give the population neurometric curve (Figure 13A). This analysis revealed that it takes ∼100 neurons in the population to detect slip events of amplitude 0.8 mm/ms^2 over the background with high efficiency ($> 99\%$). To estimate the optimal time scale of the population response in detecting a slip, we varied the time window for background and response, and generated a neurometric curve for each time window and population size (Figure 13B *Left*). A 20 ms time window was optimal for detecting slips for all population sizes (Figure 13B *Right*). Thus, the synchronous activation of ∼100 neurons S1 neurons at a time scale of ∼20 ms accurately encodes the occurrence of slip. With smaller slip sizes, more neurons are required (Figure 14). A population of ∼200 neurons can detect the smallest slip of amplitude 0.16 mm/ms^2 (with 95% accuracy).

Increase in synchrony in simultaneously recorded neurons.

The results of the simulation indicate that slips can be detected by synchronous activation of S1 neurons on a time scale of ∼20 ms. To test if slips do, in fact, increase synchrony on this time scale, we calculated, from measured spike

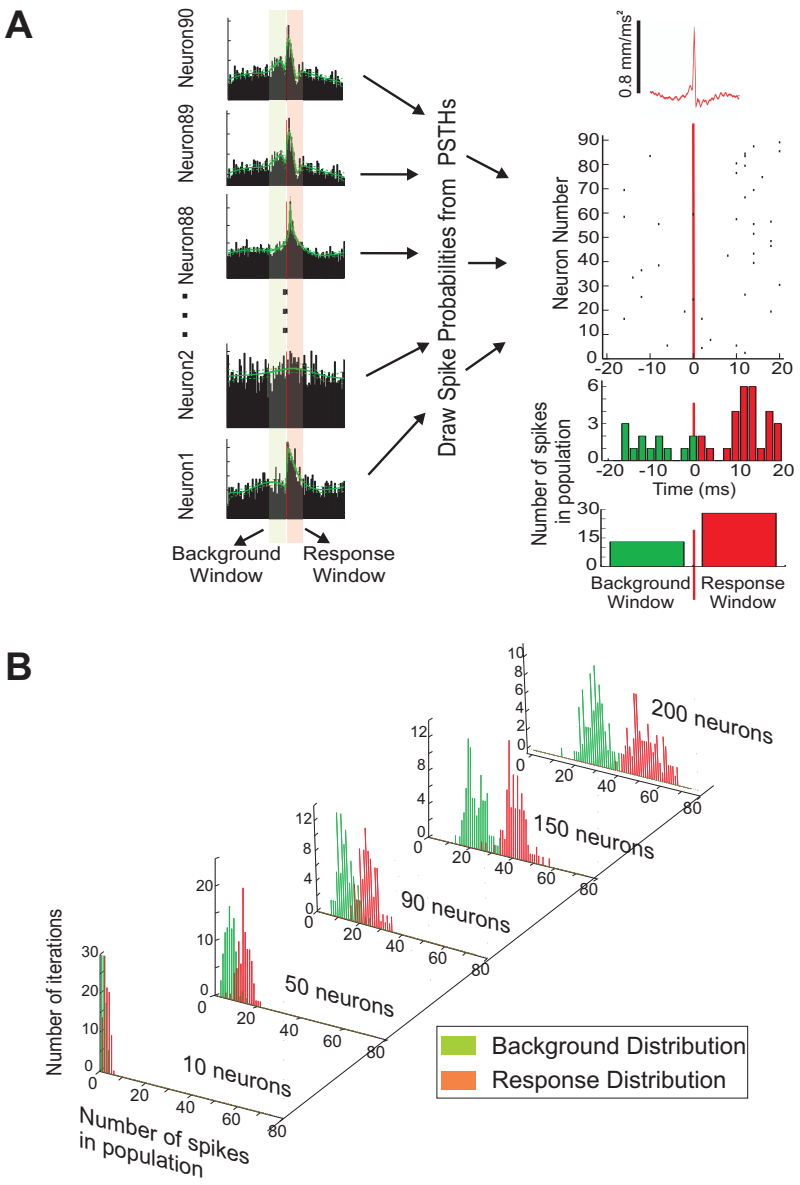

III.12 **Simulation of ensemble response to slip.** (A) Schematic of a single trial of the simulation of ensemble responses using n = 90 neurons and t = 20 ms. For each run, spikes were randomly generated from background and response windows in the slip-evoked PSTHs for each neuron in the population. Population responses were defined as the summed number of spikes in each simulated 20 ms window. Raster is for illustrative purposes - temporal dynamics within the window of length t were ignored. (B) Distribution of total number of spikes for varying population sizes in background and response windows for 100 iterations of the simulation.

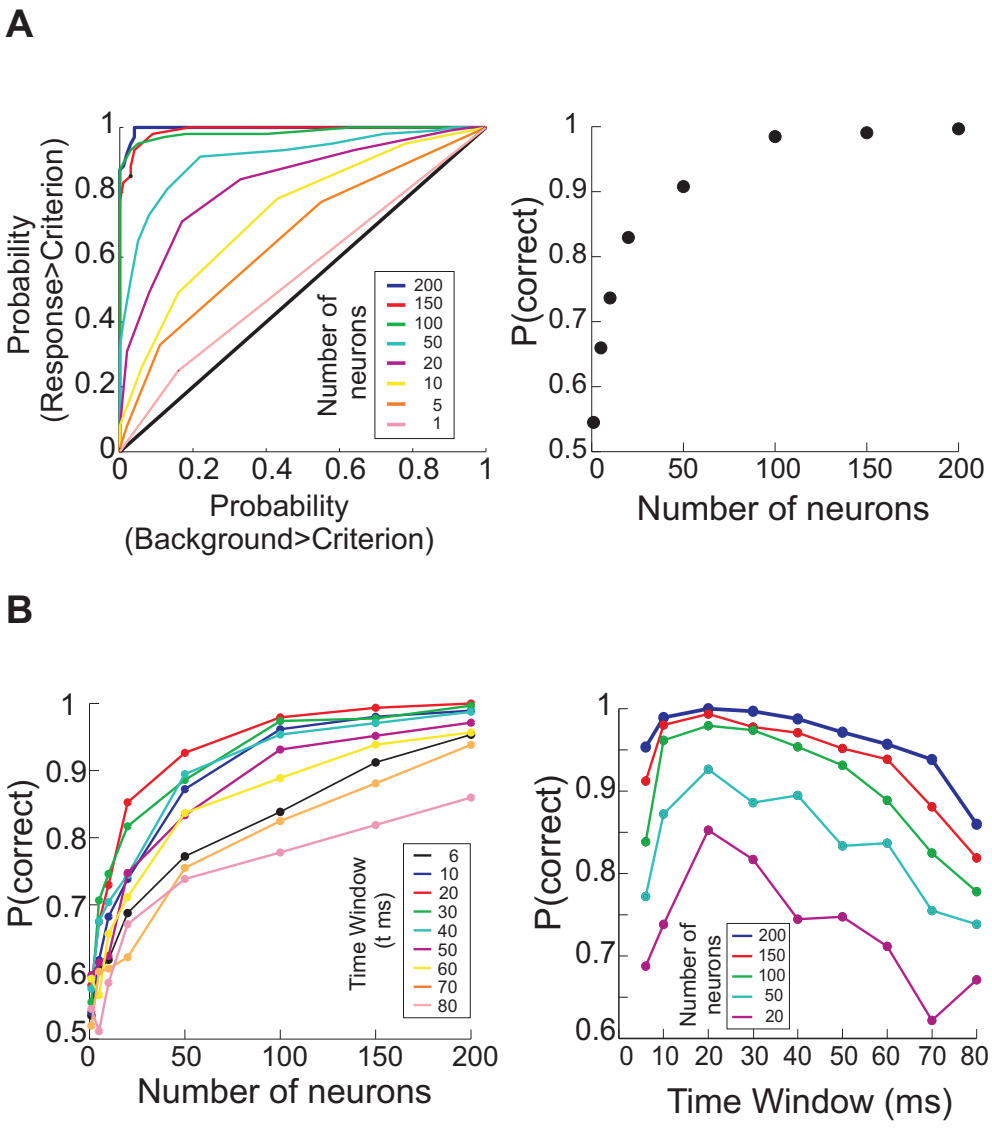

III.13 **Slips are encoded by sparse, synchronous firing in small neuronal ensembles.** (A) *Left* ROC curves for estimating the separation of background and response distributions for populations of different sizes. *Right* Performance of population in detecting a slip event (Probability(correct)) based on ROC analysis as a function of number of neurons in the population. (B) *Left* Population neurometric curves for varying time windows used for estimating the population response in the simulation. *Right* Performance of the ensemble response as a function of response time window used in the simulation.

trains, the joint spiking probability of pairs of simultaneously recorded neurons (n = 65) in response to slips vs background. Slips significantly increased synchronous

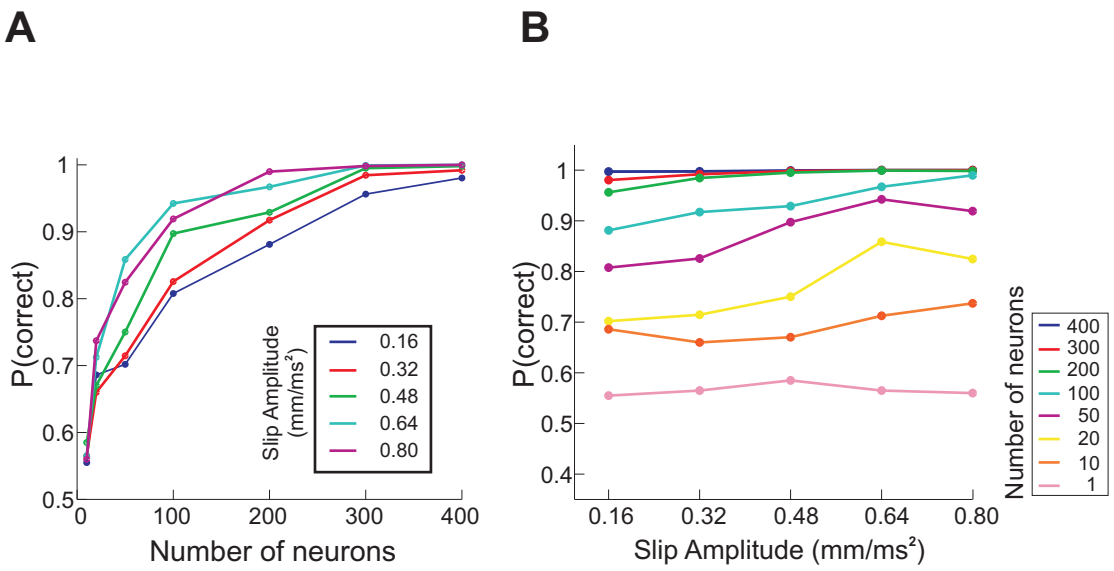

III.14 **Ensemble response to a slips of varying amplitudes.** (A) Population neurometric curves for varying slip amplitudes, using a 20 ms response window. (B) Performance of the population for increasing slip amplitudes.

activation of neuron pairs, and this effect increased with amplitude of slips (Figure 15A). This is consistent with the predicted synchrony code. Since the probability of activating a given neuron was low, the number of slips in which we saw co-activation of neurons was low. To test if more slips are detected by synchrony if a larger initial population is considered as predicted by the probabilistic simulation, we looked at synchrony in *any* pair or *any* triplet of neurons in response to a slip at recording sites with >= 3 simultaneously recorded slip-responsive neurons (n = 14 recording sites). Increase in synchrony was also seen in this analysis (Figure 15B), and co-activation of neurons was seen for a larger fraction of the slips. This analysis also showed that the observed joint spiking probability was equal or lower than the product of the individual spiking probabilities, indicating that neurons were not highly correlated (Figure 15C), justifying the assumption of independence in the simulation. Because the model assumes no correlation on the time-scale of slip responses, we measured the correlation coefficient of slip-induced activity on

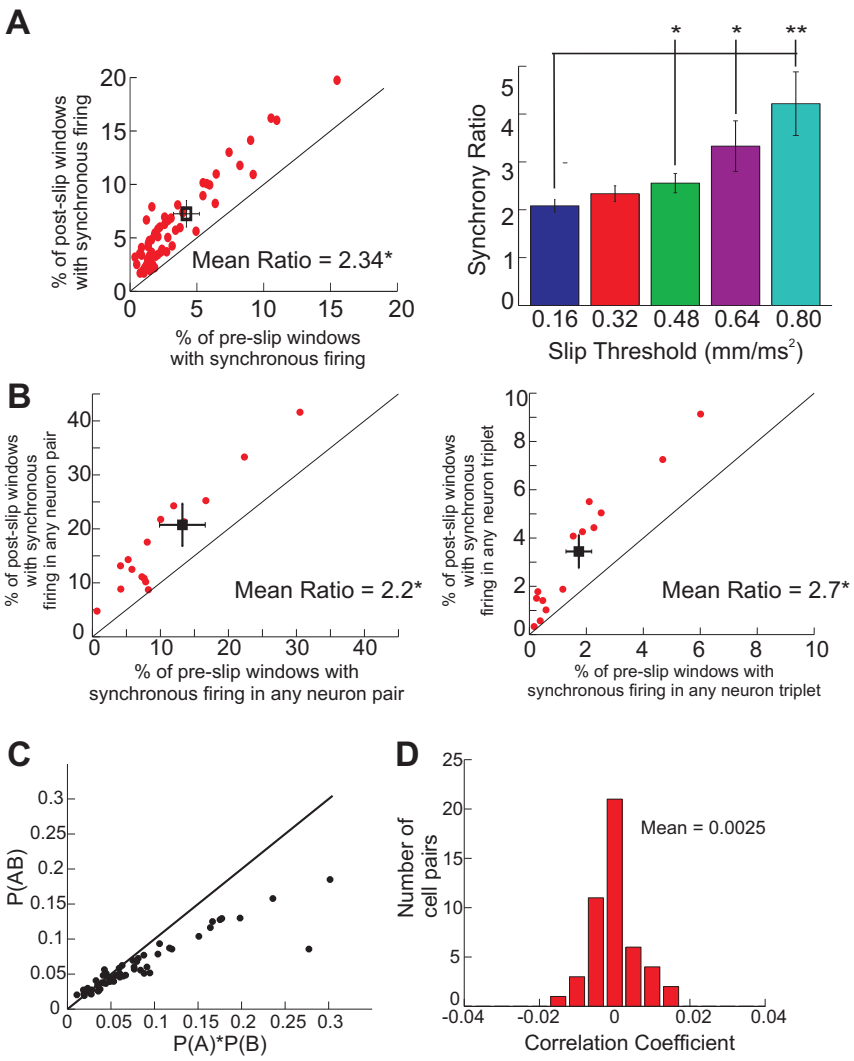

III.15 **Slips drive increase in synchrony in simultaneously recorded neurons.** (A) *Left* Increase in synchronous spiking in response to slips (Slip Threshold $\Theta = 0.32\ mm/ms_2$) in pairs of simultaneously recorded neurons. *Right* Increase in synchrony scales with amplitude of slips. (B) Increase in synchronous firing in *any* pair and triplet of neurons at a recording site in response to a slip. (C) Joint Spiking Probability (P(AB)) observed in response to a slip in pairs of neurons recorded simultaneously plotted against the expected probability if the neurons are independent. Points above the diagonal line indicate positive correlations between neuron pairs. (D) Correlation coefficient between pairs of neurons in the 20 ms slip response window calculated from the normalized JPSTH.

this time-scale between pairs of neurons from normalized JPSTHs (Joint Peri-Stimulus-Time Histograms, Aersten, et al., 1989; Narayanan and Laubach, 2006;

See Methods). The net correlation-coefficient measured in pairs of neurons was also low (Figure 15D), supporting the assumption of negligible correlations.

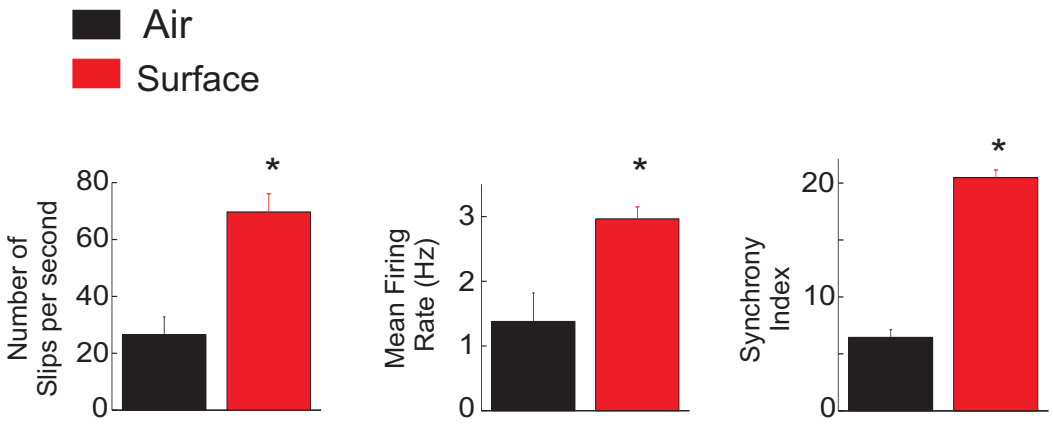

III.16 **Increase in synchronous firing during surface whisking.** Increase in number of slips, mean firing rate of neurons, and synchronous firing on a $\sim$ 20 ms time scale in pairs of neurons during surface whisking as compared to whisking in air.

The synchronous activation of neurons by slips suggests a possible mechanism for encoding of surface properties. Since slips are more frequent and larger (higher peak acceleration) on surfaces than air (Fig 1F, Wolfe et al., submitted), we predicted that in addition to an increase in mean firing rate of single neurons, there should also be an increase in synchronous activation in pairs of neurons on surfaces as compared to air. This prediction was confirmed in a subset of neurons (3 recording sites, n = 15 neurons, 22 neuron pairs, P150 surface and air) with interleaved trials on air and surface (Figure 16). Synchrony Index for pairs of neurons was defined as the percentage of 20 ms windows in which both neurons spiked (Methods). There was a significant increase in the Synchrony Index during surface whisking as compared to whisking in air. These results suggest that a sparse ensemble synchrony representation of slip-stick events in S1 may contribute to the perception of surface properties.

III.D Discussion

Our findings show that a) During natural, active whisking on surfaces, slip-stick events are one of the primary stimulus features encoded in S1. b) A sparse probabilistic ensemble representation of slip-stick motion of a whisker exists in the corresponding cortical column in S1 during active, natural sensation. Synchronous activity within small neuronal ensembles efficiently code for slips.

These results suggest that surface features are encoded by a population temporal code in S1. In our model, synchrony within sparse S1 population activity reflects the temporal sequence and amplitude of slip-stick events. We propose that as rats whisk across surfaces, whiskers slip-and-stick to create synchrony in S1 neurons, and one of the neural basis for the perception of surface palpation as against whisking in air is this sparse, synchronous population activity in S1.

Slips are fundamental features of whisking motion on surfaces encoded by sparse ensemble responses in S1

When rats are actively whisking across surfaces, we found that surface-driven spikes lead to an increase in firing rates of a majority of S1 neurons. The dominant feature of whisker motion on surfaces was slip-stick events, as has been reported before (Ritt, et al., 2008, Wolfe, et al., submitted). Slip-stick events, marked by discrete high-velocity and high-acceleration epochs, drove a precise, transient, low-probability response in a majority of S1 neurons in the barrel column corresponding to the whisker. PSTHs aligned to slip-stick events (identified as high-acceleration peaks) showed a short-latency, low-jitter peak in spiking probability. At the level of single neurons, slip responses are a sparse signal above the sparse background spiking of the neuron.

Although sparse, slips caused significant changes in firing rate in S1. The

magnitude of the slip response correlated significantly with the fractional change in firing rate on surfaces, implying that stronger the slip response, greater is the increase in firing rate. A quantitative comparison of slip-driven spikes to surface-driven spikes for all slip-responsive neurons in the population revealed that $> 30\%$ of surface-driven spikes are contributed by slips (adjusting for baseline spiking and the fractional increase in firing rate over spontaneous activity due to surfaces). This indicates that slips are one of the primary stimulus features being encoded in S1. These results are confirmed by results of a multiple regression analysis that explain variance of spiking activity of neurons as a function of kinematics of whisker motion. The instantaneous spiking rates of a majority of neurons are predicted by instantaneous values of whisker speed and absolute acceleration. Thus, when a slip occurs, it causes a rapid, transient change in velocity and acceleration, which increases the probability of spiking.

In addition to encoding timing of slips, S1 neurons also encode amplitude (the larger the acceleration of the slip, the greater the increase in spiking probability) and direction of slips. This is the first report of amplitude modulation and direction selective responses to transient, natural whisker stimuli in awake animals. We also show that ringing motion of whiskers serves to amplify the slip response by $\sim$40%.

Slip responses are sparse across the population. Only a fraction of slip occurrences lead to spikes in a neuron, and the response is predominantly single spikes. The signal-to-noise for single neurons is extremely low (even for neurons with high spontaneous rates, since slip responses are inversely correlated to mean firing rate). This leads to the question, what is the population response to a slip event; or in other words, how detectable is this sparse response above the background spiking activity in the population? Using a simulation of the experimentally observed slip responses and an ROC analysis to quantify separation of

signal and noise distributions, we estimate that synchronous activity in an initial population size of ∼100 neurons can efficiently detect slip events. The optimal time window of synchrony for detecting a slip event from the population activity is 20 ms, reflecting the time course of the slip response.

From the simulation results, we predicted that slips will drive synchronous activation of S1 neurons on a time scale of 20 ms. We confirmed this increase in synchrony in pairs and triplets of neurons recorded simultaneously. Moreover, slip-driven synchronous activity of neurons showed very little effect of correlations. Instead, neurons seem to be probabilistically activated, with the joint-spiking probability reflecting the probability of spiking of single neurons. Finally, since slips are more frequent on surfaces than air, we also predicted an increase in synchrony in S1 during surface whisking. In agreement to this prediction, we found that in addition to increase in firing rate, there was significantly more synchronous activation of neurons on surfaces as compared to air.

Neural activity in S1 underlying perception of surface properties

How surface properties are transduced into whisker kinetics and subsequently encoded in S1 has been a long-standing question. One hypotheses had proposed that resonant vibrations of whiskers during surface palpation underlies the encoding of surface properties ('resonance hypothesis', Neimark, et al., 2003; Andermann, et al., 2004). In contrast, the kinetic hypothesis posited that transient peaks in velocity driven by surface friction codes for surface properties (Arabzadeh, et al., 2005). Resolving this issue requires an understanding of what the fundamental features of whisker motion on surfaces are, and how they are represented in awake behaving animals.

Two recent studies had shown that whisker motion on surfaces in awake animals is dominated by transient slip-stick-ring events driven by friction. (Ritt

et al., 2008; Wolfe, et al., submitted). We show that slip-stick events are indeed one of the primary features represented in S1 and they drive significant firing rate changes during surface whisking. Our results, identifying slip-sticks events as fundamental elements, support the predictions of kinetic hypothesis (Arabzadeh, et al., 2005). In contrast, resonance vibrations were damped ("ringing motion") and served to amplify the slip response. This amplification of responses to elemental events by resonance vibrations has been suggested as a possible function of ringing (Hartmann, et al., 2003; Moore, 2004).

Our analysis estimated 30% as a lower bound for the contribution of slip responses to the total surface-driven increase in firing rate. The associated ringing motion further boosts the slip response. What other factors could be contributing to the increase in firing rate, and could they be additional features of whisker motion that are represented in S1? Bending of the whisker, which we were unable to measure in out setup, has been suggested to be a possibly important feature for coding of surface properties (Carvell and Simons, 1990). Bending provides a torque to the follicle and should result in a tonic response, as observed in the trigeminal ganglion (Szwed et al., 2006). Additional experiments measuring whisker motion in more than one dimension are needed to identify responses in S1 related to bending. In addition, we also frequently observed large responses at onset of whisking on surface. It is possible that initial contact with the surface is encoded by a strong phasic response, which we were unable to predict with slips. Regardless of what other features are encoded, slips, along with the associated ringing motion, account for a significant fraction of surface-driven spikes and are clearly a predominant feature of interest. Slip responses may also possibly underlie the increase in multi-unit activity seen in S1 in rats performing a roughness discrimination task (von Heimandahl, 2007)

A majority of physiology studies in reduced preparations have suggested

that neural responses in S1 to externally applied passive deflections are transient, low-probability, and preserve timing of inputs (Bruno and Simons, 2002; Pinto, et al., 2003; Brumberg et al., 2003; Gabernet, et al., 2005). The sparse representation of slips is in agreement with these predictions from anesthetized animals. The continuous motion of a whisker on a surface is decomposed into transient slip-stick events, which are represented with high precision in population activity in the corresponding cortical column in S1. Thus, precise spike timing, which is relevant for coding of transient sensory events with an explicit temporal structure, like contact with an object, is also crucial for perception of surface properties. In fact, coding of transient slip events could have, in principle, similar mechanisms to coding to contact (Szwed, et al., 2003; Curtis and Kleinfeld, submitted). In addition, sparse responses to slips are consistent with predictions that synapses are in a tonic depression state in vivo (Castro-Alamancos, 2004). A caveat to this finding is that rats were not discriminating textures in our task. It is possible that during discrimination, attention may modulate the sparse responses to slips.

These findings indicate that transient increases in synchrony of S1 neurons driven by slips could underlie the perception on surface properties, resulting in a population temporal code for spatial properties. Thus, the high temporal resolution of the neural pathways of the whisker system also possibly underlie the perception of spatial information.

Mechanism for coding of surface roughness

The representation of surface roughness (texture) is currently a topic of intense interest. Rats can discriminate between fine differences in surface roughness, with an acuity that rivals that of the human fingertip (Guic Robles, et al., 1989, Carvell and Simons, 1990). Our results also suggest a possible mechanism for coding of surface roughness. Slip-sticks events that we observe are similar to

velocity transients seen during artificial whisking on surfaces. The temporal structure of velocity transients has been shown to be unique across repeated artificial whisks, and has been suggested to underlie a code for texture ('kinetic hypothesis', Arabzadeh, et al., 2005). Recently, it has been proposed that the amplitude of slip-stick events can also code for texture in awake animals trained to whisk on surfaces (Wolfe, et al., submitted).

Our results suggest a novel synchrony coding scheme for texture roughness based on slip-stick events. Since S1 population activity reflects both, the temporal sequence and amplitude of slip-stick events with a synchrony code, we propose that texture identity is encoded by synchrony in S1. If the temporal structure of slip-stick events varies with texture, as has been proposed by the kinetic hypothesis, then the temporal dynamics of synchronous population activity in S1 will code for texture. If the amplitude of slip-stick events varies with texture in discriminating animals, then the degree of synchrony in S1 will code for texture (since synchrony scales with amplitude). The kinetic hypothesis requires that kinetic structure is unique for a texture and is repeatable across trials. There has so far been no evidence of repeatability of the temporal structure of slip-stick events in awake behaving animals. However, it is conceivable that in animals trained to discriminate textures, the whisking motor strategy is controlled so that the structure of slip-stick events is repeatable from whisk-to-whisk, and animals integrate this information across whisks to identify textures. Future experiments monitoring S1 activity in awake, discriminating animals should resolve the issue of which code is actually used.

In either coding scheme, texture identity can be decoded by reading out population activity on a time scale of 20 ms. This can be optimally achieved downstream of S1 by neurons with narrow temporal integration windows and high degree of convergence of S1 inputs. This decoding strategy is similar to the one

shown to exist in the locust olfactory system (Laurent, 2002). In the case of coding with amplitude of slip-stick events, this would lead to a firing rate code for texture in the downstream neurons. In case of the temporal structure of slip-stick events, pattern of spiking in the downstream neurons would be the code for texture. With either coding strategy, discrimination is possible with a single whisker. However, performance will be better with multiple whiskers (as has been observed behaviorally) due to integration of information across multiple columns.

Sparse representation of natural inputs in S1 in awake-behaving animals

Our data and simulation results also demonstrate that slips have a sparse representation in S1. Sparse representations in barrel cortex have been proposed based on low probability responses seen in anesthetized animals (Brecht, 2006). To our knowledge, this is the first identification of a sparse representation of natural sensory inputs in an active behaving animal in primary sensory cortex. Sparse coding, which posits that neurons encode sensory information using a small number of active neurons at any given point in time, has been proposed as a general strategy for representing information in the brain. (Olshausen and Field, 2004). Our results point to the existence of a "probabilistic population sparseness" in S1 during surface whisking. Neurons fire probabilistically when a slip occurs, and few neurons in the population are active at a given instant (a net spiking probability of 0.1 implies that $\sim$10% of neurons above the number of spontaneously active neurons in the barrel column respond to slips). However, there are no selectively large responses to a subset of stimuli.

This sparse representation is different from sparse coding strategy that has been suggested for the primary visual cortex (lifetime sparseness; Vinje and Gallant, 2000). In this scheme, since neurons are very stimulus selective, they

respond only when their preferred stimulus occurs in natural scenes. As a result, each neuron should respond very rarely, but when it does respond, it produces responses whose magnitudes are relatively large. Lifetime sparseness differs from population sparseness, which requires that only a small subset of the population of coding neurons is active in response to a given stimulus (relating to the instantaneous response of the population; Willmore and Tolhurst, 2001). For the whisker system, the number of stimulus dimensions is probably low, as compared to the visual system. Hence, stimulus selectivity is not very well-defined. For the particular case of surface properties (especially 'roughness'), slips can convey relevant information. Although it is possible that neurons may be selective to particular kinds of slips, or to the combination of phase and slip, the population synchrony coding strategy that we suggest can integrate over all these differences to represent the surface property of interest.

A sparse coding strategy is supposed to confer several advantages, such as increased storage capacity for associative memories, energy efficiency and simplification of complex representations for decoding mechanisms (Olshausen and Field, 1996; 2004). In addition, in our model, synchrony coding in the population creates a high signal-to-noise from sparse signals at the single-neuron level. Also, few spikes are required to encode a slip, since slip responses are well-separated from background activity in a sub-population of just 100 neurons. Since there are $\sim$8500 neurons in a barrel column (de kock, 2007; $\sim$5000 neurons in L4 and L5), this number is remarkably low.

These results add to a growing body of evidence that it takes a small number of neurons to drive perception and behavior in the rat whisker system (Houweling and Brecht, 2008; Huber, et al., 2008). Using selective micro-stimulation of a small number of neurons in S1 barrel cortex, one study (Huber, et al., 2008) demonstrated that rats can detect the simultaneous activation of a few hundred

neurons. Our results represent the sensory perception side of this sparseness. Neurons in S1 fire sparsely in awake behaving animals and the occurrence of a slip can be detected by $\sim$100 neurons. The synchronous activation of a small subset of neurons is sufficient to identify natural sensory inputs. Simultaneous spiking of a small sub-population of neurons is thus a very salient signal and can drive perception and behavior.

Our results also suggest that the key element of a sensory code in such sparse representations is precise timing of spikes and synchrony in the population. Many studies have revealed various cellular mechanisms for preserving temporal information in the barrel pathway (Beierlein et al., 2003; Gabernet, et al.,2005; Bruno and Sakmann, 2006). Precise timing of spikes may underlie a general coding strategy for representation of information in the whisker system. Our proposed coding strategy also relies on dynamics of population activity, rather than static receptive field properties of single neurons. The ensemble activity can be thought to be a part of an ongoing transformation of stimulus related responses to help further processing (Laurent, 2002). Given our observation of sparse population representation of slips in S1, this raises interesting questions about representation of slips in the initial stages of processing (in the trigeminal ganglion and VPM thalamus), and decoding of this representation in subsequent stages of processing.

In closing, the whisker system is being considered as a model system for integrating molecular, cellular and systems approaches to the study of neural function (Brecht, 2007; Petersen, 2007). Despite seminal studies on the physiology of the whisker system, very little is known about sensory processing due to the active nature of this system. Our results identify key stimulus features and coding strategies in the awake and active animal, and provide a starting point for further investigation of systems-level processing in the barrel pathway.

III.E Experimental Procedures

All procedures were approved by the UCSD Institutional Animal Case and Use Committee.

Behavior

A total of 12 adult female Long-Evans rats were used in this study. Rats were trained using operant conditioning techniques using water-deprivation, and received water rewards (50 μl) during behavioral training (1 hour per day) and during a 1 hour ad lib drinking period following each behavioral training session. Water was freely available on weekends. Rats on this regimen were healthy and alert, and gained weight daily. The detailed behavior training and whisker measurement procedure has been reported previously (Wolfe, et al., submitted). Briefly, rats were trained in stages to place their nose in a small port (nosepoke) and whisk across surfaces or in air to get a water reward (Figure 1). The behavioral apparatus consisted of an outer reward chamber containing a solenoid-gated drink port, and an inner measurement chamber containing the nosepoke, texture stimuli, and whisker motion recording system. Nosepoke occupancy was reported using a photo-transistor in the nosepoke port and gross whisking was assessed by four phototransistors that generated voltage pulses when the whiskers passed over them. The number of photo-transistor pulses required to trigger the noise cue and drink port water delivery was gradually increased until rats were whisking in the nose poke for $\sim$300 ms. Surfaces were 6$\times$6 cm sandpapers, glued to an aluminum plate, and positioned in the whisking path of the right whiskers 5 mm from the whisker tips, parallel to the face. Surfaces were mounted on a 4-arm plexi-glass holder attached to a stepper motor (Oriental Motor, PK264B1A-SG10). Trials were separated by the rat retreating to the reward chamber to collect the wa-

ter reward, during which stimulus could be removed for inter-leaved trials in air. Training and recording procedures were controlled by custom routines in Labview (National Instruments, Austin, TX, USA).

Whisker Measurements

The detailed whisker measurement procedure has been reported previously (Wolfe, et al., submitted). Briefly, whisker motion was measured in one dimension by casting shadows of the whiskers onto a linear CCD imaging array. The light source was a diode laser (670 nm), positioned above the rat and focused into a collimated line 60 mm long and 1 mm wide, using two cylindrical lenses rotated 90^o from one another (Figure 1C). Below the whiskers, a third cylindrical lens focused whisker shadows onto the linear CCD array (Fairchild imaging, CCD 133AEDC, 1060 elements, 13 μm width per element). The output of every other CCD element was sampled at 4 kHz frame rate using custom built electronics (UCSD Physics electronics shop) and a National Instruments data acquisition card (PCI 6111). Voltage traces from the array were stored and processed offline as described before to determine whisker position. Whisker position was recorded for 1500 ms starting with nosepoke onset. For each trial, analysis was restricted to the epoch during which the rat remained in the nosepoke. If a whisker transiently left the imaging plane, implying loss of contact with surface, whisker motion was only analyzed up to that point.

Surgery and Recordings

Rats were implanted using a chronic multielectrode micro-drive (Venkatachalam, et al., 1999) in the left hemisphere. The center of the craniotomy was targeted over the macro-vibrissa region of posteromedial barrel subfield (PMBSF) in S1, 5.5 mm lateral and 2.5 mm caudal to bregma. Implantation procedure

followed Fee, et al., 1997. Briefly, surgery was performed using sterile technique under ketamine-xylazine and isofluorane anesthesia. Anesthesia was induced using ketamine/xylazine (90 and 10 mg/kg of body weight, respectively, i.p). One dose of supplemental ketamine (20 mg/kg) was administered after $\sim$ 1 hour, and anesthesia was maintained using isofluorane for the remainder of the surgery. Isofluorane concentration (0.5%-4%) was continuously adjusted to maintain the depth of anesthesia. The surgery was divided into 2 parts, separated by 2-4 days. On the first day, a head-bolt for stability was affixed with dental cement on the skull. 6 anchor screws (which were grounded) were implanted in the skull, and a 0.5 mm silver reference wire was inserted $\sim$2 mm deep in the opposite hemisphere from the craniotomy. The second day consisted of the craniotomy, fixation of the implant, and insertion of tetrodes. Tetrodes were lowered through intact dura by applying vacuum (20 mm Hg) through the lower chamber of the microdrive till spikes were observed. Positioning of tetrodes within the barrel field was hand-mapped by stimulating whiskers, and whiskers were trimmed to leave only 1 macro-vibrissa intact. A solenoid valve was used to create air-puffs for stimulation of whiskers. Buprenorphine (0.05 mg/kg) was administered for postoperative analgesia. Rats were allowed to recover for 5-7 days before resuming water restriction and starting the recordings. Layer positioning was estimated by depth and later confirmed with histology. At the end of the experiment, 3-4 lesions were left along the electrode track as the tetrode was retracted. 100 μm across-row coronal sections (45^o to bregma-lambda line) were obtained and stained with cytochrome oxidase to recover the electrode track within the barrel field and to estimate depth of recordings. Implantation and recordings were successful in 5/12 animals, and simultaneous whisker and neural data during surface whisking were obtained in 3 animals.

The micro-drive contained upto 4 tetrodes for extracellular recordings.

Each tetrode was independently moveable through a guide tube array arranged in a hexagonal pattern with a spacing of 450 μm. Individual tetrodes consisted of four twisted polyimide-coated nichrome wires (H.P. Reid, Inc., Palm Coast, FL; single-wire diameter 12.5 μm, gold plated to 0.2-0.3 $M\Omega$ impedance). Microwires were soldered into a 10-pin connector (Samtec) attached to the skull. Neural signals were amplified (20x gain) and impedance buffered using a 16-channel head-mounted headstage amplifier (Plexon Instruments HST/8o50-G20). Headstage output was transmitted via twisted thin gauge wires to a second amplifier and bandpass filtered (Plexon Instruments PBX2/16sp-G50; 50x gain, 0.3-8 kHz band-pass). Amplifier output was digitized at 32 kHz (National Instruments PCI 6259). The spike and whisker data acquisition were performed on separate, synchronized data acquisition cards using custom code in Labview. Recordings were obtained for 2-3 weeks with electrode depths adjusted on each recording day so as to sample an independent population of cells across sessions. Multiple single-units were isolated offline using a semi-automated spike sorting algorithm (Fee, et al., 1996) implemented in Matlab by S. Mehta. A custom graphical user interface (S. Jadhav) was used to run the algorithm, evaluate the clusters in multiple dimensions, and manually improve the clustering output of the algorithm. Briefly, spike waveforms were obtained by detecting threshold crossings (3-7 s.ds above noise) on either of the 4 channels of the tetrode. 1 ms of data (32 sample-points at 32 kHz) was saved for each waveform, with spike timing defined with 0.1 ms resolution at threshold crossing. Waveforms were de-jittered, over-clustered using hierarchical clustering, and the clusters were then aggregated based on an energy and spike-timing criterion. Algorithm steps were continuously monitored using the GUI and manual re-clustering of data was performed for all recording sites by simultaneously evaluating clusters in multiple dimensions (amplitude, principal components, energy). Cluster quality was evaluated using an ISI criterion ($< 0.5\%$ violations of a 1 ms

refractory period) and isolation distance (Isolation distance > 20 in 8 dimensions, Harris, et al., 2001). In a subset of the recordings, clusters were also evaluated using the Mclust software (A.D. Redish).

Neuronal and Whisker Data

All data analysis was performed using MATLAB. For each recording session, whisker data, spike timing data for all single-units and behavior timing signals were stored in a common structure. Whisker data had a temporal resolution of 0.25 ms, and spike timing was saved with a resolution of 0.1 ms. Spike Rasters and PSTHs corresponding to whisker data were binned at 1 ms. All error-bars are s.e.m unless otherwise noted.

Whisker Motion

Retraction and protraction epochs were identified from peaks and troughs in low-pass filtered (20 Hz) whisker position data. For identifying slips, velocity and acceleration of whisker motion was calculated. Slip-sticks were identified as rapid acceleration transients for various acceleration thresholds $>= 2$ s.d.s above mean acceleration, in both the positive and negative direction. Acceleration transients were required to have a peak above threshold before returning below threshold. An interval of 2 ms was imposed between transients to unambiguously identify slips. For identifying first slips, an inter-slip-interval of 20 ms was used. Results were qualitatively similar for an inter-slip-interval of 10 ms and 30 ms. For each slip, location within whisking cycle (protraction and retraction), waveforms, and amplitudes of velocity and acceleration peaks were calculated. For all quantifications of slip responses, a threshold of 0.32 mm/ms^2 was used, unless otherwise specified. For quantifying sparseness of slip responses and simulating the population response, we divided slips into 5 cumulative amplitude ranges, named Slip

Threshold 1-5, starting with 0.16 mm/ms^2 (2 s.d.s above mean acceleration) and increasing in steps of 0.16 mm/ms^2 till the largest amplitude, Slip Threshold 5 = 0.8 mm/ms^2.

Firing Rate Modulation

For firing rate modulation plots (Figure 4), spike data was binned in 25 ms or 50 ms bins. The instantaneous firing rate plots in Figure 4B were constructed by filtering the raster data using a Gaussian filter of sigma 50 ms. For assessing firing rate modulation during surface whisking, PSTHs were aligned either to onset of nosepoke or onset of whisking. Nosepoke onset was stored as a behavior epoch using the nosepoke photo-transistor pulse. Whisking onset was defined when the whisker first appeared in the CCD trace during the nosepoke and whisking period. Lick onset was defined when the lick port photo-transistor was activated. Neurons were classified by comparing firing rates during whisking epochs (range = 125 ms - 651 ms, mean = 340$\pm$42 ms) to a pre-whisk baseline (200 ms) across all trials (t-test, $p < 0.05$).

Slip Response PSTHs

Slip-response PSTHs were constructed by aligning spike rasters to timing of slips as defined by acceleration transients (rounded to 1 ms resolution), 100 ms before and after a slip (All Slips or First Slips). Slip-aligned rasters were binned at 2 ms, and PSTHs were generated either in instantaneous firing rate units or in units of spike probability (average number of spikes/bin for a slip). To quantify slip-response PSTHs, a BARS (Bayesian Adaptive Regression Splines; Kass, et al., 2003) algorithm was used generate a fit to each All-slip-PSTH with confidence intervals. The algorithm also determined the existence of a significant peak in the fit. Slip Response Index (SRI) was defined as the peak firing rate following a slip

adjusted for baseline firing rate in the first 50 ms of the All-Slips-PSTH (Figure 5E). SRI was >=25 for slip-responsive neurons. Latency of slip response was defined as the timing of the peak, and jitter was the Full-Width-at-Half-Maximum (FWHM) of the fit. For amplitude plots (Figure 7A), slip-response PSTHs were calculated for increasing acceleration thresholds (finely spaced by 0.032 mm/ms^2). The PSTHs, in units of spiking probability, were used to generate the cumulative amplitude response plot. The threshold for a neuron was the lowest amplitude at which a significant peak response was seen. The amplitude gain was the average change in peak response for 0.1 mm/ms^2 acceleration steps. For direction-selectivity, slip-ring analysis and position encoding, a t-test was used for assessing statistical significance ($p < 0.05$). Modulation depth for direction and position selective neurons was calculated as the difference in spiking probability for the two variables, normalized to mean of the spiking probability for both variables (Modulation Depth = (x-y)/mean(x,y), where x and y are the spiking probabilities for either direction or whisking epoch.)

Slip Driven Spikes

To compare the number of slip-driven spikes to total spikes, only the 1st 250 ms from trial onset of all trials with trial length >= 250 ms was considered. For each trial, the total number of spikes in the trial was compared to the number of spikes in a 20 ms window after First slips in that trial. In a process analogous to boot-strapping, a random number of time-points equivalent to the number of first flips was selected for each trial. The number of spikes in 20 ms windows after these random time-points (the windows had to be non-overlapping with slip-response windows) was the baseline/non-slip spiking estimate for the trial.

Multiple Regression

We used the 1st 250 ms of all trials with trial length >= 250 ms for the multiple regression analysis. Only neurons with >= 20 trials of sufficient length were included in this analysis. The regression models were as described in text. Regression was also computed for individual variables (either position, speed, or acceleration). The regression outputs were the coefficients of the predictor variables, the fraction of variance explained, and whether the variance explained was significant or not. For regression with instantaneous parameters, variables were computed in sliding windows of different sizes (overlapping by window-size/2). For computing number of neurons with significant predictions with varying time windows, dynamics within trials were not considered. For predictions of spiking probability within trials, regression was computed for each trial, and an average was taken across all trials. The average values of coefficients were used to calculate mean predicted firing rate within a trial.

Simulation

The simulation was performed using a Monte Carlo procedure for numerical implementation of observed spike probabilities (Britten et al., 1992). In each iteration, a spike was generated in a given bin for a neuron by drawing a random number and comparing it to the spike probability in the corresponding bin of the slip-response PSTH for the neuron. If the probability was greater than the random number, a spike was generated. The separation of the background and response distributions was calculated using ROC analysis. A criterion number of spikes was varied from 0 to maximum observed in the simulation, and for each criterion, the probability that the number of spikes in the background and the response window was greater than criterion was calculated. The separation of the two distributions was given by the area under the ROC curve. The same procedure was repeated

for different time windows and different slip amplitudes (Slip Threshold 1-5).

Synchrony and Correlation in Data

Joint Spiking Probability was calculated for simultaneously recorded neurons (pairs and triplets) in 20 ms windows before and after a slip. For pairs of neurons, to prevent under-sampling issues due to the extremely low probabilities involved, analysis was restricted to pairs which had >= 25 spikes in the joint probability (Figures 15 A, C and D). Significance was analyzed with a t-test ($p < 0.05$). For synchrony analysis of neurons during whisking in air and surfaces, joint spiking probability was calculated in 20 ms sliding windows with 10 ms overlap for all trials. The Synchrony Index was the percentage of windows which had co-activation of neurons. The correlation coefficient (c.c.) between slip responses (20 ms after a slip) for pairs of neurons was calculated from the Joint-Peri-Stimulus-Histogram (JPSTH). The c.c. was the mean of the cross-diagonal terms of the normalized JPSTH (Aersten, et al., 1989; Narayanan and Laubach, 2006).

Acknowledgement

This chapter, in full, is being prepared for publication, Jadhav S.P., Wolfe J.H., Feldman, D.E., untitled. The dissertation author is the primary investigator and first author of this paper.

III.F References

Aertsen AM, Gerstein GL, Habib MK, Palm G (1989). Dynamics of neuronal firing correlation: modulation of "effective connectivity". J Neurophysiol 61: 900-17.

Andermann ML, Ritt J, Neimark MA, Moore CI (2004). Neural correlates of vibrissa resonance; band-pass and somatotopic representation of high-frequency stimuli. Neuron. 42: 451-63.

Anjum F, Turni H, Mulder PG, van der Burg J, Brecht M (2006). Tactile guidance of prey capture in Etruscan shrews. PNAS USA. 103: 16544-16549.

Arabzadeh E, Petersen RS, Diamond ME (2003). Encoding of whisker vibration by rat barrel cortex neurons: implications for texture discrimination. J Neurosci 23: 9146-9154.

Arabzadeh E, Zorzin E, Diamond ME (2005). Neuronal encoding of texture in the whisker sensory pathway. PLoS Biol. 3: e17.

Beierlein M, Gibson JR, and Connors BW (2003). Two dynamically distinct inhibitory networks in layer 4 of the neocortex. J Neurophysiol 90, 2987-3000.

Bensmaia SJ, Craig JC, Johnson KO (2006). Temporal factors in tactile spatial acuity: evidence for RA interference in fine spatial processing. J Neurophysiol 95: 1783-91.

Berg RW, Kleinfled D (2003). Rhythmic whisking by rat: retraction as well as protraction of the vibrissae is under active muscular control. J Neurophysiol 89: 104-17.

Brecht M, Preilowski B, Merzenich MM (1997). Functional architecture of the mystacial vibrissae. Science. 84: 81-97.

Brecht M (2006). Cortical commands in active touch. Novartis Found Symp. 270: 38-48

Brecht, M (2007). Barrel cortex and whisker-mediated behaviors. Curr Opin Neurobiol 17: 408-416.

Brecht M, Sakmann B (2002) Whisker maps of neuronal subclasses of the rat ventral posterior medial thalamus, identified by whole-cell voltage recording and morphological reconstruction. J Physiol 538: 495-515.

Britten KH, Shadlen MN, Newsome WT, Movshon JA (1992). The analysis of visual motion: a comparison of neuronal and psychophysical performance. J Neurosci 12: 4745-65.

Brumberg JC, Khatri V, Pinto DJ, Simons DJ (2003). Cortical columnar processing in the rat whisker-to-barrel system. J Neurophysiol 82: 1808-1817.

Bruno RM, Simons DJ (2002). Feedforward mechanisms of excitatory and inhibitory cortical receptive fields. J Neurosci 22: 10966-10975.

Bruno RM, Khatri V, Land PW, Simons DJ (2003). Thalamocortical angular tuning domains within individual barrels of rat somatosensory cortex. J Neurosci 23: 9565-9574.

Carvell GE, Simons, DJ (1990). Biometric analyses of vibrissal tactile discrimination in the rat. J Neurosci 56: 2638-2648.

Castro-Alamancos, M A (2004). Absence of rapid sensory adaptation in neocortex during information processing states. Neuron 41: 455-464.

Celikel T, Szostak VA, Feldman DE (2004). Modulation of spike timing by sensory deprivation during induction of cortical map plasticity. Nat Neurosci 7: 534-41.

Curtis JC, Kleinfeld D. submitted.

de Kock CP, Bruno RM, Spors H, Sakmann B (2007). Layer- and cell-type-specific suprathreshold stimulus representation in rat primary somatosensory cortex. J Physiol 581: 139-54.

Fee M, Mitra PP, Kleinfeld D (1997). Central versus peripheral determinants of patterned spike activity in rat vibrissa cortex during whisking. J Neurophysiol 78: 1144-9.

Fee MS, Mitra PP, Kleinfeld D (1996). Automatic sorting of multiple unit neuronal signals in the presence of anisotropic and non-Gaussian variability. J Neurosci Methods 69: 175-88.

Feldman DE, Brecht M (2005). Map plasticity in somatosensory cortex. Science. 310: 810-815.

Ferezou I, Bolea S, Petersen, CC (2006). Visualizing the cortical representation of whisker touch: voltage-sensitive dye imaging in freely moving mice. Neuron 50: 617-629.

Fritz JB, Elhilali M, David SV, Shamma SA (2007). Adaptive changes in cortical receptive fields induced by attention to complex sounds. J Neurophysiol 98: 2337-2346.

Gabernet L, Jadhav SP, Feldman DE, Carandini M, Scanziani M (2005). Somatosensory integration controlled by dynamic thalamocortical feed-forward inhibition. Neuron 48: 315-27.

Guic-Robles E, Valdivieso C, Guajardo G (1989). Biometric analyses of vibrissal tactile discrimination in the rat. J Neurosci 56: 2638-2648.

Harris KD, Hirase H, Leinekugel X, Henze DA, Buzski G (2001). Temporal interaction between single spikes and complex spike bursts in hippocampal pyramidal cells. Neuron 32: 141-9.

Hartmann MJ, Johnson NJ, Towal RB, Assad C (2003). Mechanical characteristics of rat vibrissae: resonant frequencies and damping in isolated whiskers and in the awake behaving animal. J Neurosci 23: 6510-9.

Houweling AR, Brecht M (2008). Behavioural report of single neuron stimulation in somatosensory cortex. Nature 451: 65-68

Huber D, Petreanu L, Ghitani N, Ranade S, Hromdka T, Mainen Z, Svoboda K (2008). Sparse optical microstimulation in barrel cortex drives learned behaviour in freely moving mice. Nature 451: 61-4.

Hutson KA, Masterton, RB (1986). The sensory contribution of a single vibrissa's cortical barrel. J Neurophysiol 56: 1196-1223.

Itoh H, Nakahara H, Hikosaka O, Kawagoe R, Takikawa Y, Aihara K (2003). Correlation of primate caudate neural activity and saccade parameters in reward-oriented behavior. J Neurophysiol 89:1774-1783

Jones LM, Depireux DA, Simons DJ, Keller A (2004). Robust temporal coding in the trigeminal system. Science 304: 1986-1989.

Kass RE, Ventura V, Cai C (2003). Statistical smoothing of neuronal data. Network 14: 5-15.

Kleinfeld D, Ahissar M, Diamond, ME (2006). Active sensation: insights from the rodent vibrissa sensorimotor system. Curr Opin Neurobiol 17: 408-416.

Knutsen PM, Pietr M, Ahissar E (2006). Haptic object localization in the vibrissal system: behavior and performance. J Neurosci 26: 8451-8464.

Krupa DJ, Wiest MC, Shuler MG, Laubach M, Nicolelis MA (2006). Visualizing the cortical representation of whisker touch: voltage-sensitive dye imaging in freely moving mice. Neuron 50: 617-629.

Lau B, Glimcher PW (2008). Value representations in the primate striatum during matching behavior. Neuron 58: 451-63.

Laurent G (2002). Olfactory network dynamics and the coding of multidimensional signals. Nat Rev Neurosci 3: 884-895

Mehta SB, Kleinfeld D (2004). Frisking the whiskers: patterned sensory input in the rat vibrissa system. Neuron 141: 181-184.

Mehta SB, Whitmer D, Figueroa, Williams BA, Kleinfeld D (2004). Active spatial perception in the vibrissa scanning sensorimotor system. PLoS Biol. 5: e15.

Minnery BS, Bruno RM, Simons DJ (2003). Response transformation and receptive-field synthesis in the lemniscal trigeminothalamic circuit. J Neurophysiol 90: 1556-1570.

Moore CI (2004). Frequency-dependent processing in the vibrissa sensory system. J Neurophysiol 91: 2390-9.

Narayanan NS, Laubach M (2006). Top-down control of motor cortex ensembles by dorsomedial prefrontal cortex. Neuron. 2006 52: 921-31.

Neimark MA, Andermann ML, Hopfield JJ, Moore CI (2004). Vibrissa resonance as a transduction mechanism for tactile encoding. J Neurosci 23: 6499-509.

Olshausen BA, Field DJ (1996). Emergence of simple-cell receptive field properties by learning a sparse code for natural images. Nature 381: 607-9.

Olshausen BA, Field DJ (2004). Sparse coding of sensory inputs. Curr Opin Neurobiol. 14: 481-7.

Panzeri S, Petersen RS, Schultz SR, Lebedev M, Diamond ME (2001). The role of spike timing in the coding of stimulus location in rat somatosensory cortex. Neuron 29: 769-77.

Petersen, CC (2007). The functional organization of the barrel cortex. Neuron 56: 339-355.

Pierret T, Lavallee P, Deschenes M (2000). Parallel streams for the relay of vibrissal information through thalamic barreloids. J Neurosci 20: 7455-7462

Pinto DJ, Brumberg JC, Simons DJ (2003). Circuit dynamics and coding strategies in rodent somatosensory cortex. J Neurophysiol 83: 1158-1166.

Rice FL, Mance A, Munger BL(1986). A comparative light microscopic analysis of the sensory innervation of the mystacial pad. I. The common fur between the vibrissae. J Comp Neurol 252: 154-174.

Ritt JT, Andermann ML, Moore CI (2008). Embodied information processing: vibrissa mechanics and texture features shape micromotions in actively sensing rats. Neuron 57: 599-613.

Romo R, Hernandez A, Zainos A (2004). Neuronal correlates of a perceptual decision in ventral premotor cortex. Neuron 41: 165-73.

Simons DJ, Carvell GE (1989). Thalamocortical response transformation in the rat vibrissa/barrel system. J Neurophysiol 1989 61: 311-30.

Stuttgen MC, Ruter J, Schwarz C (2006). Two psychophysical channels of whisker deflection in rats align with two neuronal classes of primary afferents. J Neurosci 26: 7933-41.

Szwed M, Bagdasarian K, Ahissar E (2003). Encoding of vibrissal active touch. Neuron. 40:621-30.

Szwed M, Bagdasarian K, Blumenfeld B, Barak O, Derdikman D, Ahissar E (2006). Responses of trigeminal ganglion neurons to the radial distance of contact during active vibrissal touch. J Neurophysiol 95: 791-802.

Temereanca S, Simons DJ (2003). Local field potentials and the encoding of whisker deflections by population firing synchrony in thalamic barreloids. J Neurophysiol 2003 89: 2137-45.

Vega-Bermudez F, Johnson KO, Hsiao SS (1991). Temporal factors in tactile spatial acuity: evidence for RA interference in fine spatial processing. J Neurophysiol 95: 1783-91.

Venkatachalam S, Fee MS, Kleinfeld D (1999). Ultra-miniature headstage with 6-channel drive and vacuum-assisted micro-wire implantation for chronic recording from the neocortex. J Neurosci Methods 90: 37-46.

Vinje WE, Gallant JL (2000). Sparse coding and decorrelation in primary visual cortex during natural vision. Science 287: 1273-6.

von Heimendahl M, Itskov PM, Arabzadeh E, Diamond ME (2007). Neuronal activity in rat barrel cortex underlying texture discrimination. PLoS Biol 5: e305.

Watanabe K, Lauwereyns J, Hikosaka O (2003). Neural correlates of rewarded and unrewarded eye movements in the primate caudate nucleus. J Neurosci 23: 10052-7.

Willmore B, Tolhurst DJ (2001). Characterizing the sparseness of neural codes. Network 12: 255-70.

Wolfe JH, Hill D, Kleinfled D, Pahlavan S, Feldman DE (submitted). Encoding of texture by slip-stick events versus differential resonance in the rat whisker system.

Woolsey TA, Van der Loos H (1970). The structural organization of layer IV in the somatosensory region (SI) of mouse cerebral cortex. The description of a cortical field composed of discrete cytoarchitectonic units. Brain Res 17: 205-42.

Yu C, Derdikman D, Haidarlu S, Ahissar E (2006). Parallel thalamic pathways for whisking and touch signals in the rat. PLoS Biol 4: e124.

IV

Discussion

In summary, the results of our studies advance the understanding of how surface features are represented during active tactile sensation in the rat vibrissa system in primary somatosensory cortex (S1). We show that a sparse population synchrony code in S1 encodes slip-stick events, which are one of the primary elements of active whisker motion on surfaces. This elucidates the neural representation of fundamental tactile stimuli in S1 in awake behaving animals which may underlie perception of surface properties like roughness.

A schematic of our model is presented in Figure 1. As rats whisk across surfaces, neural signals conveying surface-whisker interactions are relayed from mechanoreceptors at the base of each whisker to S1 via the trigeminal nucleus in brainstem and the VPM nucleus in thalamus (Figure 1A). Due to the force required to overcome friction, whiskers slip and stick on surfaces, resulting in a sequence of slip-stick events in time (Figure 7B). In cortical columns in S1, responses to slip-stick events of the principal whisker are sparsened across the population of neurons. At any given instant in time, spontaneous activity of neurons is low, and few neurons are active at the time scale of 20 ms. Slip lead to spiking responses in a sparse, random subset of neurons ($\sim 10\%$ above the spontaneous rate) resulting

in synchronous activity above the background rate on a 20 ms time scale. This

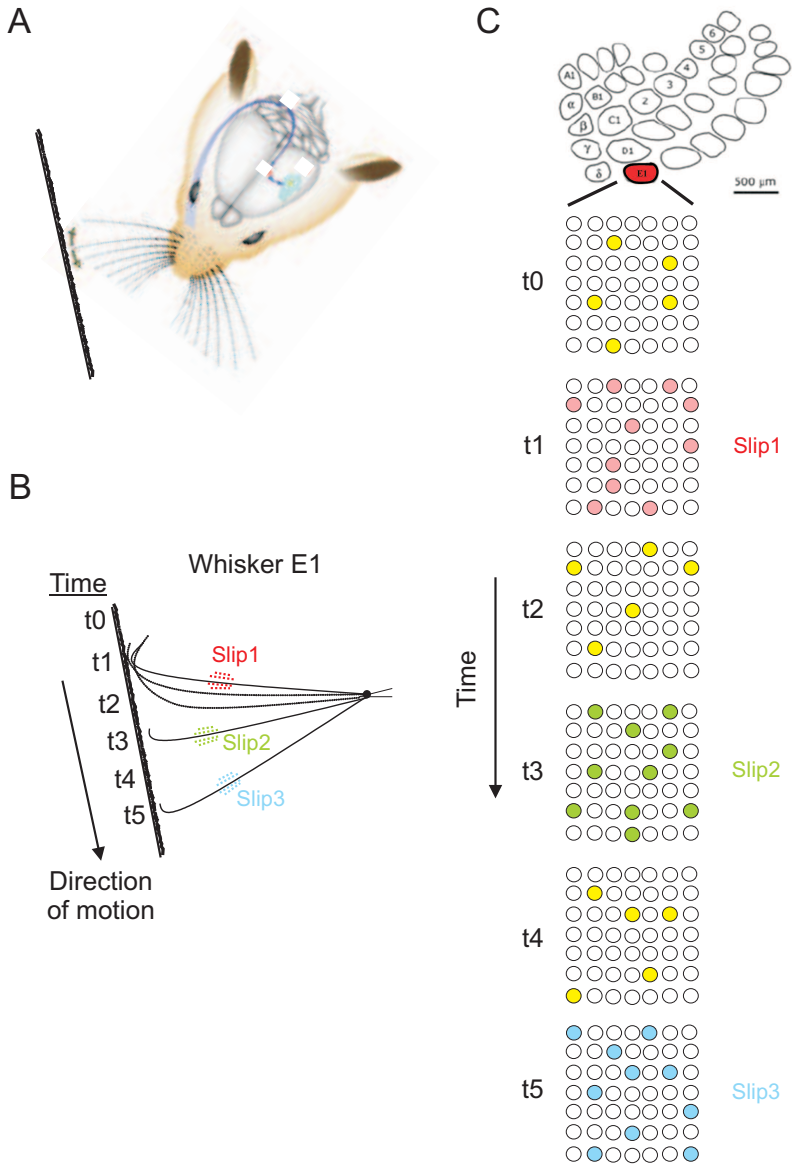

IV.1 **Schematic illustrating model.** (A) As rats whisk across surfaces, signals are relayed from mechanoreceptors to barrel cortex via the brainstem and thalamus (Illustration is from Petersen, 2007). (B) Slip-stick motion of a single whisker (E1) during forward motion (protraction). 3 slip events occurring as time progresses are illustrated. (C) Activity of a subset of neurons in E1 barrel column during surface whisking. Circles denote individual neurons. Few neurons are spontaneously active at a given instant. Each slip event results in activation of a sparse, random subset of neurons above the spontaneous rate (activity for a neuron at each time point is a single spike in a 20 ms time window).

synchronous activity is a strong signal at the population level, and dynamics of synchronous activity presumably underlies the perception of tactile features.